2016

FILTER PERFORMANCE UNDER SIMULATED REAL-WORLD CONDITIONS

Qiang Wang
wangq4, wangq4@vcu.edu

School of Engineering
Virginia Commonwealth University

This is to certify that the dissertation prepared by Qiang Wang entitled "FILTER PERFORMANCE UNDER SIMULATED REAL-WORLD CONDITIONS" has been approved by his or her committee as satisfactory completion of the thesis or dissertation requirement for the degree of Doctor of Philosophy

Dr. Da-Ren Chen, Committee Chair, Mechanical and Nuclear Engineering

Dr. Weining Wang, Mechanical and Nuclear Engineering

Dr. Hooman V. Tafreshi, Mechanical and Nuclear Engineering

Dr. Weijun Xiao, Electrical and Computer Engineering

Dr. Jing Wang, Institute of Environmental Engineering, ETH Zürich

Dr. Gary C. Tepper, Chair of the Department of Mechanical and Nuclear Engineering

Dr. Barbara D. Boyan, Dean of the School of Engineering

Dr. F. Douglas Boudinot, Dean of the School of Graduate Studies

May 23, 2016

FILTER PERFORMANCE UNDER SIMULATED REAL-WORLD CONDITIONS

A dissertation submitted in partial fulfillment of the requirements for the degree of Doctor of Philosophy at Virginia Commonwealth University.

by

QIANG WANG
M.S., School of Engineering, Virginia Commonwealth University, 2012
B.S., School of Mechanical Engineering, China Three Gorges University, China, 2010

Director: DR. DA-REN CHEN
PROFESSOR AND FLOYD D. GOTTWALD, SR. CHAIR IN MECHANICAL AND NUCLEAR ENGINEERING

Virginia Commonwealth University
Richmond, Virginia
May 2016

Acknowledgement

It was meaningful and challenging to work as a Ph.D. student in the Department of Mechanical and Nuclear Engineering at Virginia Commonwealth University. Without the precious support from people around me, it would hardly have been feasible for me to thrive in my doctoral work. Here is a small tribute to all those people.

First and foremost, I would like to express my deepest and sincere gratitude to my advisor, Professor Da-Ren Chen, for guiding me to the world of aerosol science research. His broad professional experience, immense knowledge, cheerful enthusiasm, and logical way of thinking have been of great value for me. His understanding, encouragement, patience, inspiration, motivation, and personal guidance were always invaluable and make this work possible. For me, he is not only my Ph.D. advisor, but also a lifetime friend and mentor.

I would like to express my gratitude to my dissertation committee members: Dr. Hooman V. Tafreshi, Dr. Weining Wang, Dr. Weijun Xiao and Dr. Jing Wang for their great assistance with writing this dissertation, providing useful comments, and giving me wise advice.

I wish to thank the Department of Mechanical and Nuclear Engineering, Engineering School for providing me great opportunity studying here. I am grateful to the

faculty and staff of MNE for supporting me in many ways. I especially thank Dr. Karla Mossi, who is director of graduate students in MNE.

I am indebted to all members and alumni in the Particle Lab and friends for their great help and encouragement. I am especially grateful to Jingjie Zhang, Qiaoling Liu, Hsi-Wei Yeh, Di Liu, Thamir Alsharifi, Zhenzhong Zhang, Xiuli Lin, Shaowen Chen, Laleh Golshahi and Geng Tian.

I would also thank all my friends for helping out of difficult times, and for all emotional support, entertainment and caring.

Finally, I want to express my appreciation to my parents, Huaxin Wang and Liping Tian, my brother and his wife, Fei Wang and Feng Han, and my fiancée, Xiaoyu Hu for their love, understanding, patience, endless support, and always having faith in me. To them I dedicate this dissertation.

Qiang Wang

Virginia Commonwealth University

5/23/2016

Table of Contents

List of Tables

List of Figures

Abstract

FILTER PERFORMANCE UNDER SIMULATED REAL-WORLD CONDITIONS

By Qiang Wang, M.S.

A dissertation submitted in partial fulfillment of the requirements for the degree of Doctor of Philosophy at Virginia Commonwealth University.

Virginia Commonwealth University, 2016

Major Director: Dr. Da-Ren Chen
Professor and Floyd D. Gottwald, Sr. Chair in Mechanical and Nuclear Engineering

Evaluating the performance of filter media for filtration application is essential to assure design engineers and users that the filter device will deliver promised performance for specific applications under the environmental stress. The study of particle loading characteristics of a filter medium in the laboratory setting is typically performed under the steady-state conditions, i.e., at the constant particle concentration and flow rate through filter media during the entire process. In reality, filtration products are normally operated under the situations that either the flow rate or mass concentration of particles passing through media is varied in time. The success of translating the data collected in the laboratory setting to predict the performance of filter media in the field is thus very limited. In order to bridge the gap between the laboratory testing and real-world performance of filter media, it is

necessary to investigate the performance of filter media under the real-world conditions, i.e., unsteady flow rate or mass concentration.

Particulate Respirator filters have been widely utilized in industrial and daily life to protect individuals from inhaling harmful particles. New filter media for respirator applications continuously are in high demand to meet various challenges in personal particulate matter (PM) protection. The US National Institute for Occupational Safety and Health (US NIOSH) certificates particulate respirators in accordance with Title 42 Code of Federal Regulations (CFR) Part 84. This standard testing is only operated under constant flow conditions. To better understand the performance of respirator filter media in real-world applications, it is thus necessary to evaluate the performance of filter media under realistic flow conditions such as simulated human breathing. A new advanced testing setup will be introduced and applied to systematically investigate the performance of various respirator filters under cyclic flow. In addition, a flat filter testing apparatus was built, which is capable of adjusting the testing flowrate (or face velocity) and particle mass concentration under the controlled patterns.

HVAC entrance filter panels are widely used in aircraft to maintain proper air quality in the passenger cabin, but it has been reported that HVAC filter panels are often not-well utilized in practical circumstances. The non-uniform particle deposition pattern on HVAC filter panels was diagnosed be the most possible reason reducing the lifetime of HVAC filter panels, and normally only partial area on the filter panel were effectively utilized. A typical HVAC system takes up a rather large space which is impossible to meet based on school

laboratory conditions, as well as the actual layout in the cargo area of aircraft. Thus, numerical modeling and simulation would be an alternate method to deal with this problem instead of experiments. Computational fluid dynamics (CFD), is applying numerical methods and algorithms to solve and analyze problems; it is primarily employed to study the performance of pleated HVAC filter media under non-uniform particle loading in this study.

The overall goals of this research are (1) to study the performance of filter media under unsteady conditions (i.e., the performance of respirator filter media under simulated breathing conditions); and (2) to investigate the issue of particle non-uniform deposition on HVAC filter panels. A new experimental setup was developed to accomplish the former goal. The numerical modeling tool, Computational fluid dynamics (CFD), was applied to achieve the latter objective.

CHAPTER 1 Introduction and Overview

1.1 Introduction to Aerosol Filtration

Aerosols, or airborne particles, are present throughout our environment either by nature or through human being activities. They come in many different forms, such as dust, mist, fume, smoke, smog, and fog. These aerosols affect visibility, climate and human health and quality of life. For example, viruses, pollen, and bacteria carrying aerosols, could cause severe breathing problems, lung infection, and other sicknesses if inhaled. In semiconductor manufacturing, the deposition of a foreign particle on the wafer could kill the chip if it is larger than one half the minimum device feature size. Cabin air must be cleaned to remove aerosols and odors inside an airplane, train, subway or bus to ensure a healthy environment for the passengers. It's also been noticed that particulate and oil mist emissions from engine tail pipes and engine crank case ventilation systems are carcinogens, therefore they are highly regulated in developed countries. More generally, much particulate pollution is generated and emitted during production and transportation processes, such as chemical, electronic, mineral, and power plants, and it must be controlled to comply with regulations. In addition, sometimes aerosol particles are very damageable to machinery relying on clean air or liquid for operation. One common example is intake air for combustion engines. The particulate contaminants in air, if not removed before introduced to the combustion chamber, could lead to non-reversible engine damage immediately, especially in a dusty environments where engines operate, such as mining plants, deserts, and construction areas where a fair amount of flying dust exists.

Based on the various physical mechanisms and the different collection substrates, particulate control technologies can be classified into six categories: solid plate impaction (e.g. impactor), virtual impaction, centrifugal impaction (e.g., cyclones), liquid impingement (e.g., scrubbers), filtration, and the use of external force fields (e.g., electrical precipitators and magnetic filters). Among all these possible categories, filtration technology is known as the most economical method for achieving high removal efficiency, especially for fine aerosol particles. Air filtration technology has been extensively applied in industrial and human daily life as the most economical means for collecting submicron sized particles from a gas stream with high efficiency. Some of the most popular application of air filtration will be given in the following.

Air filtration applications

Respiratory equipment is commonly utilized to provide personal protection from various kinds of noxious gases, vapors, and aerosol hazards, which could cause harm and even lead to death, if inhaling wood dust, coal dust, spray painting, pesticide spraying and aerosol transmissible diseases such as influenza, diphtheria, SARS (Severe Acute Respiratory Syndrome). Compared to surgical face masks, which have not traditionally protected the wearers but have been used to keep mouth generated particles away from harming a patient in a healthcare situation.

(a) Face mask **(b) Cartridge respirator**

Figure 1.1 Typical respirator seen on the market

Diesel engine air intake suppliers are facing increasing challenges because vehicle manufacturers demand higher performance in a smaller volume while minimizing life cycle costs. This challenge is mainly from the design and performance of the air filter. The air filter collects particulates from the air in order to protect the engine from damage. Engine wear rates have been calculated to decrease by a factor of 10 when high efficiency air filters were utilized instead of standard efficiency filters. Considerable progress in engine-intake air filtration recently has been made by introducing in line, flow-through fluted and pleated filters, and nanofiber filter media. Figure 1.2 is a diagram of one type of air induction system, where nanofiber media is used in the filter.

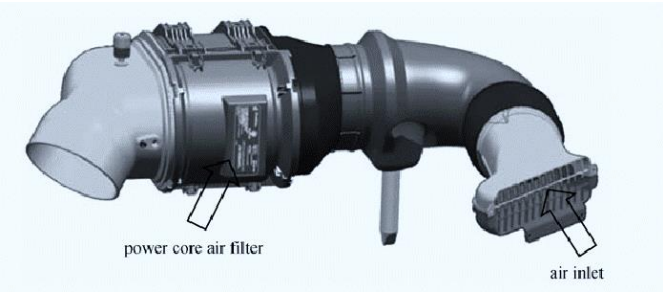

Figure 1.2 Example of engine in-take air filter system

In addition to the PowerCore technology which is protected by almost 30 featured patents, other companies have developed their own fluted air filter designs and contend in the market place of engine in-take air filtration. The major companies are composed of Cummins, Mann-Hummel, and Baldwin, and their products are shown in Fig. 1.3. These highly compacted filter systems are becoming even smaller and lighter due to OEM's (Original Equipment Manufacturer) requirement which entails to use the hood space fully, integrate multiple mechanical and electrical functionalities for fuel economy and emission reduction.

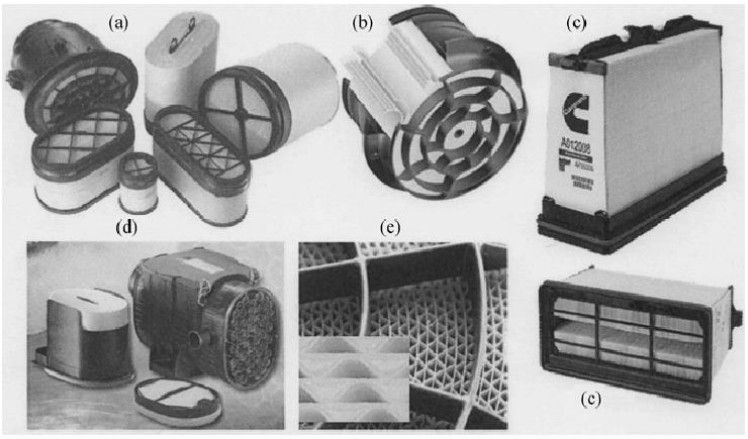

Figure 1.3 In-line fluted and pleated air filters (a) PowerCore (Donaldson), (b) Channel flow (Baldwin), (c) Direct flow (Cummins), (d) PicoFlex (Mann-Hummel), (e) Block of flutes [16]

Heating, ventilating, and air-conditioning (HVAC) systems are normally installed in public, private, and governmental buildings, such as offices, retail facilities, schools, transportation terminals, and public venues (for example, sports arenas, malls, coliseums). And air-filtration and air-cleaning systems are implemented in HVAC systems. Air-filtration and air-cleaning systems could remove different contaminants from a building's airborne

environment. The efficiency of a particulate air filter to remove particles depends upon the size of the particulate combined with the type of filter used and HVAC operating conditions. Larger-sized aerosols can be collected by lower efficiency filters, but the effective removal of small-sized aerosols requires a high efficiency filter. Particulate air filters are classified as mechanical filters and electrostatic filters (electrostatically enhanced filters), and they both are fibrous media and used extensively in HVAC systems to remove particles, including biological materials, from the air. When pleated filters are used, extra filter media are included to decrease the air velocity through the filter media. This enables the filter to increase collection efficiency for a given pressure drop.

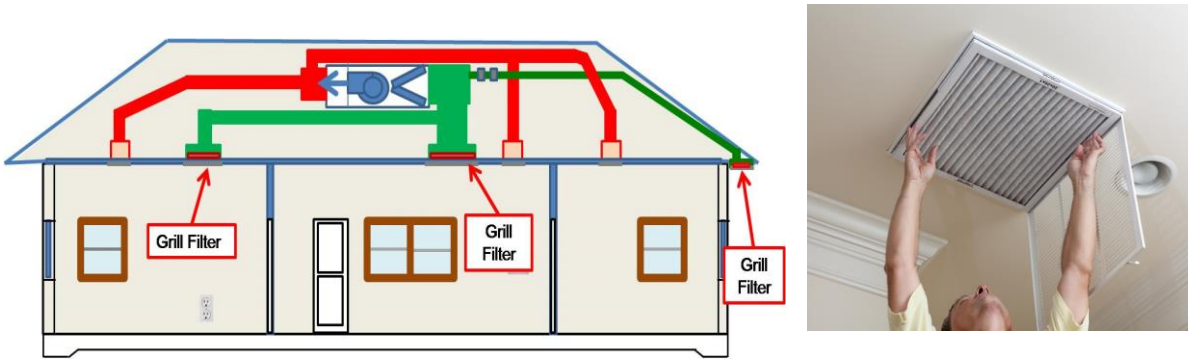

Figure 1.4 HVAC system with filter medium

The air filtration system has to meet widely varying conditions at a nuclear plant and may comprise a multitude of elements, subsystems, and ancillary equipment. The strictest safety and protection regulations are enforced, and everything is designed for fail-safe operations. The prevention of very low concentrations of airborne contamination is foundational to the nuclear facility's safe operation and an important factor for cost

efficiency. This is the reason that the nuclear industry has brought major contributions to the development of new and improved air cleaning equipment. All air and other gaseous effluents are exhausted through a ventilation system utilizing High Efficiency Particulate Air (HEPA) and carbon filters in order to get rid of radioactive particulates and gases. A nuclear air cleaning system protects the public and plant operating personnel from airborne radioactive particles and gases which could be generated or released by the nuclear reactor during fuel fabrication, radiochemical or laboratory operations. HEPA and ULPA (Ultra Low Penetration Air) filters are the major air filters that are used for protecting the handling of nuclear products. Applications in nuclear power plants include control room emergency air supply systems and exhaust systems connected to containment vessels. Processing or manufacturing plants also control radioactive exhaust from prepared materials. Because of the application's sensitive nature, strict guidelines established by the Department of Defense Approval of HEPA filter manufacturers and may include testing by the Department of Energy.

Figure. 1.5 Nuclear power plant

Air filtration principle

There are two main types of principles for particle capture, either by mechanical means or by electrostatic attraction. The particle capture by mechanical means comes into effect without the influence of attractive forces between the airborne particles and the filter fibre. These include: (1) direct interception, which involves a particle following a streamline and being captured if it comes into contact with fibre; (2) inertial impaction, in which capture is effected by the deviation of a particle from a streamline because of its own inertia; (3) diffusional deposition, where the combined action of airflow and Brownian motion brings a particle into contact with a fibre; and (4) gravitational settling, the mechanism of which requires no description. But the effect of gravity during filtration will depend on the direction of airflow, with the result that gravitational settling may either augment or diminish the transport of particles towards the fibres. Thus, it will not be discussed in detail in the following section. Particle capture by electrostatic attraction also plays an important role in air filtration process. The attraction of particles by a uniformly charged fibre illustrates that the drift velocity under the influence of the attractive electric field takes the particle towards the fibre while the convective velocity of the air tends to carry it past.

Figure 1.6 shows these four different popular collection mechanisms govern particulate air filter performance: inertial impaction, interception, diffusion, and electrostatic attraction). The first three of these mechanisms apply mainly to mechanical filters and are influenced by particle size.

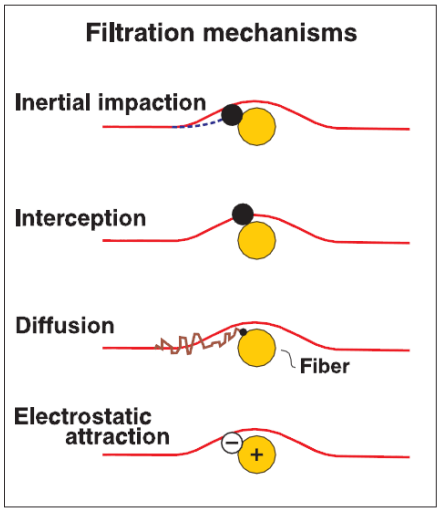

Figure 1.6 Four primary filter collection mechanisms.

Understanding filter loading behavior is an important issue for filtration researchers and engineers. Macroscopically, there are two major parameters—pressure drop and collection efficiency—used in characterizing filtration performance. The filter medium penetration is another useful factor which means the fraction of particles that pass through the media (that is also the ratio of downstream aerosol concentration to upstream aerosol concentration):

$$P = \frac{N_{out}}{N_{in}}$$

where particles' number is N. Thus, the collection efficiency can be written as:

$$E = 1 - \frac{N_{out}}{N_{in}} = 1 - P$$

The pressure drop across a filter is proportional to both its area weight and thickness when the filtration velocity is constant and the filter homogeneous. The collection efficiency of a filter increases by increasing solid volume fraction or decreasing filter fibre diameter.

The filter medium penetration for a specific particle size is given by the following expression:

$$P = \exp\left(-\frac{4\alpha_f \eta Z}{\pi(1-\alpha_f)d_f}\right)$$

where η is the particle collection efficiency of a single fibre, d_f is the fibre diameter, Z is the filter thickness and α_f is the filter packing density. As mentioned above in the principle of filtration section, diffusion, interception and impaction are three particle removal mechanisms operating concurrently within the filter. The problem concerning the assessment of collection efficiency when more than one collector mechanism is important has occupied the attention of investigators before. As pointed out by Ramarao (1994), the simplest approach is to assume that collection efficiencies due to individual mechanisms are additive:

$$\eta = \Sigma\eta_i$$

Thus, the total single fibre efficiency η is then defined as:

$$\eta = \eta_D + \eta_R + \eta_I$$

For the sake of brevity, we selected some of the popular well-known expressions and described them in the following part. Lee and Liu (1982) indicated that only diffusion and

interception are involved in particle collection, with the minor role of impaction mechanism in the range of particle size (between 0.1 and 0.3 μm). They proposed the expression as

$$\eta_R = 0.6\frac{1-\alpha_f}{K_u}\frac{R^2}{(1+R)}$$

$$\eta_D = 2.6(\frac{1-\alpha_f}{K_u})^{1/3}Pe^{-2/3}$$

with

$$K_u = -\frac{\ln \alpha_f}{2} - 0.75 + \alpha_f - 0.25{\alpha_f}^2$$

The single fiber efficiency due to impaction was proposed by Brown (1993) for moderate values of Stokes number,

$$\eta_I = \frac{Stk^3}{Stk^3 + 0.77Stk^2 + 0.22}$$

1.2 The Motivation of Dissertation

As known, it is extremely critical to obtain accurate evaluation of filter media before introduced to various applications. The evaluation of particle loading characteristics of a filter medium in the laboratory setting is typically performed under the steady state conditions, which includes: the air face velocity distribution over the filter media sample is controlled as constant, and it is assumed that a uniform dust concentration is attained over the filter surface during the entire testing of the filter loading process. In the real world, both the flow rate and air face velocity passing through the tested filter media are not always

constant as assumed above. Especially when the filtration devices are installed in an exposure environment, exchanging air between the inside room and outside door. For example, Heating, Ventilation and Air-Conditioning (HVAC) Systems built in office or school buildings are always operating during the day in order to maintain the quality of indoor air, keep comfortable relative humidity, and retain constant temperature for people working inside. In contrast, when at night, the HVAC system will be shut down or operated under low performance in order to lower the energy cost. Thus, the flow rate and face velocity through filtration device will be down to zero or a small value at night. It is obvious that the filter media would be operated under periodical flow rates: two modes which contain both daytime and night flow rates. Furthermore, the particle concentration would also vary from daytime to evening, which affects the dust deposition on the filter panel. The second common example is the engine-intake air filtration system used in piston engine application, which uses one or more reciprocating pistons to convert pressure into a rotating motion. The filter media is playing a critical role in collecting unexpected particles and protect the engine safely. The piston engine is operating under reciprocating movement, as a result, the generated flow rate passing through the chamber and filter will be always regularly oscillating when the piston engine is working. The next typical example is a respirator, which is designed to protect the wearer from inhaling harmful dust, gases, fumes, or vapors. To characterize respirator filter media which filters out airborne particles by mechanical filtration is also under the standard filter media testing methods where a constant flow rate passing through the media was utilized, but actually the flow rate varies as a certain pattern

when people breathe. There are also many other existing examples to demonstrate the flow rate passing through filter media is dynamic instead of constant. It is almost undocumented that the filter media testing experts in the industrial world take the actual flow rates and challenge aerosol concentration into account for the filter media testing standards.

Therefore, the success of translating the data collected in the laboratory setting to predict the performance of filter media in the fields is thus very limited. In order to bridge the gap between the laboratory testing and real-world performance of filter media, it is necessary to investigate the loading behavior of filter media under dynamic particle loading conditions as in the real-world. To study the effect of dynamic particle loading on filter media, we developed a lab-scale flat filter test facility which is capable of varying testing flow rate and mass concentration of challenge particles under the controlled patterns. The particle loading characteristics of several filter media will be characterized under controlled-variation conditions. By the comparison of loading curves obtained under both steady and unsteady testing conditions, the effect of unsteady particle loading on filter media can be observed and quantified.

To maximize the efficiency of an HVAC system, especially for HVAC filter media which are used to regulate indoor air quality, is significant. HVAC filters are widely used in aircraft to maintain proper air quality in the passenger cabin, but it has been reported the HVAC filter panels are often not-well utilized in practical circumstances. The non-uniform particle deposition pattern on HVAC filter panels was diagnosed be the most possible reason reducing the lifetime of HVAC filter panels, and normally only a partial area on the filter

panels was effectively utilized. To understand the effect of non-uniform particle loading on pleated HVAC filter panels installed in aircrafts would be meaningful based on our study. However, there are many practical, difficult issues in front of us to conduct and operate experiments for this work. Normally, a typical HVAC system takes a rather large space which is impossible to meet based on school laboratory conditions, as well as the actual layout in the cargo area of aircraft.

Thus, modeling and simulation would be an alternate method to deal with this problem instead of experiments. Computational fluid dynamics, usually known as CFD, is applying numerical methods and algorithms to solve and analyze problems; it is primarily employed to study the performance of pleated HVAC filter media under non-uniform particle loading in this study. With the assistance of CFD tools, we are allowed and able to build a reasonable geometric model in order to simulate the realistic problems and investigate them. Application of this study will provide a better understanding of the flow field and particle behavior around the pleated HVAC entrance filter medium installed in aircrafts.

1.3 The Objective of Dissertation

The overall goal of this research is to investigate the loading behavior of filter medium under unsteady particle loading conditions, simulating real world situations. Our study also deals with modeling the flow field, particle motion, and particle deposition on HVAC filter panel. In order to study unsteady particle loading on filter media effect, we

developed a novel testing method which is able to evaluate various respirator filter medium precisely. Different types of respirator filter media were provided for the evaluation with the new testing method. In addition, a flat filter test apparatus was also built that was capable of adjusting the testing flowrate (or face velocity) and mass concentration of challenge particles under the controlled patterns. With the comparison of loading behaviors obtained under steady and unsteady testing conditions, we are able to quantify the effect of unsteady particle loading effect on these filter media. The other part of this study is to develop numerical models which can describe the flow field distribution, pressure drop, particle trajectories and particle loading profile during the non-uniform particle loading process on the pleated filter which was installed in HVAC entrance panels. Detailed plans are further described below in the form of objectives.

Objective 1: Study the loading behavior of filter media under dynamic loading conditions.

i. Develop an advanced new experiment setup for respirator filter media testing
ii. Evaluate the performance of respirator filter medium under periodic flow conditions
iii. Develop a lab-scale filter medium testing facility
iv. Investigate the effect of particle loading rate on the performance of filter media

Objective 2: Investigate the performance of HVAC entrance filter panel under non-uniform particle loading

i. Build 2D model to calculate the loading curve of filter under loading condition
ii. Evaluate the effect of pleat geometry and point-released locations on HVAC entrance filter panel performance under non-uniform particle loading
iii. Investigate particle loading under the presence of flow obstruction near the HVAC entrance
iv. Model the dust cake growth on filter medium in 2D model
v. Establish 3-D numerical model for investigating the flow field and particle behavior around clean pleated HVAC entrance filter panels

1.4 Dissertation Structure

The dissertation contents are structured to address the two major objectives in the following manner: the first part, including chapters 2, 3, 4 and 5, focuses on the experimental study on the performance of filter media under unsteady conditions; the second part, containing chapters 6 and 7, focuses on the computer modeling investigating the performance of HVAC entrance filter panels under non-uniform particle deposition.

In chapter 1, an overview of aerosol filtration technologies and their needs, applications, major principle and challenges is presented. A general introduction including the background, motivation and overall research objectives of this study is given.

In chapter 2, the filter media loading behavior with selected models are introduced and reviewed. Some of the concepts and methods are chosen and applied to analyze and model our experimental and simulation data of the filter loaded with solid particles.

In chapter 3, an advanced new testing method, including the background information, detailed testing method, setup design, experimental results and discussion are described for evaluating various standard respirator filter media.

In chapter 4, the performance of respirator filter media are investigated under simulated human breathing conditions. Five types of respirator filter media were evaluated, including two single-layer fibrous filters, one single-layer charged filter, and two composite filters. In addition, another fibrous filter medium and a nano-fiber medium were also tested under cyclic flow conditions. The flow with Sinusoidal pattern and inhalation-only were selected as filter media testing conditions. The individual effects of breathing frequency and peak flow rate are discussed. Furthermore, modeling of particle peak penetration is also developed.

In chapter 5, experiments were performed to systematically study the effect of dust loading rates (i.e., test particle mass concentration times total test flowrate) on the loading curve of high efficiency filter media. Two types of filter media, glass fiber filter and charged electret filter, were loaded with two test dusts, Arizona road dust (ARD) and Ultrafine dust. Five dust loading rates and two filter face velocities (i.e., 10 and 20 cm/sec) were varied in this study. The effect of the loading rate was further quantified by data analysis. An empirical equation was also proposed to describe the loading curves obtained in this study.

In chapter 6, computational fluid dynamics, usually abbreviated as CFD, are utilized to build up a 2-D numerical model of the HVAC entrance filter panel to study their

performance under non-uniform particle deposition. The 2-D model for calculating the loading curve is developed. The effect of filter panel pleating geometry and point-release locations of particles on HVAC filter performance are studied and discussed under non-uniform loading. Also, the performance of HVAC filter panels in presence of flow obstruction is also considered and investigated.

In chapter 7, a 3-D numerical model is established based on the 2-D model for evaluating the performance of HVAC entrance filter panels. The flow field and particle behavior around clean HVAC entrance filter panels are calculated and discussed.

In Chapter 8, the accomplishments of this dissertation are summarized; the research also explores issues, challenges and future efforts.

CHAPTER 2 Review of Models for Filter Media Loading Behavior

2.1 Introduction

A filter is often composed of fibrous materials which removes solid particulates such as dust, pollen, mould and bacteria from the air, and the process of filtration is dynamic. The collection efficiency of filtration continuously improves as particles are trapped in the media matrix or deposited on the surface of the filter. While the media filtration efficiency improves, the pressure drop across filter media monotonically increases with the formation of particle dendrites on the fibers. The increase of pressure drop is undesirable, because it either reduces the filtration velocity or increases the load on the air movers, like a pump. Besides, a critical pressure drop is typically utilized as an indicator to monitoring the lifetime of filter media. Thus, understanding filter loading behavior is a significant issue for filtration researchers and engineers. Macroscopically, filter loading behavior is characterized by the filter pressure drop ratio as a function of loaded mass or volume, where the pressure drop ratio is defined as the ratio of the instant loaded-filter pressure (ΔP) to the filter initial pressure drop (ΔP_0). The loading capacity of the filter can then be defined as the loading mass/volume at the critical pressure drop.

Previously, many studies have shown that filter loading behavior (i.e., the pressure drop vs. the loaded particle mass/volume per unit filter area) is affected by the properties of particles (e.g., particle size distribution, particle concentration and charging status), the structure of the filter media (e.g., fibrous filter, fabric filter, granular filter, and membrane

filter), the filtration face velocity, and other environmental conditions (e.g., relative humidity, temperature). For a typical low efficiency fibrous filter media loaded with solid particles, the loading phase generally progresses through three stages: depth filtration, a transition regime, and surface filtration. (Fig. 2.1) At the beginning, particles load onto the fibers, starting to form dendrites, and the pressure drop gradually increases in a liner pattern, which is depth filtration. As the loading continues, the pressure drop experiences a steeper increase, into the transition regime. In the final step (surface filtration), the dendrites join together and create a dusk cake on the surface of filter media. The pressure drop linearly increases until either the dust cake is mechanically restructured by the large pressure drop, or the filter clogs.

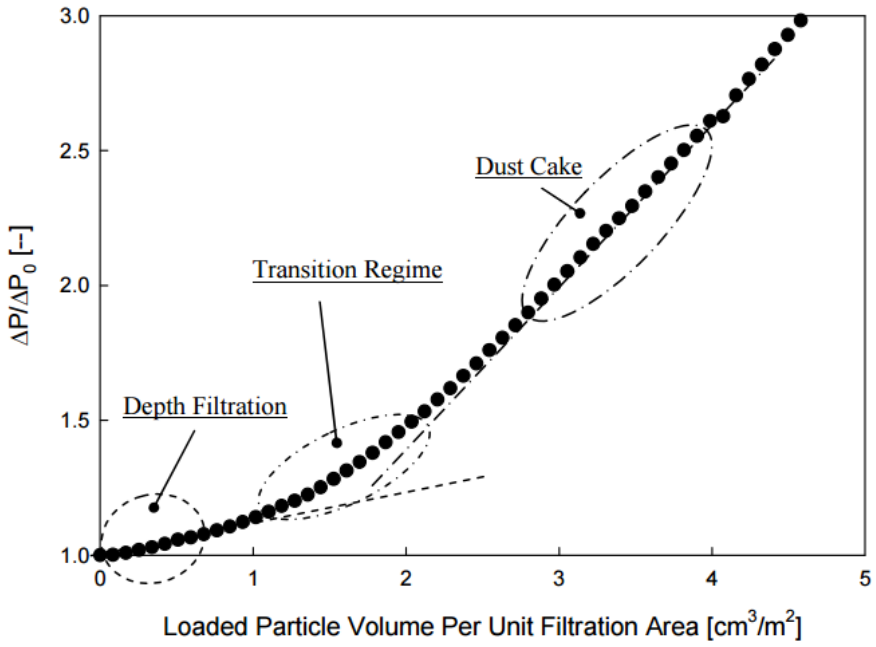

Figure 2.1 Typical loading behavior for fibrous filter loaded with solid particles

2.2 Pressure Drop of Clean Filter

Many relationships have been proposed to calculate the pressure drop across clean fibrous filters. One fundamental model to predict the pressure drop across clean fibrous media is based on the summation of the drag forces of all the fibers. When at low Reynolds numbers ($\rho U d_f/\mu<1$), the drag force on a cylinder fiber array can be approximated by the product of flow velocity (U), viscosity (μ), and a drag coefficient (F), and the pressure drop of clean filter (ΔP_0) can be estimated as:

$$\Delta P_0 = L_f \mu U F, \quad \text{and } L_f = \frac{4\alpha_f Z}{\pi d_f^2} \tag{2.1}$$

where L_f is the total length of all filter fibers per unit filtration area, F is the drag coefficient, Z is the filter thickness, α_f is the filter packing density and d_f is the fiber diameter. The accuracy of Eq. 2.1 highly depends on the drag coefficient F. The expression of F proposed by Happel (1959), Kuwabara (1959), and Stechkina and Fuchs (1963) are all derived theoretically by solving the flow field in a system of parallel circular cylinders at a condition of low Reynolds number, but with different boundary conditions. However, experiment results indicate that the expression in estimating clean filter drop is not accurate as the empirical expression proposed by Davies (1952). Werner and Clarenburg (1965) did extensive experiments to test glass fiber filters with packing densities ranging from 0.039 to 0.084, and showed better agreement with the predication of Davies. The reason may be attributed to the theoretical models not considering the random orientation of the fiber cylinders and the flow interference between them.

For Davies' expression (1973), the pressure drop across clean fibrous filter media can be written in terms of fluid viscosity (μ), face velocity (U), filter thickness (Z), fiber mean diameter (d_f), and packing density (α_f):

$$\Delta P_0 = \mu Z U \frac{64\alpha_f^{1.5}(1+56\alpha_f^3)}{d_f^2}, \qquad when \;\; 0.0006 < \alpha_f < 0.3$$

$$\Delta P_0 = \mu Z U \frac{64\alpha_f^{1.5}}{d_f^2}, \qquad when \;\; \alpha_f < 0.006$$

We should be aware that these equations are semi-empirical and do not account for the fiber size variation in the filter media. The study of Jackson and James (1986) also shows that the prediction begins to deviate from the experimental test when the packing density is below 0.001.

Hosseini and Tafreshi (2010) developed virtual 3-D models to mimic the internal microstructure of a fibrous structure for predicting and simulating the pressure drop and collection efficiency of clean filter. However, the problem is that simulating is expensive.

2.3 Pressure Drop of Loaded Filter

The pressure drop across loaded filters has been extensively studied, and some researchers have attempted to build mathematic models to simulate the process of pressure drop evolution for a filter loaded with solid particles under different filtration regimes. Within the microscopic level, the pressure drop increase across a loaded filter is due to the additional flow resistance contributed by the deposited particles. Deposited particles can

form particle dendrites and further disturb the original flow field. The mechanisms of the particle dendrite are similar to the mechanical filtration mechanisms, and they are closely related to the particle size. Kanoaoka et al. (1986) summarize the different particle deposition patterns (dendrite morphology) on a single fiber and showed the continuous changes of the patterns with the particle Peclet number (Pe) and Stokes number (Stk). The difference between these deposition patterns creates various flow resistance resulting in different pressure drops across loaded filters. However, the link between the microscopic dendrite structure, loaded particle mass, and pressure drop is still unclear. The paramount challenge is investigating and quantifying the particle dendrite structure on loaded filters, especially for polydisperse submicron particles.

Payatakes and Tien (1976) had first to develop theoretical models to simulate particle dendrite growth and their effect on filter penetration and pressure drop. However, the model is quite complicated and requires two density functions: the dendrite age distribution function and the dendrite number distribution function which are extremely hard to estimate in reality. Some researchers have proposed different methods to calculate the drag force on a dendrite, but achieved limited success. Kanaoka and Hiragi (1990) proposed another theoretical model to predict the pressure drop of a dust-loaded filter based on the drag theory. The proposed model is only applicable if the effective fibre diameter and the drag coefficient of a dust-loaded fibre are given as a function of accumulated volume of captured particles.

Another approach to account for particle collection by filter media is developed by Bergman et al. (1978), who assumed that the filter may be considered as a medium with two

types of fibres during the particle deposition process. The first sort is composed of the initial fibres, the second of the collected particles forming dendrites. In this model, the two pressure drops are independent. In addition, to correct the interference between the dendrites and filter fibers, they increased the fiber and dendrite volume fraction by the factors $(L_f + L_p)/L_f$ and $(L_f + L_p)/L_p$ respectively. Based on Darcy's law and the corrected Davie's empirical expression for the factor F, the total pressure drop is summarized as

$$\Delta P_0 = 16\pi\mu U \left[\left(\alpha_f \frac{L_f + L_p}{L_f} \right)^{0.5} L_f + \left(\alpha_p \frac{L_f + L_p}{L_p} \right)^{0.5} L_p \right]$$

where α_p is the packing density due to deposited particle and L_p is the total length of the "new" fiber formed by the particle dendrites. The L_p could be calculated by the equation as,

$$L_p = \frac{4\alpha_p Z}{\pi d_p^2}.$$

Substituting L_p to above equation of ΔP_0 gives,

$$\Delta P_0 = 64\pi\mu U \left(\frac{\alpha_f}{d_f} + \frac{\alpha_p}{p} \right) \left(\frac{\alpha_f}{d_f^2} + \frac{\alpha_p}{d_p^2} \right)^{0.5}$$

Nevertheless, by comparison with experimental data, Vendel et al. (1990) show the pressure drop is underestimated during the loading process of particle in Bergman's model. They suspected the reason may be from the assumption of uniform deposition and diameter

of particle in the filter medium. Thomas et al. (1990, 2001) extend Bergman's model by dividing the filter into various layers with thickness Z_j and assumed particles homogeneously deposited in each layer of the filter. However, the model developed by Thomas requires repeat calculations of the collection efficiency, the loaded particle mass, and the packing density of each layer.

For a HEPA filter, heavily loaded filter, or fabric filter, surface filtration is dominant. The loaded particles typically develop dust cake. The total pressure drop across a loaded filter consists of two parts. One is attributed to the pressure drop across clean filter (ΔP_o), and the other is from dust cake (ΔP_c). Thus, the pressure drop across a loaded filter can be written as,

$$\Delta P_0 = \Delta P_o + \Delta P_c$$

Much work had been performed to experimentally and theoretically investigate the pressure drop across the dusk cake built up on the filter surface. Among the more recent studies, Endo and Chen proposed the following equation to calculate pressure drop of dust cake for the cases of randomly packed dust cake with the consideration of particle polydispersity and shape:

$$\Delta P_c = 18\mu u_s H \frac{(1-\varepsilon)\upsilon(\varepsilon)}{\varepsilon^2} \frac{\kappa}{d_{vg}^2 exp(4ln^2\sigma_g)}$$

where $\mu, u_s, H, \kappa, d_{vg}$ and σ_g are fluid viscosity, superficial velocity, cake height, dynamic shape factor of particles, and the geometrical mean diameter and standard deviation of test particles, respectively. ε and $v(\varepsilon)$ are the cake porosity and void function.

CHAPTER 3 Advanced Testing Method to Evaluate the Performance of Respirator Filter Media

3.1 Introduction

Respirators have been applied for the personal protection either in indoor or outdoor environments, where the particulate matters (PM) at the threshold concentration level are potentially present. New filter media for respirator applications are continuously in high demand to meet various challenges in the personal PM protection. The testing of respirator filter media and respirators is of critical importance for its applications. The regulation to certify particulate respirator filters for use in industrial, chemical, biological, radiological and nuclear applications had been published by US National Institute for Occupational Safety and Health (US NIOSH). The detailed information of the regulation can be found in Title 42 *Code of Federal Regulations (CFR)* Part 84, in which the filtering facepiece respirator media are challenged by Sodium Chloride (NaCl) or oil aerosol with the mass median diameter (MMD) of 300 nm under a constant flow rate of 85 L/min. However, the particle penetration through a filter medium is in general dependent on factors such as size distribution of aerosol particles, face velocity, relative humidity, and physical properties of filter media. In reality, respirator filter media experiences cyclic flow because of the breathing of a human being. To better understand the performance of respirator filter media in real-world applications it is thus necessary to evaluate the performance of filter media under realistic flow conditions.

Previous studies had investigated the effect of cyclic flow on the particle penetration of respirators. The pioneer study was reported by Jordan and Silverman, in which a fiberglass filter was tested with particles of 0.78 μm Count Median Diameter (CMD) and a geometric standard deviation, σ_g of 1.13. The work concluded that penetration measured under constant flow conditions may either under- or over- estimate that obtained under cyclic flow conditions, depending on the time-averaged mean air velocity. In another early publication by Stafford *et al.*, [3] the authors measured the penetration of seven monodisperse polystyrene latex particle (PSL) ranging from 0.176 to 2.02 μm and one dioctylphthalate (DOP) aerosol of 0.3 μm through respirator filter cartridges under three cyclic breathing flow conditions with mean inspiratory flow (MIF) rates of 30, 35 and 53 L/min. It was found that the maximal particle penetration through a respirator filter medium was consistently higher under cyclic flow conditions as compared to that under constant flow conditions. In early studies, two Log Alamos-designed light-scattering photometers were used to measure the aerosol concentrations at the upstream and downstream of filters. All the conclusions were relied on the measurement technology which determines the accuracy of the results.

N95 respirators have shown superior performance under various flow conditions compared to other types of respirators and surgical facemasks. A laser particle spectrometer (LAS-X) was applied by Qian *et al*. to measure the particle size distribution in the study of N95 facepiece respirator performance challenged by microbial and inert particles. The above study concluded that N95 respirators provide higher filtration efficiencies under medium/low work load conditions when the flow rate is less than 85 L/min. Wang *et al*.,

measured the penetration of 0.3 μm polystyrene latex (PSL) particles through N95 and P95 cartridges under various cyclic flow conditions. Four cyclic flow patterns (i.e., two sinusoidal, one trapezoidal and one exponential waveforms) having the same equivalent minute ventilation (defined as volume of the half of the cyclic flow per minute) of 50 L/min, were selected in their study. The upstream and downstream aerosol concentrations were measured by a laser particle spectrometer (LAS-X). The work concluded that the highest particle penetration was found when the media tested under the cyclic exponential-flow pattern, in which peak inhalation flow rate (PIFR) was the highest. The cyclic flow with the trapezoidal-waveform (having the lowest PIFR) resulted in the lowest particle penetration (among all the cyclic flow testing). Compared with the data obtained under cyclic flow evaluation, filter media evaluated at the constant flow condition has the lowest particle penetration.

Facemask seal is also needed to be considered in evaluating the performance of respirators. Grinshpun *et al.* studied the performance of an N95 filtering facepiece particulate respirator and a surgical mask using an electrical low pressure impactor (ELPI). The work focused to differentiate the contribution of two air pathways, i.e., via the faceseal leakage and through filter medium, for particles in the size range from 0.03 to 1.0 μm under realistic breathing conditions. The work indicated that facial/body movement had pronounced effect on the relative contribution of two penetration pathways. The use of ELPI enabled the measurement of instantaneous particle size distribution. Particles in high concentration at the downstream of test filter media are required because of low detection limit of

electrometers used in the ELPI for particle concentration measurement. It becomes challenging to use ELPIs in the evaluation of filter media in the HEPA grade.

The other instruments used to study the performance of respirator filter medium for particles in sub-micrometer size range are scanning mobility of particle sizers (SMPSs). Bałazy *et al.* indicated that the N95 respirators may not provide the expected protection against small viruses. A significant fraction of airborne viruses penetrates through some surgical masks, providing very low protection against aerosolized infectious agents in the size range of 10 to 80 nm. The wide-range particle spectrometer (WPS) was used to sample aerosol inside and outside of respirators in this study. Note that a laser particle spectrometer (LPS) was included in WPS to extend the measurable range of particle size up to 10,000 nm. Haruta *et al*. used PSL particles for testing N95 filtering facepiece respirators (FFRs) under various cyclic and constant flow conditions. In their investigation, they only enabled the scanning mobility sizer module of WPS to measure aerosol concentrations at both sides of respirators. The work reported that the particle penetration of filters varied under different cyclic flow rate conditions. Mahdavi *et al*. proposed a procedure to study the individual contribution of BF and PIFR on the performance of N95 filtering facepiece respirators, in which a scanning mobility particle sizer (SMPS) was operated to measure particle concentrations at the up- and down-stream of filter media. The aerosol measuring time for SMPS method in the work was set at 360 sec. It was concluded that the PIFR variation had a more significant contribution to the particle penetration of respirator filters, but the effect of breathing frequency on the respirator performance was negligible.

We questioned the previous findings of negligible breathing frequency effect on the respirator performance. It is because the SMPS measurement cycle used in the previous study was set at 360 sec. Measured particle size distributions was in fact the average of 124 and 252 breathing cycles when the BF were set at 24 and 42 BPMs (breath per minutes), respectively. We thus hypothesized that the reported observation was due to the testing method and measurement technique. The objectives of this work are thus (1) to examine our hypothesis; (2) to develop a new testing method for studying the individual effect of BF and PIFR on the performance of respirator filter media; (3) to perform a pilot study to demonstrate the feasibility of the new testing method. In the following sections we first described the new testing method to investigate the performance of a respirator filter media under cyclic flow conditions. For comparison, SMPS was also applied in the setup as particle sizers to measure the penetration of the same filter media under the same cyclic flow conditions. The data collected in our work were then shown in the section of Result and Discussion.

3.2 New Testing Method and Experiment Design

3.2.1 New Testing Method

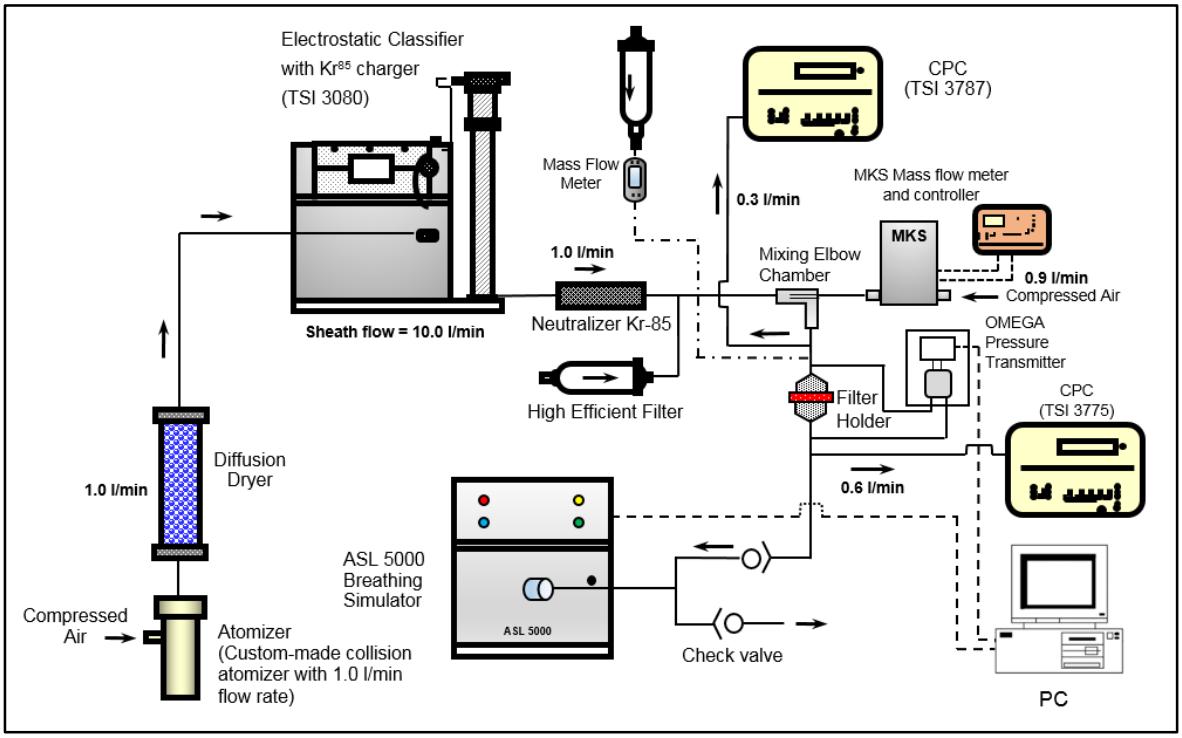

Figure 3.1 Schematic diagram of experimental setup for the new testing method

The schematic diagram of our experimental setup is shown in Figure 3.1. Polydisperse droplets were generated by atomizing sodium chloride (NaCl) solutions via a custom-made Collison atomizer. Polydisperse solid particles were obtained by passing polydisperse droplets through a diffusion-type dryer with silica gel as the desiccant. Once generated, polydisperse solid particles were introduced into a Kr^{85} bipolar aerosol charger and a differential mobility analyzer (DMA TSI model 3081) to classify particles of desired sizes based on their electrical mobility. Both aerosol and sheath flowrates of the DMA were set at 1.0 and 10.0 LPM, respectively. After the size classification electrical charges on DMA-classified particles were minimized by delivering them through a 10 mCi Kr-85

neutralizer (TSI Model 3012). It is because electrical charge level on particles could affect the particle penetration though filter media.

Because of cyclic flow testing, a mixing chamber, in which a constant and particle-free flow of 0.9 L/min was injected to mix with classified aerosol flow, was placed at the upstream of filter test section to provide sufficient flowrate for the CPC measurement. A mass flow controller (MKS Type 1179A) was used to control the 0.9 L/min flowrate. In the test section, the filter media was placed in a 47mm filter holder. The effective test area of filter media was 15.3 cm^2. Differential pressure transmitter (OMEGA PX-655) was used to measure the pressure drop across the filter media. Two identical sampling ports were located in the up- and down- streams of the filter holder for particle measurement. Condensation particle counter (CPC; TSI Model 3775) and water-based CPC (TSI Model 3787) were applied to measure the up- and down- stream concentrations of test particles, respectively. Both CPCs have the sampling time of 0.1 sec (i.e., 10 Hz) for measuring particle concentration. Particle penetration of filter media was derived by taking the ratio of downstream concentration to the upstream. In this study, each test run lasted for 4 minutes after the flow in the setup reached the periodical status. Prior to each run, the background CPC readings were also checked to ensure the zero reading.

Because of particle loss in the filter holder and two CPC models used in the setup, a calibration experiment was performed to correlate the readings of two CPCs before the testing. No filter media was in the holder during the calibration experiment.

A human breathing simulator (Model ASL5000, IngMar Medical, PA, US) was used to provide the cyclic flow condition. Two one-way valves (Model BE 130-22B, Instrumentation Industries, Inc., US) were installed at the inlet of the breathing simulator for inhalation-only testing. Prior to each test, the flow condition was verified by a mass flow meter (TSI Model 4143).

To test the performance of respirator filter media under the worst scenario, we selected particles at the most penetration particle size (i.e., MPPS) under the constant-flow condition at the rate of MIFR (Mean Inhalation Flow Rate) to challenge filter media. The MPPS of test filter media was measured prior to its cyclic flow testing. For the test filter medium A studied, the measured MPPS was at ~ 150 nm under the face velocity of 10 cm/s. The selection of 10 cm/s face velocity is because the flow rate of 85 L/min is applied to test respirator filter media with the surface area of 135 cm^2 in the testing standard (Title 42 *Code of Federal Regulations (CFR)* Part 84), resulting in the face velocity of 10.6 cm/s. For the reference, the basic properties of the test respirator filter media are given in Table 3-1.

Table 3-1. Basic properties of respirator filter media used in this study. Filter medium A was primarily used in our pilot study. Filter medium B was used in the part of study to demonstrate the applicability of proposed testing method for HEPA filter media

Filter Media	Media Type	Basic Weight [g/m^2]	Pressure Drop at Flowrate of 1 L/min [inH_2O]	Thickness [mm]	Permeability [m^2]
A	Borosilicate glass	75.4	0.135	0.43	2.62E-12
B	HEPA Membrane Filter	13.69	1.285	N/A	N/A

3.2.2 Experimental Design

Flows in multiple sinusoidal waveforms were selected in this study. Two BFs of 6 and 25 breaths/min (BPM) and two PIFRs of 9.42 and 18.14 L/min were chosen as the flow testing conditions. Table 3-2 summarizes the key parameters for four selected cyclic flows. Three replicates were performed at different days for each test condition.

TABLE 3-2. Characteristics of cyclic flows designed in this pilot study

Cyclic Flows	Breathing Frequency (stroke/min)	Peak Inhalation Flow at test area of 15.3 cm^2 (L/min)	Peak Inhalation Flow at test area of 135 cm^2 (L/min)	Tidal Volume (liter/stroke)	Peak Face Velocity (cm/s)
1	6	9.42	82.94	0.5	10.24
2	25			0.12	
3	6	18.14	159.97	0.96	19.70
4	25			0.23	

The selection of these cyclic flow testing conditions is to match the NIOSH standard flow testing condition and breathing patterns of adult human beings. The relationship among the flow rate, face velocity and effective area is expressed as *Flow rate = Face Velocity* × *Effective Area*. Because of the use of filter holder having effective testing area of 15.3 cm^2, we matched the test face velocity with that defined in the NIOSH standard testing for N95 mask, in which the testing area of respirator is approximately 135 cm^2 at the constant flow rate of 85 L/min (resulting in the face velocity of 10.6 cm/s). To match the face velocity defined by NIOSH, test flow rate in our study was lower than 85 L/min because of smaller filter testing area used. The PIFR of 9.42 L/min was selected as equivalent testing condition

to the NIOSH standard test. We also selected one higher PIFR (i.e., 18.14 L/min) to study the effect of PIFR on the particle penetration of the test respirator filter media.

To test the effect of breathing frequency on the performance of the respirator filter media, BF was chosen as 6 and 25 BPM. The selection of BF is based on the earliest data available on spontaneous breathing frequency of human beings, obtained from Quetelet on 300 subjects and Hutchinson on 1714 adult subjects. The wide BF ranging from 6 to 31 breaths per minute were observed in adults.

3.3 Result and Discussion

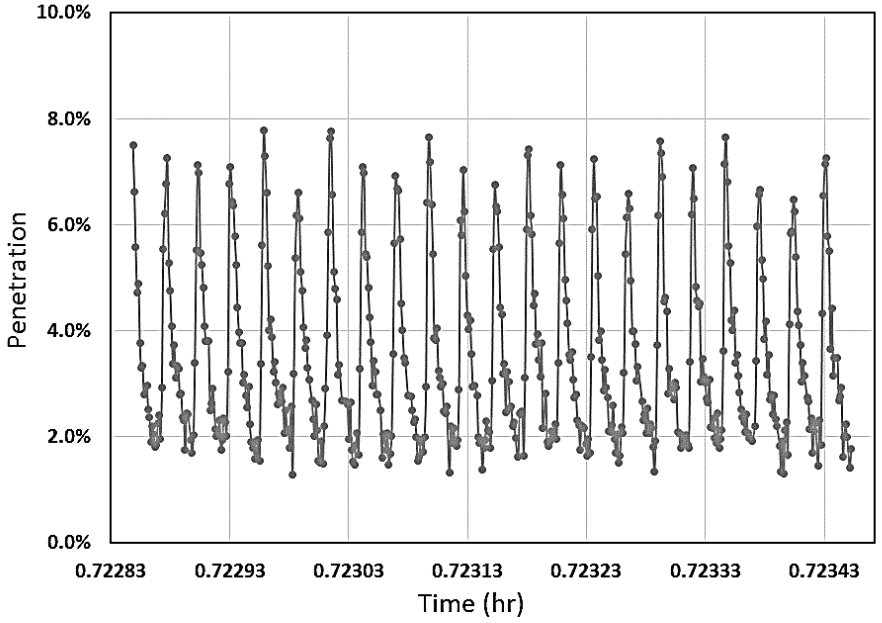

Figure 3.2 Measured instantaneous penetration values through test filter media at the particle size of 150 nm and PIFR of 18.14 L/min via the new testing method

Figure 3.2 shows a typical time-dependent particle penetration of test filter media (at the particle size of 150 nm and PIFR of 18.14 L/min) measured by the new testing method (at the sampling frequency of 10 Hz). The characteristics of breathing cycle are clearly shown in the figure. Detailed data analysis of the time-dependent penetration is expected to provide more information on underlined mechanisms involved in the cyclic flow conditions.

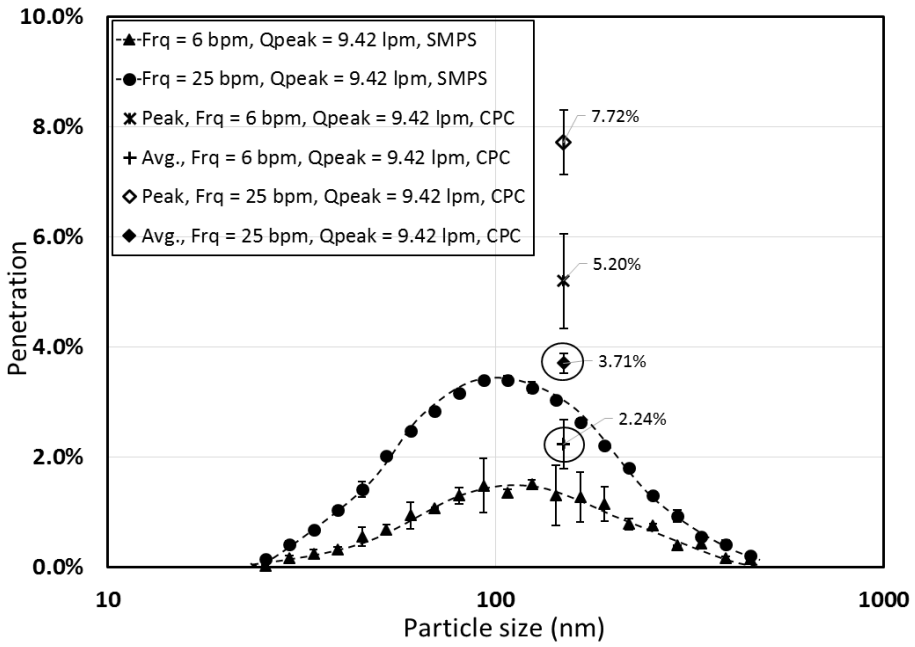

(a) At PIFR = 9.42 L/min

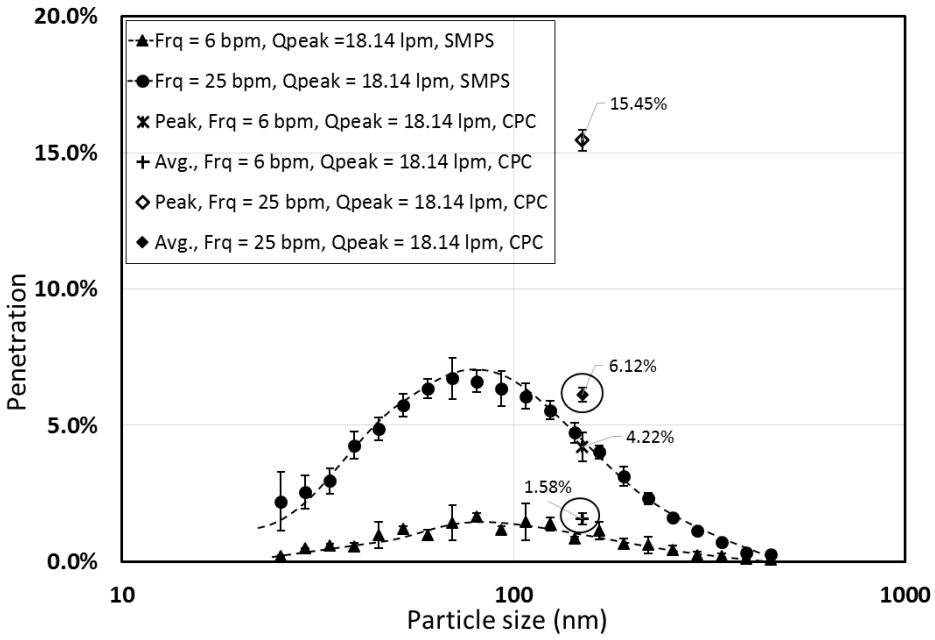

(b) At PIFR = 18.14 L/min

Figure 3.3 Penetration values through test filter media via the new testing method and testing with SMPS as particle sizers at PIFR values of (a) 9.42 L/min, and (b) 18.14 L/min

Figure 3.3 shows the particle penetration through the test filter media, measured both by the new testing method and the method with SMPS as particle sizers, under the selected cyclic flow conditions. Among previous literature the maximum particle penetration of respirator filter media was selected to determine the worst-scenario performance of respirator filters. It is observed from the figure that the value of maximum particle penetration for a respirator filter medium cannot be obtained by the testing methods with SMPS. Fig. 3.3a shows the particle penetration through the filter medium under 6 and 25 BPM (at the PIFR of 9.42 L/min). Because of the use of MPPS in the new testing method, only two data points were included in Fig. 3.3a. The SMPS-measured data shows that the

most penetrating particle size is ~ 120 nm, and the peak penetrations are approximately 1.5% and 3.4% for BF of 6 and 25 BPM, respectively. For the new testing method, the measured particle penetrations of test respirator filter media are 5.2% and 7.72% for 6 BPM and 25BPM, respectively. Note that the maximal penetration data given in Fig. 3.3 (obtained by the new method) is the average of peak particle penetration measured in multiple breathing cycles. The numbers of measured data points for the above average were 48 and 200 in the cases with 6 and 25 BPM, respectively. It is found that the penetration data measured by the new method are a factor of two higher than those measured via the testing using SMPSs as the sizers. Also included in Fig 3a are the cycle-averaged penetration calculated based on the instantaneous penetration measured in the new method. The cycle-averaged values are slightly higher than those measured with SMPSs.

For the flowrate condition of 18.14 L/min PIFR (given in Fig. 3.3b), the peak penetration values of 1.47% and 6.6% were measured with the SMPS testing method for BFs of 6 BPM and 25 BPM, respectively. The peak penetration of 4.22% and 15.45% for 6 and 25 BPM BF, respectively, were obtained via the new method. Similar to that observed in the case of 9.42 L/min PIFR, the measured peak penetration via the new testing method were more than two times higher compared to those measured by the testing with SMPSs. The cycle-averaged penetration calculated based on instantaneous penetration measured using the new method are also shown in Fig. 3.3b. Again the cycle-averaged values are in higher than those measured via the testing with SMPSs as the sizers.

Figure 3.3 confirms that our hypothesis for the previous investigation of BF effect on respirator filter media. Because of relatively long measuring time of SMPS (related to the breathing cycle time), the effect of breathing frequency on the filter penetration was "smoothed" or "averaged" in the previous testing methods with SMPSs as the sizers.

To demonstrate the importance of sampling frequency of aerosol instruments used in the cyclic flow testing methods, we re-tested the filter media A using the new testing method but with the sampling frequency of CPCs set at 1 Hz instead of 10 Hz set in the new testing method. Figure 3.4 shows the comparison of measured peak penetrations of test filter media under two CPC sampling frequencies of 1 and 10 Hz. At the BF of 6 BPM (Fig. 3.4a), the difference in the measured penetrations was negligible at the CPC sampling frequency of 1 and 10 Hz in the case of 9.42 L/min PIFR. As the BF increased to 25 BPM, (Fig. 3.4b), the measured penetrations are close at the PIFR of 9.42 L/min. Significant difference in the particle penetration was observed at the PIFR of 18.14 L/min and breathing frequency of 25 BPM, in which the measured peak penetration was 10.84% and 15.45% at the 1 and 10 Hz CPC sampling frequencies. However, the difference between the penetration values at 1 and 10 Hz was insignificant at 6 BPM. The smoothing of BF effect on the filter penetration was again observed in the new testing method with CPCs set at the low sampling frequency, resulting in lower penetration values at lower sampling frequency. All the following measurements were set at 10 Hz CPC sampling frequency.

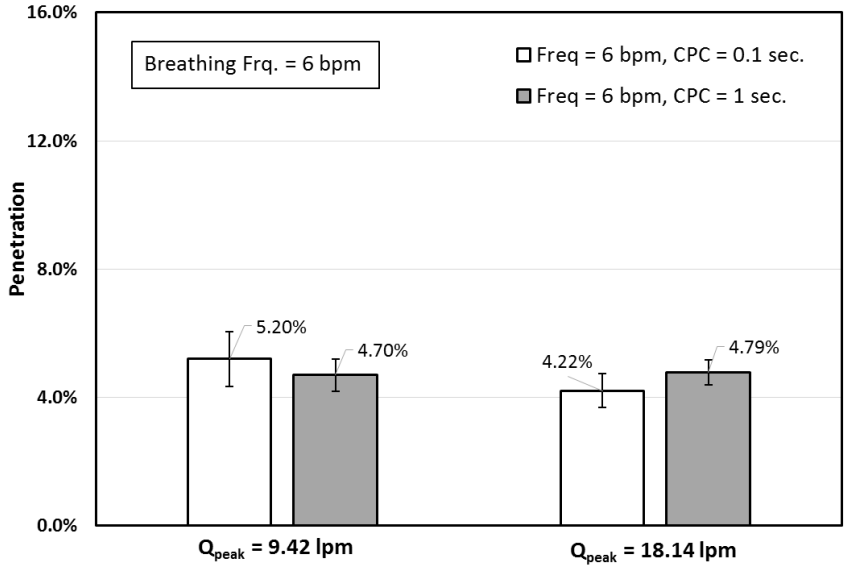

(a) At BF = 6 BPM

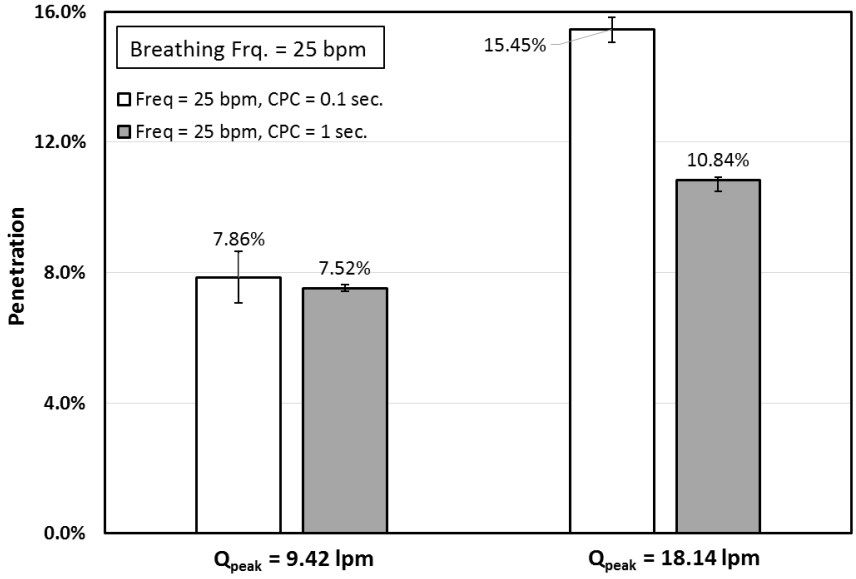

(b) At BF = 25 BPM

Figure 3.4 Comparison of the penetration of filter media A measured via the new testing method having two CPCs with the sampling frequency set at both 1 and 10 Hz. The size of test particles was 150 nm at breathing frequencies of (a) 6 BPM, and (b) 25 BPM

The selection of MPPS in the new testing method is of importance for the worst scenario testing. Figure 3.5 shows the measured peak penetration of the test filter media at the particle size of 300 nm and PIFR of 18.14 L/min. The measured peak penetration values through the test filter media are 2.21% and 3.62% for BF of 6 and 25 BPM, respectively, which are less than those observed at the MPPS of 150 nm.

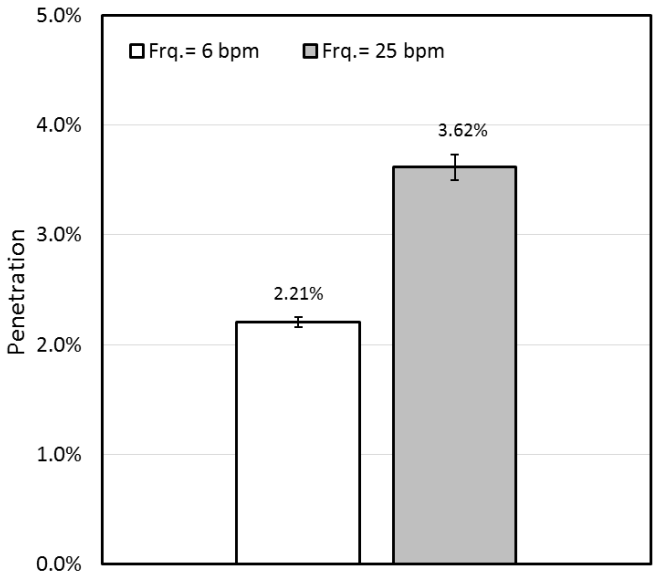

Figure 3.5 Penetration values through test filter media A at the particle size of 300 nm and PIFR of 18.14 L/min

To show the general application of the new testing method we applied it to measure the performance of a HEPA membrane filter B. The basic information of filter medium B is also listed in Table 3-1. Figure 3.6 shows the BF effect of membrane filter penetration at the PIFR of 18.14 L/min. The MPPS of this membrane filter was around 60 nm. The measured peak penetration of test membrane filter was 0.17% and 0.51% at the BFs of 6 and 25,

respectively. A factor of three between the penetration values at the two BFs was again observed via the proposed testing method. The result given above would be difficult to obtain via the testing with SMPSs. It is because of insufficient particles at the downstream of HEPA membrane filters in order to obtain reliable particle size distribution measurement.

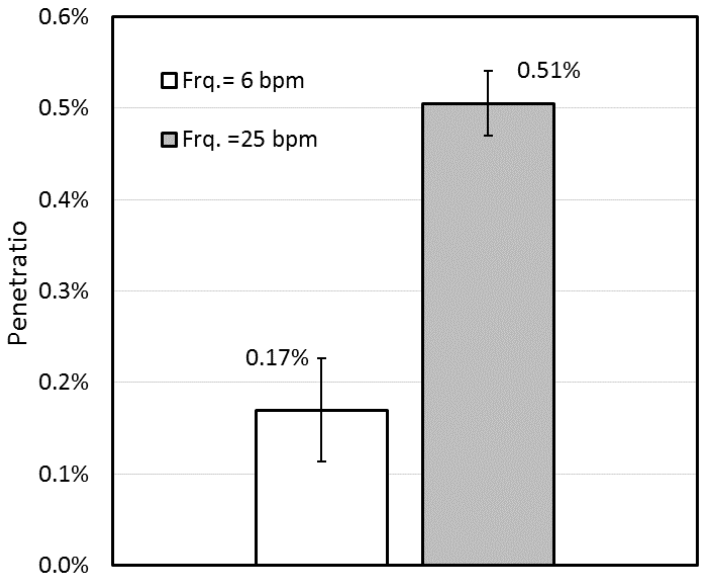

Figure 3.6 Penetration values through HEPA membrane filter at PIFR of 18.14 L/min

3.4 Summary

A new testing method is proposed to study the performance of respirator filter media under cyclic flow condition, which models the flow conditions in real-world applications. Instead of using polydisperse test aerosol, respirator filter media was tested using DMA-classified particles with the size having the maximal penetration, which is evaluated at the equivalent constant flowrate (MIFR; Mean Inhalation Flow Rate). Two CPCs were used in the method to measure the up- and down- stream concentrations of classified particles, from

which the particle penetration could be derived by taking the ratio of the two concentrations. Because of 0.1-second sampling time of CPCs, the new testing method is able to measure close-to-instantaneous particle penetration through respirator filter media. Via the new testing method, the individual effects of BF and PIFR on the performance of respirator filter media can accurately be studied. A pilot study was performed to illustrate the new testing method.

In the study, we measured the penetration of a selected respirator filter media under cyclic flow conditions. Cyclic flows with the sinusoidal wave patterns, simulating an adult human breathing pattern, were applied. Two breathing frequencies, i.e., 6 and 25 BPM and two different peak inhalation flow rates, i.e., 9.42 and 18.14 L/min were chosen. The study was performed under the inhalation-only condition. The above measurements were performed with the new testing method and compared with the results obtained using SMPSs as the particle sizers. Because of relatively long measuring cycle time of SMPS to measure the entire particle size distribution (compared with the breathing cycle time), the smoothing effect of breathing frequency (i.e. lowering the average values) on the peak particle penetration of filters was observed. Different from what reported in the previous work, the effect of BF on the particle penetration of respirator filters was in fact significant.

The importance of the selection of CPC sampling frequency and particle size were also illustrated in this pilot study. In addition, the effect of BF on the filter penetration under cyclic flow conditions was further confirmed when applying the new testing method to a HEPA membrane filter.

CHAPTER 4 Performance Evaluation of Respirator Filter Media under the Simulated Breathing Conditions

4.1 Introduction

Filtering facepiece particulate respirators are commonly utilized for personnel protection in industrial and chemical, radiological, biological and nuclear applications. With the development of technology, novel filter media for respirator have been continuously manufactured in high demand to meet various challenges in the personal particulate matter (PM) protection. It is thus essential to assess the performance of respirator filter media by industry and individual to assure design engineers and users that respirator will deliver promised performance for specific applications under the environmental stress. The National Institute for Occupational Safety and Health (NIOSH), in cooperation with the Mine Safety and Health Administration (MSHA) issued new regulations for certificating particulate respirator filters in 1996. The detailed information of this regulation has been listed in Title 42 *Code of Federal Regulations (CFR)* Part 84, where the particulate respirator filters are tested against a salt or oil charge-neutralized aerosol at a constant flowrate of 85 L/min. The testing aerosol has a mass median diameter (MMD) of 300 nm that is assumed to be the most penetrating particle size (MPPS). This standard testing method is only limited to constant flowrate condition whereas air flow through filters is cyclic due to the nature of human breathing in practical applications. It is thus necessary to evaluate particulate respirator filter under simulated human breathing conditions, i.e., at cyclic flow.

A few studies have already investigated the performance of particulate respirator filters under cyclic flow and compared the performance of respirator filters under constant flow with cyclic flow. One of the pioneer studies was reported by Stafford *et al.* (1973), in which the authors tested the penetration of seven monodisperse polystyrene latex particle (PSL). These PSL particles ranged from 0.176 to 2.02 μm and passing through respirator filter cartridges under three cyclic breathing flow. It was observed that the peak particle penetration through a respirator filter medium were higher under cyclic flow conditions as compared to that under equivalent constant flow conditions. The similar observation was also reported in the work by Brosseau et al. (1990). These studies proved that the performance of respirator was different under steady and unsteady flow conditions that more particles passed through respirator filter at cyclic flow testing, thus it is critical and meaningful to systematically study this effect because of the issue of human health.

A recent work of filter media testing under cyclic flow conditions by Wang *et al.* (2012) measured the penetration of 0.3 μm polystyrene latex (PSL) particles through N95 and P95 cartridges under various cyclic flow. Four waveforms, including two sinusoidal, one trapezoidal, and one exponential cyclic flow patterns, all having an equivalent minute ventilation (minute volume of the cyclic flow), were applied in the study. The results indicated that the highest particle penetration was observed when the filter media was tested under the cyclic flow of exponential pattern which had the highest peak inhalation flowrate (PIFR). The cyclic flow with the trapezoidal-pattern, having the lowest PIFR, resulted in the lowest particle penetration among all the cyclic flow measurement. The particle penetration

with the testing of two sinusoidal-flow patterns, having the same PIFR but different tidal volumes and frequencies, were at the similar level. However, the lowest penetration was obtained from filter media tested at the constant flow condition (with equivalent minute ventilation flow) compared with that under cyclic flow evaluation. Besides, Eshbaugh et al. (2009) and Haruta et al. (2008) reported that the particle penetration of filters was higher under cyclic flow when compared with that under constant flow. The contribution of PIFR on the penetration of respirator was thus identified by these research, but the effect of breathing frequency, the other important parameter, was still unknown on the performance of respirator filter.

Limited effort had been devoted to study individual effect of breathing frequency (BF) and PIFR on the particle penetration of respirator filter media. Mahdavi et al. (2014) proposed a procedure to study the individual contribution of BF and PIFR on the performance of N95 filtering facepiece respirators. The particle penetration of filter media under two PIFRs (i.e., 135 and 360 l/min) and two BFs (i.e., 24 and 42 breaths per minute, BPM) was studied in their work. All measurements were performed by using two different experimental setups: the first setup had inhalations and exhalations through filter media while in the other only inhalation flows was included. The authors observed a huge enhancement of particle penetration through filters by increasing the PIFR from 135 to 360 l/min under the same BF. Only a very small increase in the particle penetration was observed by increasing the BF from 24 to 42 BPM with the same PIFR. It was thus concluded that the PIFR variation had much contribution to the particle penetration of respirator filters and the

effect of breathing frequency on the respirator performance was negligible. In addition, there was nearly no difference of filter performance when the samples were operated under both setups. However, they used a scanning mobility particle sizer (SMPS) to measure particle concentration at the up- and down-stream of filter media. The previous finding of negligible breathing frequency effect on the respirator performance is questionable. It is because the SMPS measurement cycle used in the previous study was 360 sec. Measured particle size distributions was in fact the average of 124 and 252 breathing cycles when the BF were set at 24 and 42 BPMs (breath per minutes), respectively. We thus suspected that the reported observation was due to the testing method and measurement technique. Moreover, the polydisperse aerosol in high concentration was applied to challenge respirators. Test respirators would be quickly loaded up because of high aerosol concentration. It is known that loaded filter media typically have better particle collection than clean filter media. Recently, an advanced testing method was developed by our group to evaluate the performance of respirator filter medium, specifically for studying the individual effect of BFs and PIFRs on the particle penetration through respirator filter medium. This advanced method consists of the use of DMA (Differential Mobility Analyzer)-classified particles with maximum penetration particle size (MPPS). Instead of SMPS, two condensation particle counters (CPCs) were utilized to measure the particle concentrations at the upstream and downstream of test filter media at the same time. CPCs sampling frequency with 10Hz was used that close-to-instantaneous particle penetration could be determined. This new testing method was utilized to systematically investigate the effect and contribution of breathing

frequency and peak inhalation flowrate on the performance of various respirator filter media in this study.

The objectives of this study are thus: (1) to study the individual effect of breathing frequency and peak inhalation flowrate on the penetration of respirator filter medium with new method; (2) to evaluate the performance of various respirator filter medium (5 types) under simulated human breathing conditions; (3) to develop a semi-theoretical numerical model to quantitatively analyze and predict the effect of cyclic flow on the performance of respirator filter medium.

4.2 Experimental Setup and Design

4.2.1 Experimental Setup

The experimental setup that was recently developed and introduced by our group was again utilized in this study. A custom-made Collison Atomizer was used to generate polydisperse aerosol by atomizing sodium chloride (NaCl) solutions with concentration of 0.1% by volume. Polydisperse solid aerosol were obtained by passing polydisperse droplets through a diffusion-type dryer with silica gel as the desiccant. Polydisperse solid aerosol were then introduced into a Kr^{85} bipolar aerosol charger and a differential mobility analyzer (DMA TSI model 3081) was used to classify particles based on their electrical mobility. Aerosol and sheath flowrates of the DMA were set at 1.0 and 10.0 LPM, respectively. After the DMA electrical charges on DMA-classified particles were neutralized by delivering classified particles stream through a 10 mCi Kr-85 neutralizer (TSI Model 3012). It is

because depending on the extent of electrical charge on particles the particle penetration though filter media could be affected.

An elbow mixing chamber, in which a constant particle-free flow of 0.9 l/min was injected additionally to mix with classified aerosol flow during the cyclic flow process, was placed in front of filter testing section in order to provide adequate flow for the CPC measurement. The 0.9 L/min flow was supplied and controlled by a mass flow controller (MKS Type 1179A). In the testing section, filter media was placed in a filter holder (Pall Model 2220) with 47 mm OD. The effective test filtration area for media is 15.3 cm^2 with this filter holder. Differential pressure transmitter (OMEGA PX-655) was included to monitor and record the pressure drop across filter media. Two identical sampling ports were located in the up- and down- streams of the filter holder for particle sampling and measuring. Condensation particle counter (CPC; TSI Model 3775) and water-based CPC (TSI Model 3787) were utilized to measure the up- and down- stream concentrations of test aerosol, respectively. Both CPCs have a sharp response time of 0.1 sec. (i.e., 10 Hz) for measuring particle concentration. Particle penetration of filter media was calculated by taking the ratio of downstream concentration to the upstream. In this study, the data were collected for 4 minutes in each test once the cyclic flow in the setup reached reproducible periodical status. Due to particle loss in the filter holder and two CPC models used in the setup, a calibration experiment was performed to correlate the readings of two CPCs and find the baseline penetration values before each filter test. No filter media was in the holder during the

calibration experiment. Additionally, the background CPC readings were also checked to ensure zero reading before each run.

Table 4-2. Summary of tested sinusoidal cyclic flow conditions

Cyclic Flow Types	Breathing Frequency (breath/min)	Peak Inhalation Flow at test area of 15.3 cm^2 (L/min)	Peak Inhalation Flow at test area of 135 cm^2 (L/min)	Tidal Volume (liter/breath)	Peak Face Velocity (cm/s)	Mean Inhalation Flowrate at test area of 15.3 cm^2 (L/min)
1	6	9.42	82.94	0.5	10.24	6
2	12			0.25		
3	25			0.12		
4	6	13.57	119.43	0.72	14.74	8.64
5	12			0.36		
6	25			0.17		
7	6	18.14	159.97	0.96	19.70	11.55
8	12			0.48		
9	25			0.23		

*The face velocity for testing a typical N95 respirator having the surface area of 135 cm^2 (at the defined 85 L/min flowrate) is ~ 10.6 cm/sec.

The cyclic flow was generated by a human breathing simulator (Model ASL5000, IngMar Medical, PA, US). The reason to use human breathing simulator was because of five types of tested filter medium belonging to respirator filter medium. Two one-way valves (Model BE 130-22B, Instrumentation Industries, Inc., US) were placed at the inlet of the breathing simulator for inhalation only testing. Prior to each testing, test flow condition was further verified by a mass flow meter (TSI Model 4143). The details of cyclic sinusoidal flow patterns used in testing filter media are given in Table 4-2.

With the consideration of worse scenario testing, particles at the maximal penetration size (i.e., MPPS under constant flow condition) were selected to challenge filter media. The MPPS of test filter media under constant flow condition was measured prior to cyclic flow testing. For four out of five filter media, the measured MPPS was approximately 100 nm under the face velocity of 10 cm/s. The MPPS was 150 nm only for one of the filter media (type-3 with details given in Table 4-1).

Table 4-1. Basic properties of respirator filter media used in this study. Filter medium 1, 2, and 3 belong to single-layer fibrous media. Filter media 4 and 5 are composite media

Filter Media	Media Type	Basic Weight [g/m^2]	Pressure Drop at Flowrate of 1 L/min [inH_2O]	Thickness [mm]	Permeability [m^2]
1	Fibrous	80.27	0.090	0.63	5.02E-12
2	Fibrous (charged)	56.44	0.015	0.94	5.51E-11
3	Fibrous	79.61	0.115	0.84	5.51E-12
4	Fibrous (Composite)	86.46	0.035	0.93	1.80E-11
5	Fibrous (Composite)	78.39	0.030	0.94	2.32E-11

4.2.2 Experimental Matrix

Five different types of respirator filter media were selected for this study. Two of them, types 1 and 3, properties given in Table 1, are classified as single-layer fibrous respirator filter media. Type-2 belongs to charged fibrous filter media. The other two types

of respirator filter media, types-4 and -5, are two composite filters. The basic properties of these test respirator filter media are given in Table 4-1. Three filter samples, identical in dimensions, were randomly cut from batch filter media sheets and evaluated for each cyclic flow condition.

Cyclic flow with the sinusoidal wave pattern was selected in this study, and only inhalation flow was considered. Three breathing frequencies (BFs) of 6, 12 and 25 breaths/min (BPM) and three peak inhalation flow rates (PIFRs) of 9.42, 13.6 and 18.14 L/min were chosen as the flow testing conditions. Table 4-2 summarizes the parameters for the nine groups of cyclic flows applied in this study, and the diagram of the sinusoidal cyclic flow is shown in Figure 4.1. Three sets of data replicates, taken at different days, were considered for each test condition.

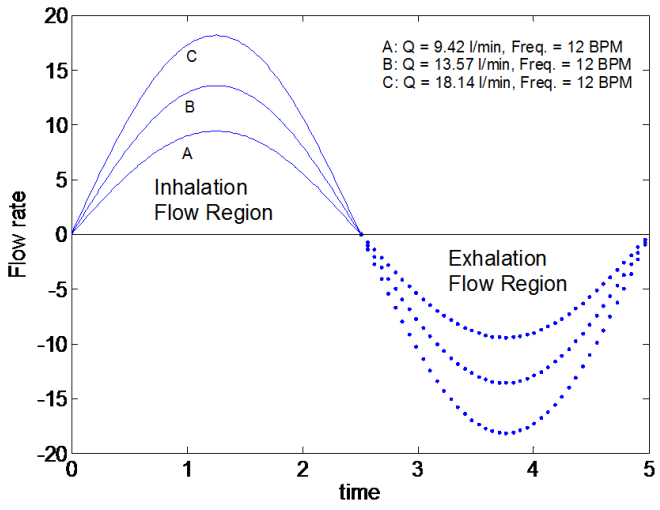

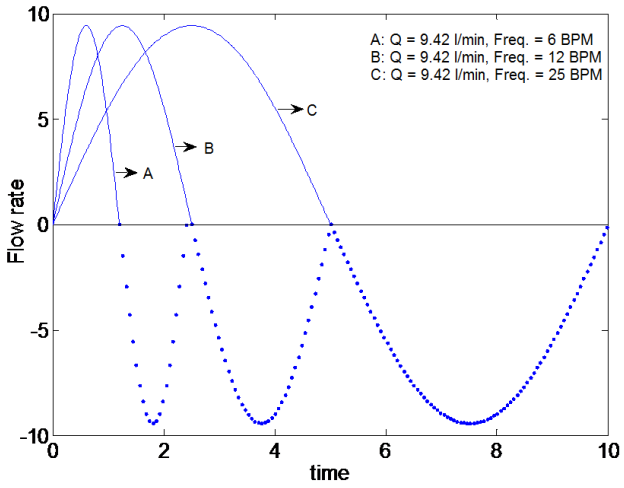

Figure 4.1 Diagram of sinusoidal wave pattern used in this study

The reasons for selecting cyclic flow testing conditions are to match the NIOSH standard flow testing condition and breathing patterns of adult human beings. The relationship among the flow rate, face velocity and effective area could be expressed as *Flow rate = Face Velocity* × *Effective Area*. Despite the use of filter holder with effective testing area of 15.3 cm^2 in our study, we matched the face velocity in our study with that defined in the NIOSH standard testing for N95 mask, in which the testing area of respirator is approximately 135 cm^2 at the constant flow rate of 85 L/min, resulting in the face velocity of 10.6 cm/s. To match the face velocity defined by NIOSH, test flow rate in our study was scaled down because of the smaller filter area used herein, but still the test flow rate was a reasonable inhalation flow expected with human beings. The PIFR of 9.42 L/min was selected resulting in equivalent testing condition to the NIOSH standard test in terms of face velocity. We also selected two higher PIFR, i.e., 13.6 and 18.14 L/min, to investigate the PIFR effect on the particle penetration of test filter medium. To test the effect of cyclic flow

frequency on the performance of filter medium, BFs were chosen as 6, 12 and 25 BPM. This selection was based on the earliest data available on spontaneous breathing frequency of human beings, Quetelet (1842) on 300 subjects and Hutchinson (1850) on 1714 adult subjects. The very wide BF ranging from 6 to 31 breaths per minute were observed in adults, and these data appear to be the most extensive data published so far.

4.3 Results and Discussion

4.3.1 Effect of Breathing Frequency

Figure 4.2 shows the comparison of peak penetration through filter medium type-1, measured with our developed testing method under the selected cyclic flow conditions and constant flow condition at mean inhalation flow rate, MIFR, which is 2 times tidal volume times breathing frequency. The maximum penetration data given here are the average of peak penetration measured from multiple cycles. It is observed from the figure that the peak penetration for filter medium type-1 is the minimum value under constant flow with MIFR in each PIFR group of 9.42, 13.6 and 18.14 L/min compared to the cyclic flow patterns. When PIFR is 9.42 L/min, the smallest peak penetration is 8.68% at constant MIFR flow, and the peak penetration values are 13.04%, 17.22% and 20.42% for BF of 6, 12 and 25 BPM, respectively, meaning penetration increases with increasing breathing frequency. The same observation could be made with the other two peak inhalation flowrates: PIFR equal to 13.6 L/min and 18.14 L/min.

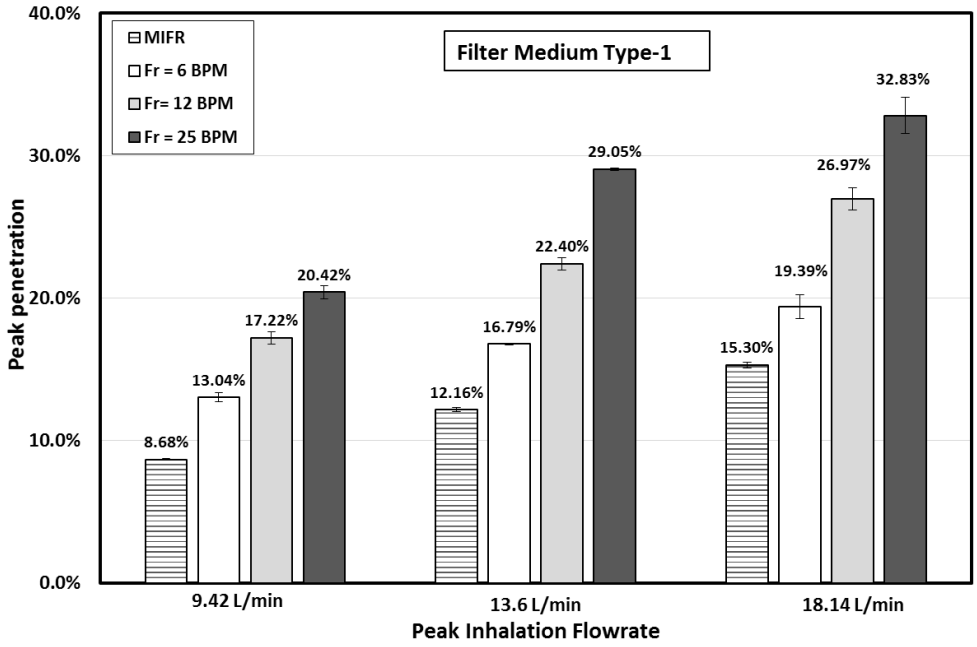

Figure 4.2 Comparison of the peak penetration of filter medium type-1 with different breathing frequencies under three different peak inhalation flowrates (PIFRs)

In order to understand the contribution of breathing frequency to the peak penetration of respirator filter medium type-1, the relationship between peak penetration ratio and breathing frequency is given in Figure 4.3. The peak penetration ratio has been defined as the ratio of peak penetration under cyclic flow with different breathing frequency to the penetration value under constant flow with equivalent corresponding MIFR, which could be considered as the reference penetration value for each group of PIFRs. The value of penetration ratio is one, if no cyclic flow is applied; thus, the effect of cyclic flow and breathing frequency could be identified by the peak penetration ratio, illustrated in Figure 4.3. For PIFR of 9.42 L/min, the value of ratio is 1.4 at BF of 6 BPM, and it increases to 1.9 as BF increases to12 BPM and keeps increasing to 2.2 as BF reaches 25 BPM. Almost 60%

increase in penetration ratio is obtained as BF increases from 6 to 25 BPM. For PIFR of 13.6 and 18.14 L/min, similar conclusion could be made from the plot.

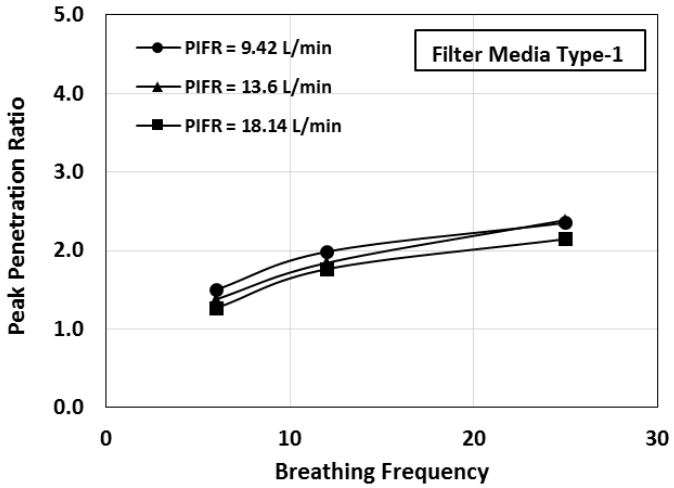

Figure 4.3 The ratio of peak penetration with each cyclic flow condition to constant flow at MIFR vs breathing frequency for filter media type-1

For respirator filter medium type-3, which is another single-layer fibrous filter, Figure 4.4 gives the particle peak penetration values under different breathing frequencies and peak inhalation flow rate conditions. The peak penetration values under equivalent constant flow rate MIFR are 3.35%, 4.42% and 5.28% for PIFR of 9.42, 13.6 and 18.14 L/min, respectively, and are lowest for each group of PIFRs compared to the penetration values obtained with cyclic patterns. The trend is clear as for the filter media type-1 in the way that the peak penetration is increasing as the breathing frequency increases for all PIFR cases. Additionally, to assess the effect of breathing frequency on filter penetration, Figure 4.5 has been plotted to illustrate the contribution of breathing frequency to penetration. The

peak penetration ratio is increased to 2.7 at BF of 25 BPM from 1.5 at BF of 6 BPM. Therefore, the breathing frequency of cyclic flow directly affects the peak penetration ratio.

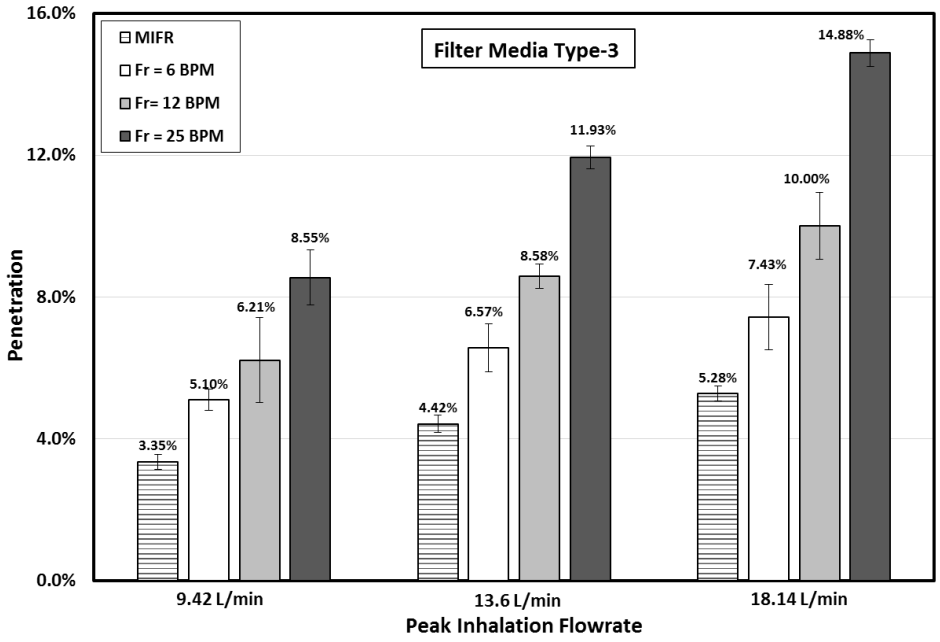

Figure 4.4 Comparison of the peak penetration of filter media type-3 with different breathing frequencies under three different peak inhalation flowrate conditions

The similar effect of breathing frequency on peak particle penetration was also confirmed for other respirator filter media in this study, listed in Table 1. However, the difference does exist among respirator filter media with different structures. The detailed discussion on the effect of filter structure is given in the following section.

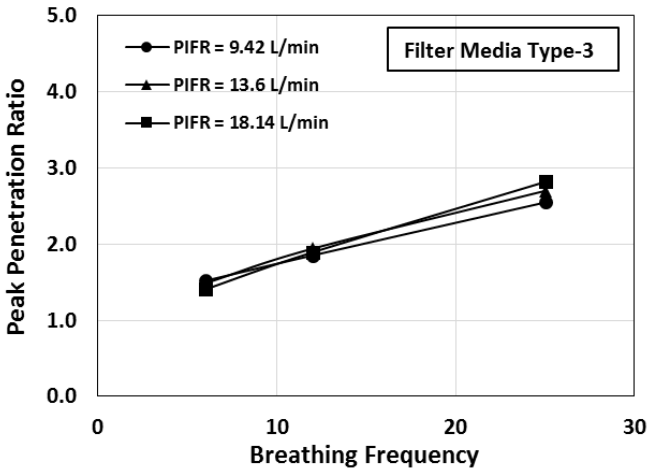

Figure 4.5 The ratio of peak penetration with each cyclic flow condition to constant flow at MIFR vs breathing frequency for filter media type-3

4.3.2 Effect of Peak Inhalation Flow Rate

From Figure 4.2, the peak penetration values measured with respirator filter media type-1 are 8.68%, 12.16% and 15.3% for PIFR of 9.42, 13.6 and 18.14 L/min, respectively, under constant flow of MIFRs. For cyclic flow at breathing frequencies of 6, 12 and 25 BPM, the peak penetration is also increasing with increasing PIFRs from 9.42 to 18.14 L/min. It thus can be concluded that higher PIFR values result in more penetration. Figure 4.6 (a) shows the relationship between peak penetration ratios and PIFR, where the y-axis is the ratio of peak penetration under cyclic flow to the penetration at corresponding constant flow MIFR. It is observed from the Figure 4.6 (a) that the values of ratios remain nearly constant for different PIFRs and BF of 6, 12 and 25 BPM. For filter medium type-3, Figure 4.6 (b) shows that the peak penetration increases by increasing PIFRs at 25 BPM, but this ratio doesn't change noticeably due to variation of PIFR at the other two breathing frequencies of

6 and 12. Thus, it can be concluded that the PIFRs have negligible effect on the peak penetration ratio. This conclusion was also applicable to the other types of respirator filter media tested in the study (Table 4-1).

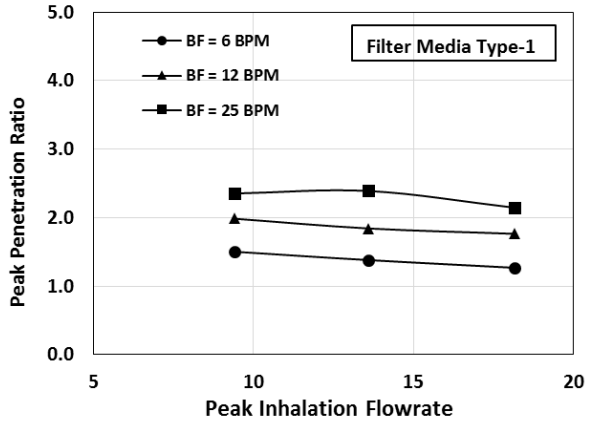

(a) Media type-1

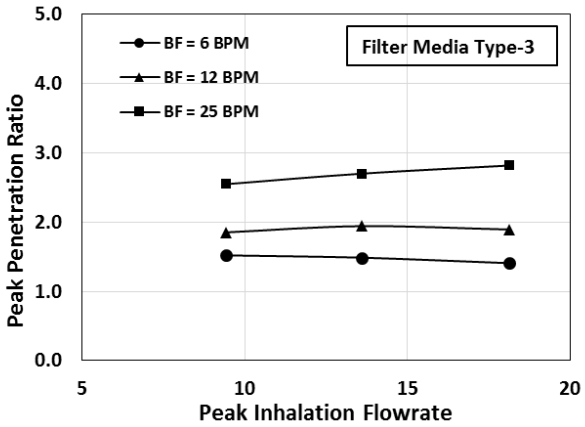

(b) Media type-3

Figure 4.6 Peak penetration ratio vs peak inhalation flowrate for filter media (a) type-1 (b) type-3

4.3.3 Effect of Filter Medium

Five types of respirator filter media were tested in this study to investigate their performance under cyclic flow similar to human breathing conditions. Respirator filter media type-1 and type-3, both belong to single-layer fibrous media, have already been discussed in previous section on the performance with cyclic flow. In this section, the investigation is focused on the other types of respirator media. Media type-2 is a charged single-layer fibrous medium, which has primarily been used in face masks. The comparison of peak penetration plot for type-2 is consistent with the results for type-1 and -3 filter media. The values of peak penetration under MIFR are the lowest for each PIFR group of 9.42, 13.6 and 18.14 L/min, respectively; the breathing frequency enhances the peak penetration under cyclic flow condition. The plot for comparison of peak penetration are included in the appendix. Figure 4.7(a) shows the peak penetration ratio vs breathing frequency for filter media type-2. It is found that all three data points at PIFR of 9.42, 13.6 and 18.14 L/min almost overlap with each other at BF of 6, 12, 25 BPM, and it indicates that the PIFR has minor effect on the penetration ratio of charge media type-2. The ratio increases to 2.5 at BF of 25 BPM from 1.5 at BF of 6 BPM, which is a trend similar to what has been observed with media type-1 and 3. Thus, for media type-2 with electrical charge, we get the consistent conclusion that there is a direct relation between breathing frequency and the peak penetration ratio.

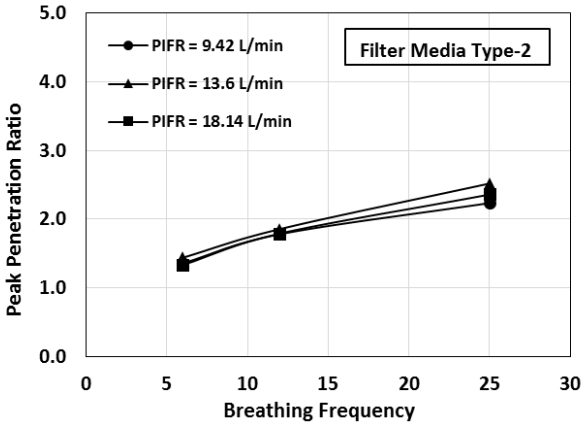

(a) Media type-2

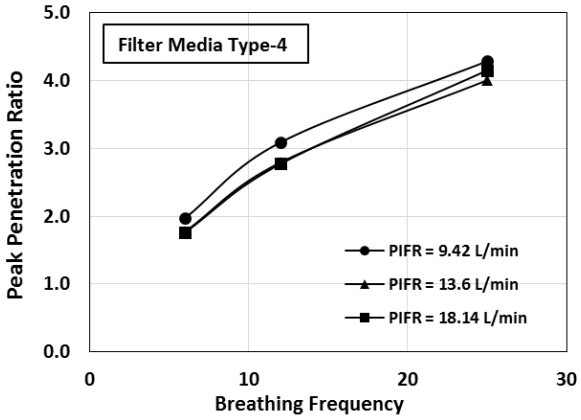

(b) Media type-4

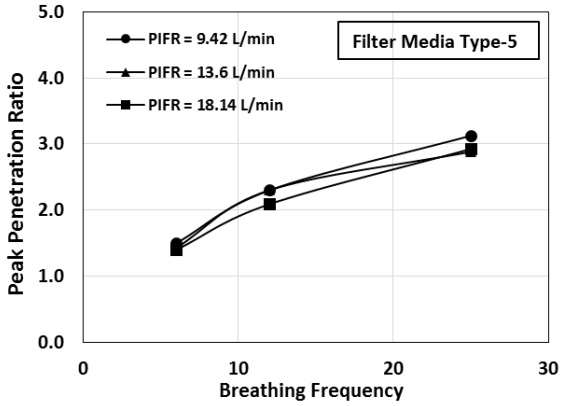

(c) Media type-5

Figure 4.7 Peak penetration ratio to breathing frequency of filter media (a) type-2 (b) type-4 (c) type-5

Respirator filter media type-4 and 5 are classified as composite media, since both have multiple layers. The figures showing the peak penetration under MIFR and cyclic flow at three breathing frequencies are included in the appendix. The trends mentioned above hold true for these types of filter media as well. Figures 4.7 (b) and (c) show the relationship between the peak penetration ratio and the breathing frequency for types 4 and 5 filter media, and it is noticed that the values are different from other previously-discussed cases. In Figure 4.7 (b), the ratio is about 2.0 at BF of 6 BPM for media type-4, and the ratio is 4.2 at BF of 25 BPM, which are much higher values than the other cases, presented above. At each BF, all three PIFR data points slightly differ from each other. For media type-5 in Figure 4.7 (c), the peak penetration ratio is 3.0 at BF of 25 BPM. It is thus concluded that the effect of breathing frequency is more obvious with composite filter media compared to single-layer filters with and without charge. The increase in the peak penetration ratio with breathing frequency is more pronounced with the use of cyclic flow patterns with composite filter media. The reason is mostly due to the structure of respirator filter media.

4.4 Modeling of Particle Penetration at MIFR

As discussed above, the effect of breathing frequency and peak inhalation flow rate are observed and confirmed on peak particle penetration of respirator filter media under cyclic flow conditions. It would be interesting and meaningful to predict the peak penetration under various BFs with a numerical model. Thus, a semi-theoretical model was developed based on previous discussion to calculate the peak penetration at cyclic flow as follows.

4.4.1 Modeling of Particle Penetration at MIFR

Single-fiber theory has widely been used to predict the collection efficiency of particles for an individual fiber under constant flow since last century. Equation (4.1) shows the penetration of filter media relating the macroscopic properties of filter to the microscopic properties of single-fiber and its efficiency, E_{Σ}, where $\alpha, t,$ and d_f are solidity, thickness and fiber diameter, respectively. The key to obtain the penetration, *P*, is determining the value of E_{Σ} (the single fiber efficiency). The overall efficiency of a filter, E, is a function of this single fiber efficiency, E_{Σ} :

$$\boldsymbol{P = 1 - E = e^{-rt} = \exp\left(\frac{-4\alpha E_{\Sigma} t}{\pi d_f}\right)} \qquad \textbf{(4.1)}$$

The overall particle collection efficiency of an individual fiber is the sum of collection efficiency of different mechanisms. Equation (4.2) is a general expression for total collection efficiency of a fiber, where $\boldsymbol{E_R, E_I, E_D, E_{DR}}$ are collection efficiencies for interception, impaction, diffusion and interception mechanisms. Thus, it is key to determine the collection efficiency due to each mechanism. These filtration mechanisms have been discussed in details by Hinds (1999) and Davies (1973)

$$\boldsymbol{E_{\Sigma} = E_R + E_I + E_D + E_{DR}} \qquad \textbf{(4.2)}$$

The single-fiber efficiency for interception $\boldsymbol{E_R}$ is given by Lee and Ramamurthi (1993) as Equation (4.3),

$$E_R = \frac{(1-\alpha)R^2}{K_u(1+R)} \quad (4.3)$$

where $R = \frac{d_p}{d_f}$ (ratio of particle diameter to filter diameter) is a dimensionless parameter, *Ku* is the Kuwabara hydrodynamics factor, another dimensionless factor compensating for the effect of distortion of the flow field around a fiber due to its proximity to other fibers. *Ku* only depends on the solidity, α, (i.e., 1-porosity)

$$K_u = -\frac{1}{2}ln\alpha - \frac{3}{4} + \alpha - \frac{1}{4}\alpha^2 \quad (4.4)$$

The single-fiber efficiency for impaction E_I is given by Davies (1973) as Equation (4.5),

$$E_I = \frac{Stk}{4K_u^2} \quad (4.5)$$

where Stk is the Stokes number, and the expression of Stk is as Equation (4.6), in which ρ_p, C_c, U_0, η are particle density, Cunningham correction factor, face velocity and air viscosity, respectively. The expression for Cunningham correction factor is Equation (4.7) when $d_p < 1$ μm and Equation (4.8) when $d_p < 0.1$ μm.

$$Stk = \frac{\rho_p d_p^2 C_c U_0}{18\eta d_f} \quad (4.6)$$

$$C_c = 1 + \frac{2.52\lambda}{d} \quad (4.7)$$

$$C_c = 1 + \frac{\lambda}{d_p}(2.34 + 1.05\exp(-0.39\frac{\lambda}{d_p})) \quad (4.8)$$

The single-fiber efficiency due to diffusion $\boldsymbol{E_D}$ is a function of dimensionless Peclet number $\boldsymbol{Pe}$, given by Stechkina and Fuchs (1966) as Equation (4.9) which is based on experimental measurements of filter efficiencies,

$$\boldsymbol{E_D = \left(\frac{1-\alpha}{Ku}\right)^{\frac{1}{3}} Pe^{-\frac{2}{3}}, \qquad Pe = \frac{d_f U_0}{D}} \qquad \textbf{(4.9)}$$

Another term to account for collection due to interception of the particles is often included as Equation (4.10), given by Hinds (1999).

$$\boldsymbol{E_{DR} = \frac{1.24R^{2/3}}{(KuPe)^{1/2}}} \qquad \textbf{(4.10)}$$

The total collection efficiency of respirator filter could be calculated based on the single-fiber theory and measured properties of filter medium from experiments in our study. Respirator filter media type-1 and type-3 were chosen here to calculate the penetration from theory, and then the predicted theoretical penetration curves were compared with experimental data as shown in Figure 4.8. It is clear that the experimental and the theoretical values are in good agreement with each other at different flow rates.

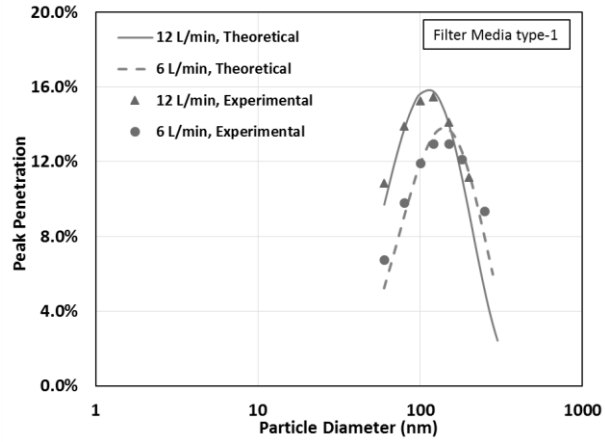

(a) Filter media type-1

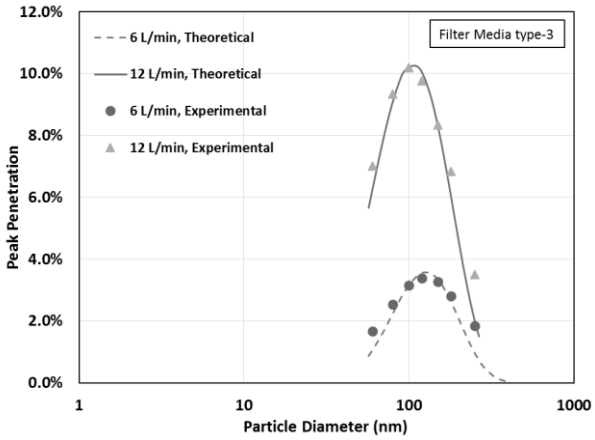

(b) Filter media type-3

Figure 4.8 Comparison of penetration calculated with single-fiber theory with experimental measurements for (a) Filter media type-1 (b) Filter media type-3

4.4.2 Fitting Function of the Peak Particle Penetration Ratio

For filter media type-1, one curve as a peak penetration ratio function of breathing frequency was selected to fit all the data of peak penetration ratio previously given in Figure

4.3. Figure 4.9 (a) shows the plot of this fitting curve function for peak penetration ratio, and the best fitting function was determined as Equation (4.11)

$$f(BF)_1 = 2.5872(1 - exp^{-0.0316BF}) + 1 \qquad \textbf{(4.11)}$$

For filter media type-3, another curve was chosen to fit the data in Figure 5 as a peak penetration ratio function of breathing frequency. Again, Figure 4.9 (b) gives the plot of fitting curve for those peak penetration ratio, and the best fitting function was also found as Equation (4.12),

$$f(BF)_2 = 3.9699(1 - exp^{-0.0224BF}) + 1 \qquad \textbf{(4.12)}$$

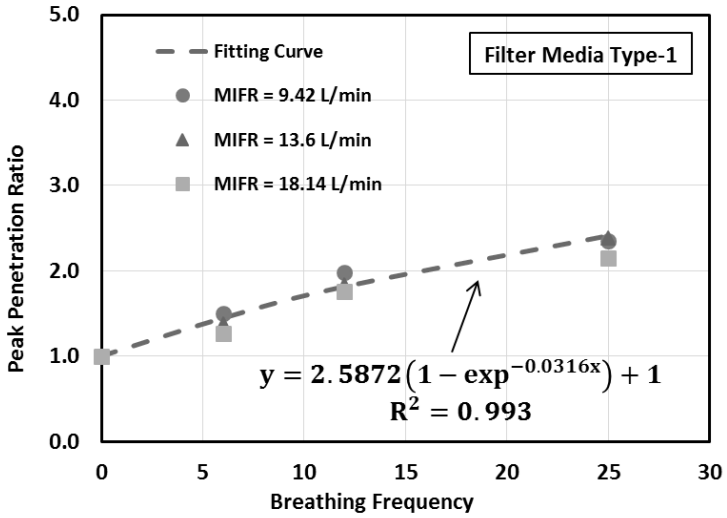

(a) Filter media type-1

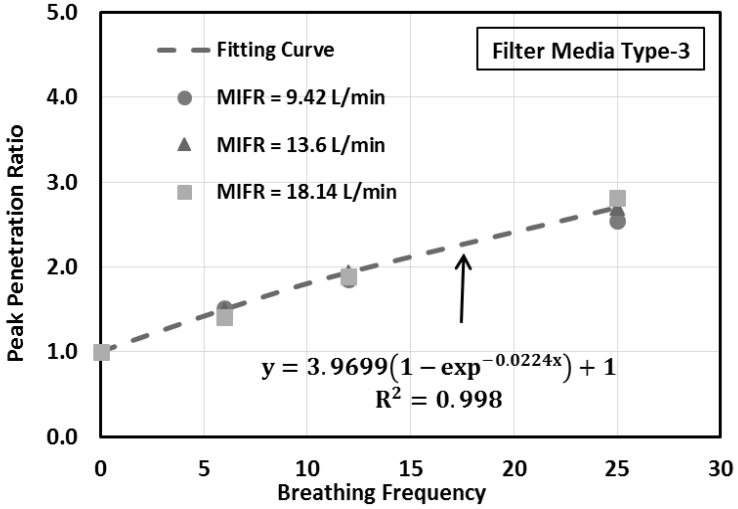

(b) Filter media type-3

Figure 4.9 Comparison of peak penetration ratio between semi-theoretical model and experimental for (a) Filter media type-1 (b) Filter media type-3

4.4.3 Semi-theoretical Modeling for Peak Particle Penetration at Various BFs

It is hypothesized that the peak particle penetration under cyclic flow at various BFs could be predicted as the product of penetration calculated by single-fiber theory under MIFR (discussed in section 4.1) and the ratio of peak penetration (discussed in section 4.2), the expression of which is shown in Equation (4.13). This semi-theoretical model for predicting peak penetration at various BFs thus consists of two parts: one is the experimental fitting ratio of peak penetration (section 4.2), the other part is theoretical penetration of single-fiber theory (section 4.1).

$$P = f(BF) \times \exp\left(\frac{-4\alpha E_{\Sigma} t}{\pi d_f}\right) \qquad (4.13)$$

To assess our hypothesis and proposed semi-theoretical model for predicting the peak penetration of respirator filter media at various BFs, media type-1 and 3 were selected for this model validation. In Figures 4.10 (a) and (b) the dashed lines are standing for the peak penetration from developed semi-theoretical model under cyclic flow conditions, while single symbols are for measured actual experimental data. As observed from both Figures 4.10 (a) and (b), the lines of semi-theoretical predicted peak penetration match with the peak penetration values measured experimentally at cyclic flow with various BFs and PIFRs. Thus, this proposed semi-theoretical model is verified and could be used to predict the particle peak penetration under cyclic flow conditions for various single layer fibrous filter media.

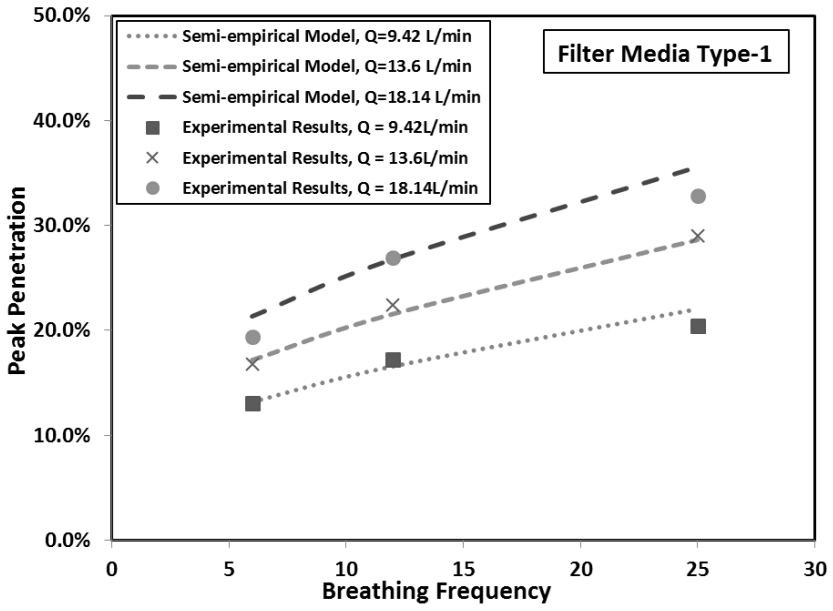

(a) Media type-1

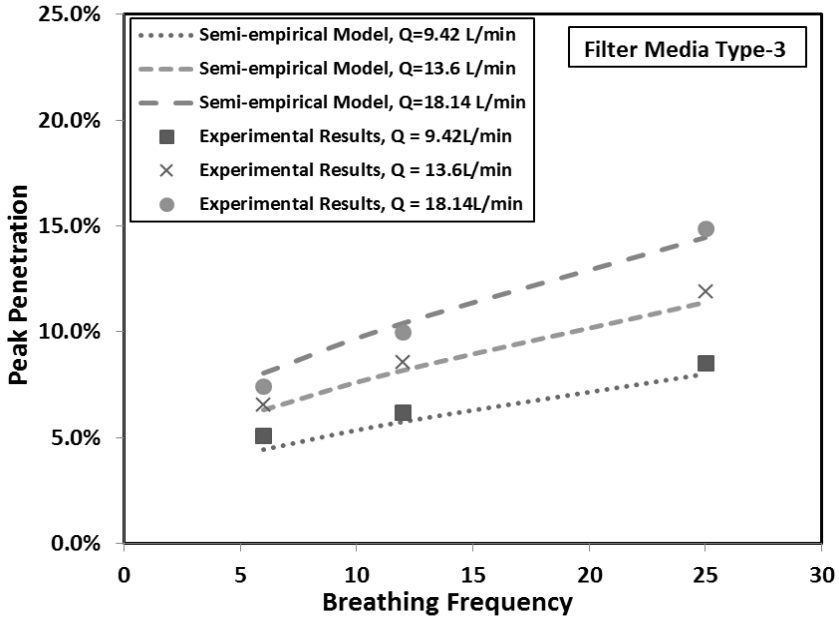

(b) Media type-3

Figure 4.10 Comparison between semi-theoretical modeling and experimental results for (a) media type-1 (b) media type-3

4.5 Summary

The performance of different types of respirator filter media, including two single-layer fibrous media, one charged fibrous media and two composite media, have been investigated with an advanced testing method under the worse scenario in this study, by testing the filter media with the most penetrating particle size. Two CPCs were used in the method to measure the up- and down- stream classified particle concentrations simultaneously during the experiments. Due to 0.1-sec. sampling time of CPCs, it was possible to measure close-to-instantaneous particle concentration through filter media. These tests were operated under cyclic flow with sinusoidal pattern flow, but only inhalation part

was considered. With the advanced method, the individual effect of BF and PIFR on the performance of respirator filter media could be accurately studied.

In the study, we measured the penetration of five respirator filter media under cyclic flow conditions. Cyclic flow with sinusoidal wave patterns which simulates human breathing patterns were applied and only inhalation was considered in the experiments. Three breathing frequencies, i.e., 6, 12 and 25 BPM and three different peak inhalation flow rates i.e., 9.42, 13.6 and 18.14 L/min were selected. The penetration of respirator filter media were also tested under constant flow condition, i.e., equivalent mean inhalation flow rate (MIFR) for each peak inhalation flow rate (PIFR) conditions. Peak penetration was determined and compared for each cases. The effect of BF and PIFR were confirmed that the peak penetration increases by increasing of BF or PIFR. Peak penetration ratio, defined as the ratio of peak penetration and the penetration from corresponding MIFR, was also discussed. It is concluded that the peak penetration ratio increases as BF increases, while the value do not significantly change at various PIFRs within the conditions considered in this study.

Furthermore, a semi-theoretical model was developed to predict the peak penetration of respirator filter media under cyclic flow with various BFs. It consists of two parts: one is the fitting function of peak penetration ratio, and the other is the penetration calculated by single-fiber theory. Two sample examples were given to assess the proposed model. Because the peak penetration of the semi-theoretical model are matching the results of the experimental, this semi-theoretical model was confirmed and verified. Therefore, the semi-

theoretical numerical model could be used to predict the peak penetration of respirator filter media under cyclic flow conditions.

CHAPTER 5 Effect of Dust Loading Rate on the Loading Characteristics of High Efficiency Media

5.1 Introduction

Filtration systems have been used in many industrial sectors such as chemical, nuclear, food, mineral processing industries. Examples of filtration applications include the cleaning of the particulate in exhausts of smelters and coal-fired power plants, the processing of nuclear and hazardous materials, the air purification for semiconductor manufacturing cleanrooms, the respiratory protection and the recovery of powder material. Filter media are the essential component of any filtration systems. The primary parameters to characterize the performance of filter media are the pressure drop and filtration efficiency of filter media. In general, the pressure drop across filter media increases when they are loaded with particles while the particle collection efficiency of loaded filter media improves. The increase of filter pressure drop under the loading condition is attributed to the particle deposition in the media and the dust accumulation on the filter front surface. Understanding the factors affecting the filter pressure drop, eventually being able to estimate the filter pressure drop under the particle loading condition, is of importance in determining the lifetime of filter media being applied.

The particle loading process of fibrous filter media generally precedes through three different phases: After the initial particle collection, the performance of filter media is in the depth filtration regime in which particles are collected inside the media. During the depth filtration regime the filter pressure drop gradually increases as particles continue to be

collected. Filter media are then in the so-called transitional regime when a significant percentage of void space in filter media is occupied with particles. The filter pressure drop in transitional regime increases faster as compared to that in the depth filtration. In the last phase of filter media performance, particles are collected on the filter surface (i.e., surface filtration), where the particle cake starts to establish and buildup on the filter surface. The filter pressure drop increases dramatically when they are in the surface filtration regime. For high efficiency filter media, the performance of filter media will stay in the first two phases for only a short period of time and quickly move to the surface filtration regime.

Filtration research has been focused on the investigation of filter media performance under various operational and environmental conditions, such as filtration face velocity, particle types, relative humidity and temperature, and so on. However, the effect of particle loading rate on filter loading performance curve had never been systematically investigated in the literature. The only work relevant to the above subject was reported by Saleem and Krammer (2007). In the above study, the authors considered the factors of face velocity and dust concentration on the formation of dust cake layers in a pilot-scale jet-pulsed bag-house filter system. Three levels of particle mass concentration (i.e., 7.32, 4.81 and 4.53 g/m^3) were tested. They found that the cake density and resistance were higher at lower dust concentration and the filtration velocity had more effect on the filter pressure drop and cake property (i.e., cake density and specific cake resistance) as compared to the dust concentration effect. The tested range of dust concentration was however limited.

5.2 Experimental Setup and Design

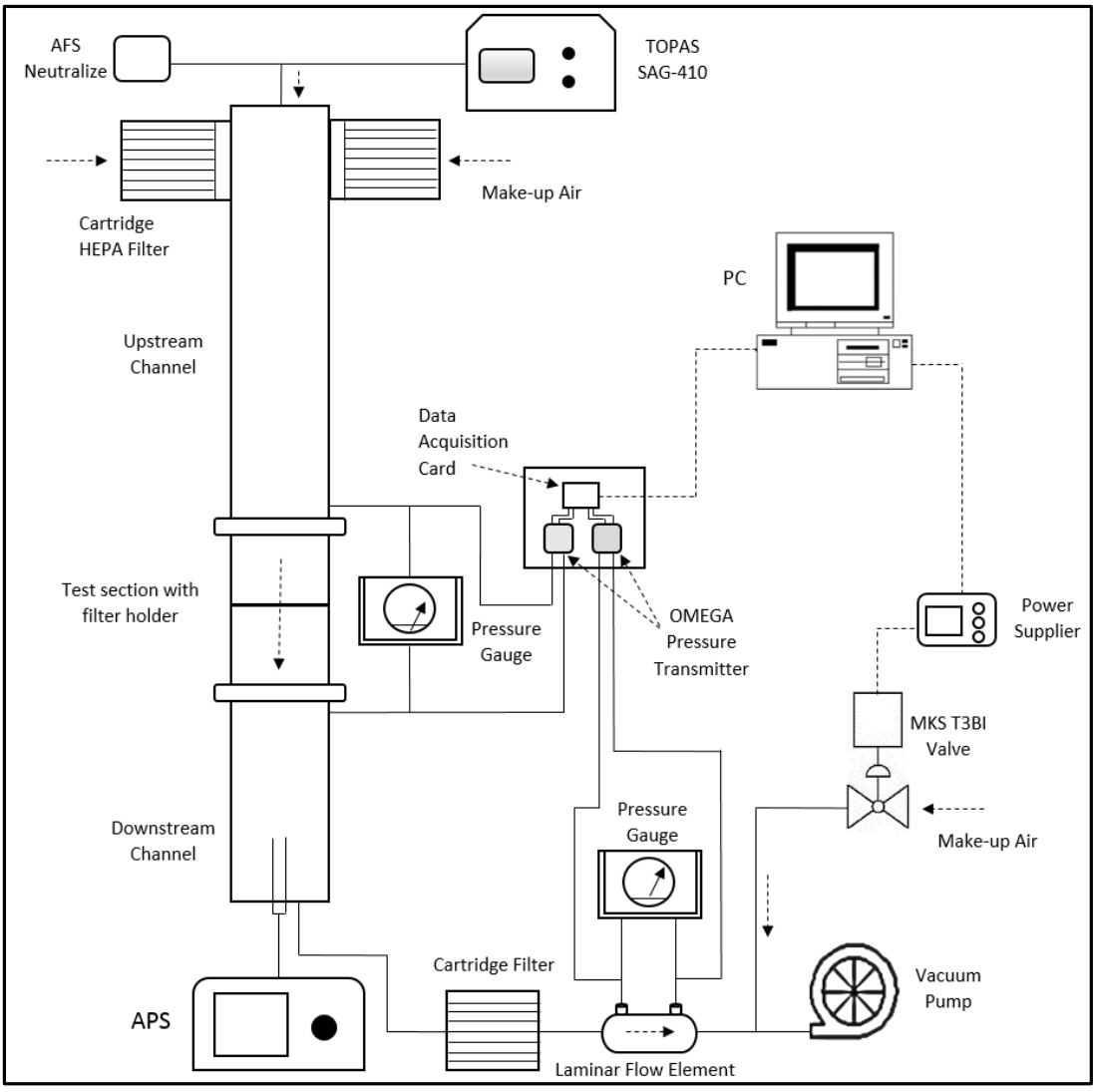

Figure 5.1 Schematic diagram of the filter testing setup used in this study

The schematic diagram of our experimental setup for this study is shown in Fig. 5.1. The setup consists of upper flow channel, test section and lower flow channel. Dry test powders were airborne as test aerosol by a dust disperser (TOPAS SAG-410), and injected

into the upper flow channel from the top. Prior to the aerosol injection the electrical charge level of airborne particles was reduced by mixing the stream with bipolar ion flow (from an AC corona discharger with airflow controller AFC; Simco-Ion Industrial Group, Hatfield, PA, US). Two high efficiency filter cartridges were also included at the setup top to provide clean make-up air flow for filter testing. A custom-made filter holder was located in the test section of the setup. The effective test area of filter media is designed as 100 cm^2. Differential pressure transmitters (OMEGA PX-655) were used to measure the pressure drop across test filter media. All the pressure drop data was recorded by a computer via a data acquisition card (USB-1208FS-Plus, Measurement Computing Corporation, MA, US). Two ports were included in the upper and lower flow channels to insert probes for particle sampling and measurement. At the downstream of lower flow channel vacuum pumps were used to drive the test flow through the test setup. The total flowrate through the setup was monitored by a laminar flow element, LFE (model Z50MC2-2, Meriam Process Technologies, Cleveland, OH, US). Two differential pressure gauges (one is OMEGA differential pressure transmitter and the other a mechanical pressure gauge from Dwyer Instruments Inc.) were used to measure the pressure drop of LFE. Because the total flow driven by vacuum pumps was higher than that required for filter testing, a bypass flow channel with a MKS T3BI high speed throttle valve was further included in the test setup to balance the flow. A close PID control loop was used to adjust the valve opening in order to achieve the desired flow rate through the filter test section.

ISO 12103-1, A3 Medium test dust, known as Arizona Road Dust (ARD), and ISO 12103-1, A1 ultrafine test dust (Powder Technology Inc., Burnsville, MN, US) were selected as test particles in this study. TOPAS SAG-410 and SAG-410/U were used to disperse ARD and Ultrafine dust, respectively. ARD was measured by Aerodynamic Particle Sizer (APS, TSI 3321), ultrafine test dust by Optical Particle Sizer (OPS, TSI 3330).

Two different HEPA filter media were tested for this study: borosilicate glass fiber medium (A) and electret filter media (B). Table 5-1 lists basic properties of two test filter media. To investigate the effect of face velocity, each filter medium was further tested at two face velocities (i.e., 10 and 20 cm/sec). In the study five particle loading rates were used to test filter media. Based on our experimental data, the variation of repeated loading rates could be successfully controlled within 5%.

Table 5-1 Characteristics of tested filter media

Filter Media	Materials	Thickness [mm]	Basic Weight [g/m^2]	Permeability [m^2]	Fiber Effective Diameter [μm][a]	Solidity
A	Borosilicate glass	0.33	93.4	4.14E-13	2.09	0.12
B	Electret	0.40	80.0	2.83E-12	0.28	0.20

[a]Fiber effective diameter was calculated by Kuwabara's cell models.

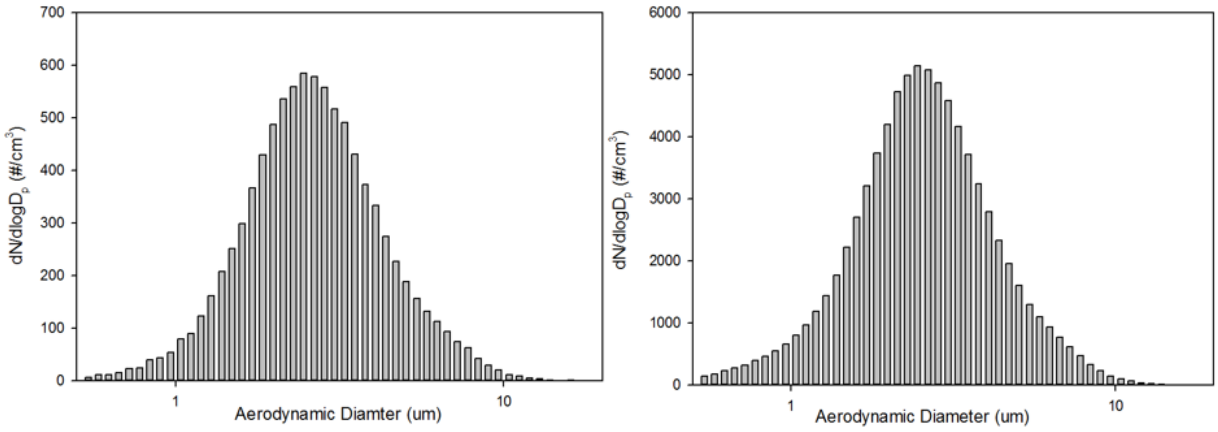

(a) ARD, mass conc. = 0.32 µg/cm^3 **(b) ARD, mass conc. = 7.08 µg/cm^3**

Figure 5.2 Particle size distribution of different loading rates under face velocity = 10 cm/s

For each particle loading rate the size distribution of dispersed particles in the upper flow channel was characterized by APS. Repeated measurements of the size distributions of dispersed ARD particles at lowest and highest loading rates were taken at different days in our study, evidencing that the size distributions of test particles remains the same at various loading rates. (Fig. 5.2)

In this study experiments were carried out to systematically investigate the effect of particle loading rate on the performance curves of high efficiency filter media under the steady flow operation (at two constant face velocities of 10 and 20 cm/sec). Two different filter media (glass fiber and electret filter media) were used in this study. Two types of dusts (i.e., ARD and ultrafine dusts) were selected for this test. Based on the collected experimental data a semi-empirical model was further proposed to quantify the effect of particle loading rate on the filter pressure drop.

5.3 Experimental Results

5.3.1 Effect of Test Particle Mass Concentration

Figure 5.3 shows the loading curves of test filter media under various test particle mass concentrations when loaded with ARD at the face velocity of 10 cm/sec. In general both filter media experienced the similar filtration phases during the loading: i.e., depth, transitional and dust cake (or surface) filtration. Because of HEPA filter media, the filtration status was quickly transitioned to the surface filtration after a short period of loading time. Five dust mass concentration levels were randomly selected for testing each filter medium. All five loading curves followed the typical loading characteristics of fibrous filter media. However, the slopes of pressure drop increase in the dust cake (or surface) filtration regime were very different. The slope of filter pressure drop in the surface filtration was decreased as the particle mass concentration was increased. The similar trend on the slope change of filer pressure drop in the surface filtration regime was also observed for the filter medium B. Obviously, the permeability of dust cake formulated at low particle mass concentration loading condition is lower as compared to that formed at high mass concentration loading.

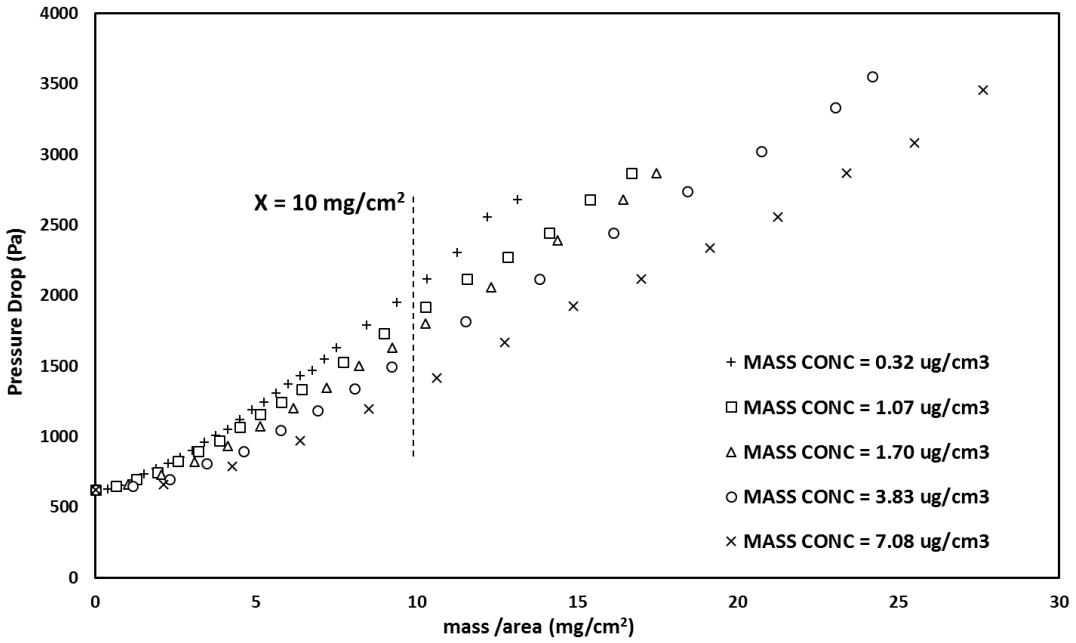

Figure 2 (a)

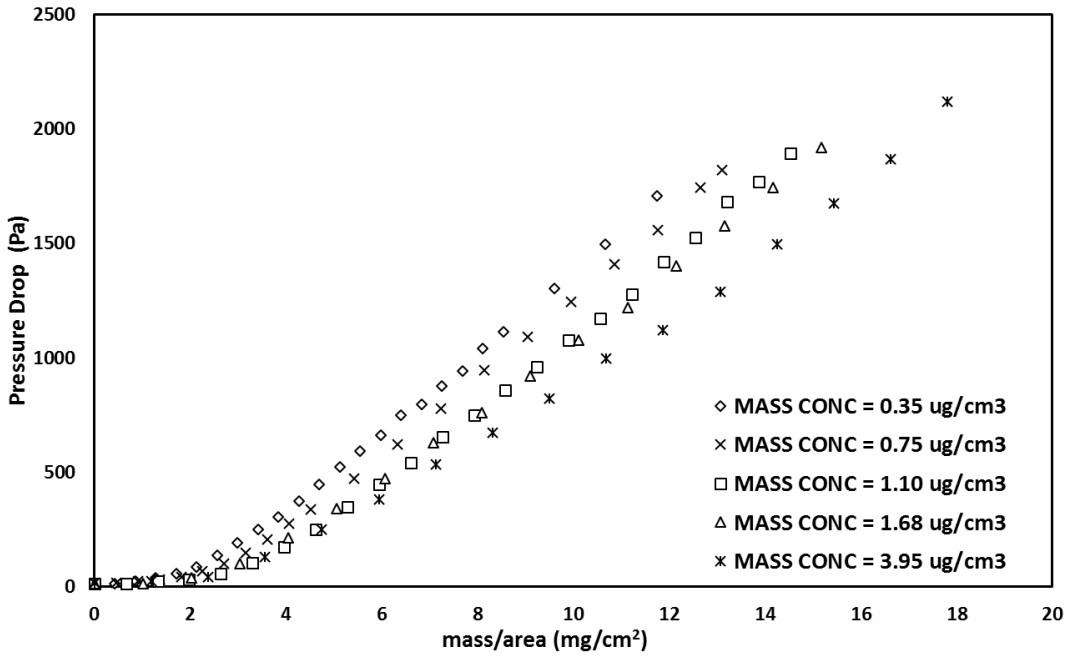

Figure 2 (b)

Figure 5.3 Loading of ARD on filter media (a) A and (b) B Solid particle (ARD) at various loading rates and with the face velocity = 10 cm/sec.

We thus hypothesize that for low mass concentration loading particles had more intra-particle spacing when they moved in air. When they were collected on the filter surface they had more time and space to arrange themselves without the interference of incoming particles, thus establishing a denser cake micro-structure. At high mass concentration loading, particles collected on the filter surface had much less time and space to arrange them in a stable condition, resulting in a loose micro-structure (as a result of interference from incoming particles). To confirm the above hypothesis we applied the technique developed by Schmidt and Löffeler to fix the micro-structures of test filter media under the low and high mass concentration loading conditions and observed the samples under SEM (model SU-70, Hitachi High Technologies America Inc., Gaithersburg, MD, US). Figure 5.4 shows the SEM images of the side view of filter medium A after being loaded at both low and high particle mass concentrations. The dust amount on both cases were kept nearly the same for both cases. It is obvious that for the case with low mass concentration loading, more particles were deposited inside the medium and the porosity of dust cake was less when compared to that for the case with high mass concentration loading (Fig. 3b).

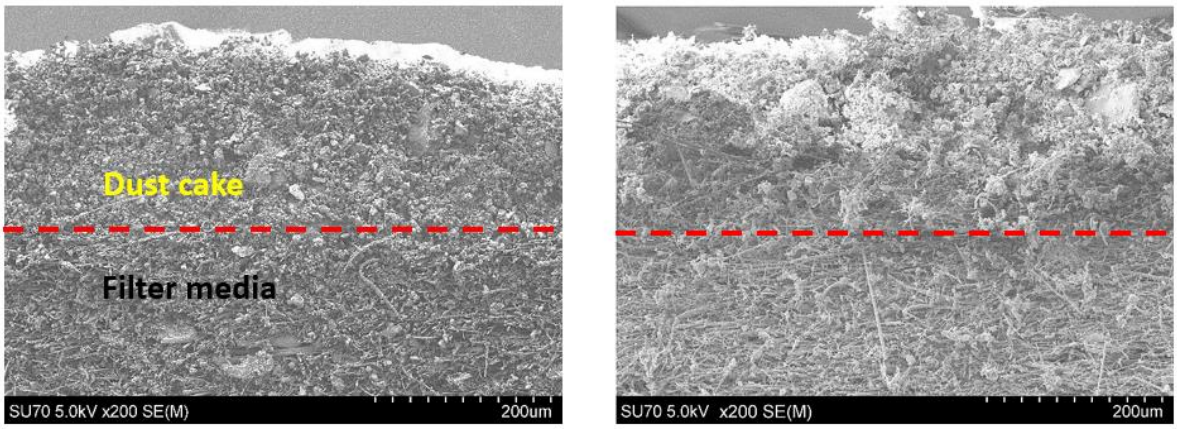

(a) At the rate of 0.32 µg/cm³ (b) At the rate of 7.08 µg/cm³

Figure 5.4 SEM images of the cross-section of loaded filter medium A at the face velocity of 10 cm/s (a) at the rate of 0.32 µg/cm3; (b) at the rate of 7.08 µg/cm3

5.3.2 Effect of Particle Size

ISO 12103-1, A1 ultrafine test dust was also selected as test aerosol in this study. Figure 5.5 shows the loading curves of test filter media A and B at low and high particle mass concentration loading (with the face velocity of 10 cm/sec). It is found that the filter pressure drop at low particle mass concentration loading is higher than that at high concentration loading. However, the effect of particle mass concentration in these cases is not as obvious as that observed in the cases with ARD. The particle size should be the primary factor for the above observation. When ultrafine particles were loaded to filters, they required less time and space to be stabilized, resulting in more fine particles deposited inside the media and later built up denser dust cake layer on the filter surface (as compared to that with ARD). The effect of particle concentration on the filter loading curves was thus reduced.

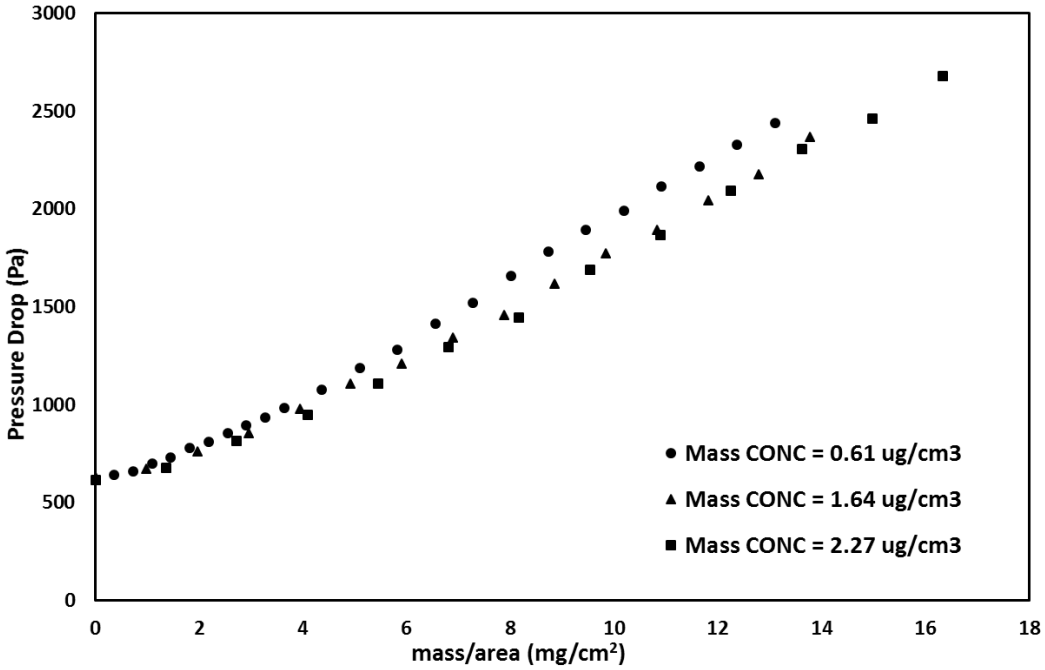

Figure 5.5 (a)

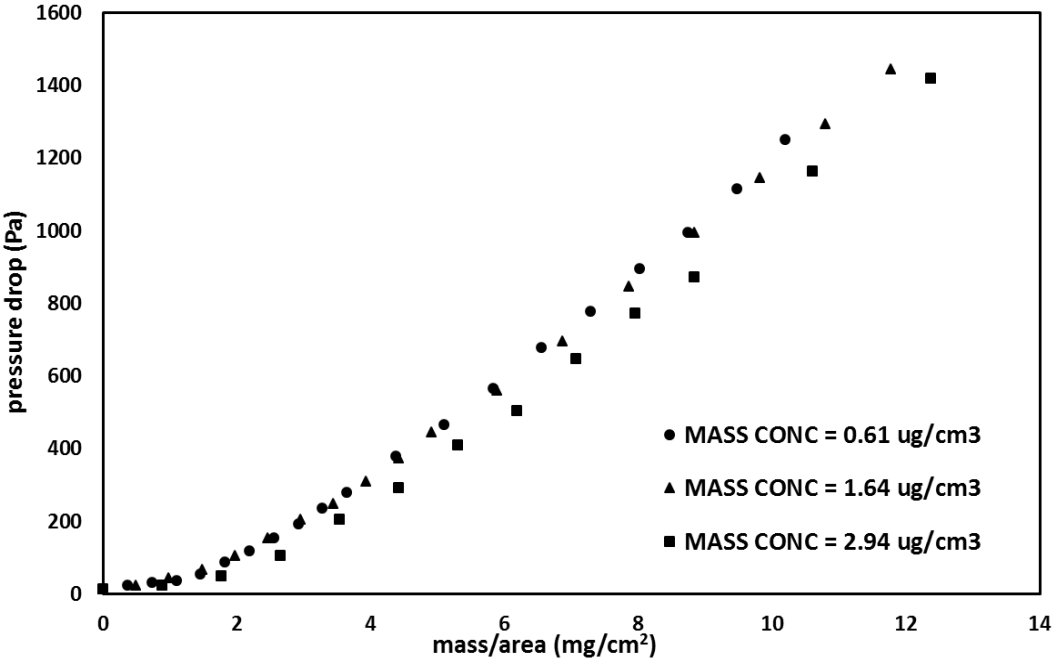

Figure 5.5 (b)

Figure 5.5 Ultrafine dust loading behavior with various loading rates on (a) A and (b) B type filters with the face velocity = 10 cm/sec.

5.3.3 Effect of Face Velocity

The effect of flow rate or face velocity on the dust cake compaction and cake resistance had been studied. In the above work, the cake resistance was found to increase with the increase of filtration velocity. Additionally, the cake porosity decreased and cake specific resistance increased when the face velocity increased. In this part of study, we further tested the filter media at the face velocity of 20 cm/sec in order to find out the effect of face velocity.

Figure 5 shows the comparison of loading curves for Filters A and B at the face velocities of 10 and 20 cm/sec. Because of the experimental conditions, we could only adjust the mass concentration in the cases with two face velocities as close as possible (not exactly the same unfortunately). The ratio of filter pressure drop to face velocity was used in the y axis in Fig. 5.6. The reason for using the above ratio is based on Darcy's law, where the filter pressure drop is linearly proposal to the face velocity, and the slope of the linear relationship depends on the microstructure of loaded filter media. By using the above ratio, one can decipher the influence on the microstructure of loaded filter media attributed to the face velocity. It is evidenced that the effect of face velocity on the microstructure of loaded filter media is negligible under our experimental condition.

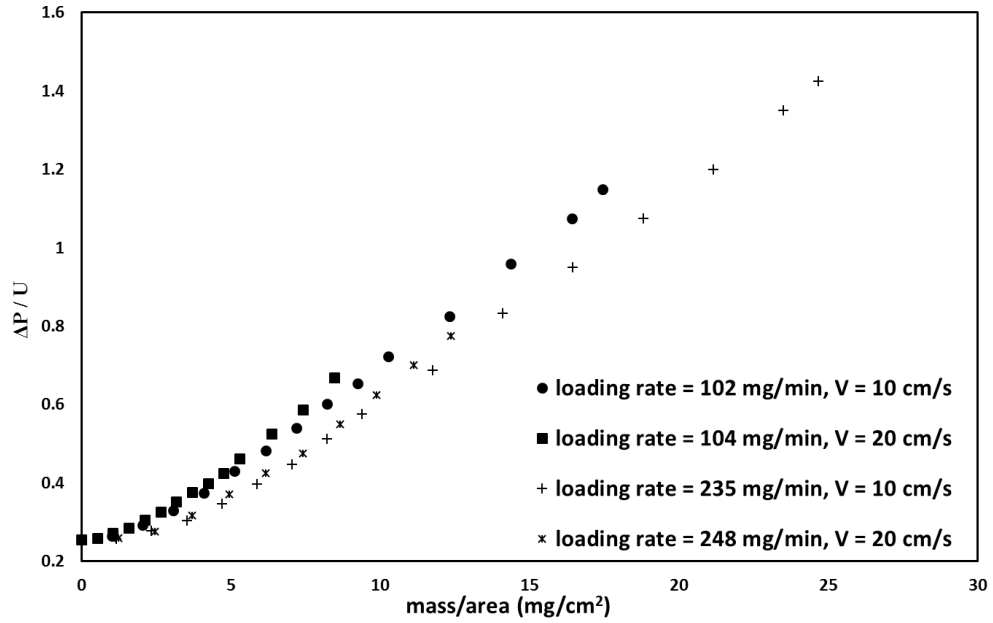

Figure 5.6 (a)

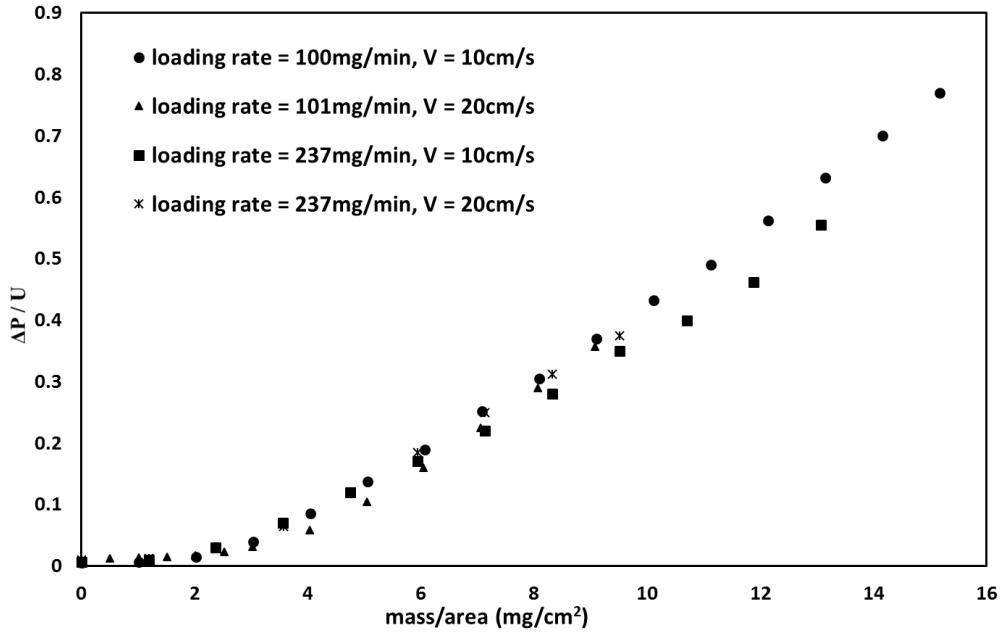

Figure 5.6 (b)

Figure 5.6 The filter loading behavior of filter (a) A and (b) B at two velocities on filter A when loaded with ARD

5.3.4 Qualitative analysis of experimental data

5.3.4.1 For the dust cake

Since a high efficiency filter media is used, the majority of particles are collected on the filter surface and built up the dust cake layer. The effect of loading rate on the microstructure of filter dust cake can be revealed by further qualitative analysis. Much work had been performed to experimentally and theoretically investigate the pressure drop across the dust cake that built up on the filter surface. Among the more recent studies, Endo and Chen proposed the following equation for the cases of randomly packed dust cake with the consideration of particle polydispersity and shape:

$$\Delta P_c = 18\mu u_s H \frac{(1-\varepsilon)\upsilon(\varepsilon)}{\varepsilon^2} \frac{\kappa}{d_{vg}^2 exp(4ln^2\sigma_g)} \qquad (5.1)$$

where $\mu, u_s, H, \kappa, d_{vg}$ and σ_g are fluid viscosity, superficial velocity, cake height, dynamic shape factor of particles, and the geometrical mean diameter and geometric standard deviation of test particles, respectively. ε and $\upsilon(\varepsilon)$ are the cake porosity and void function. By re-arranging *Eq. (5.1)*, the following equation can be derived as:

$$\Delta P_c \cdot A_{cake} = \mu u_s \kappa \frac{M}{\rho_p} \frac{1}{d_{vg}^2 \exp(4ln^2\sigma_g)} \frac{18\upsilon(\varepsilon)}{\varepsilon^2} \qquad (5.2)$$

where M is the mass of deposited dust and A_{cake} is the area of dust cake and the total volume of dust particles deposited on the filter surface can be calculated as $A_{cake} \cdot H \cdot (1-\varepsilon)$. *Eq (5.2)* can then be manipulated as

$$F(\varepsilon) = \frac{18\upsilon(\varepsilon)}{\varepsilon^2} = \frac{\Delta P_c \cdot A_{cake}}{M} \cdot \frac{\rho_p \cdot d_{vg}^2 exp(4ln^2\sigma_g)}{\mu u_s \kappa} \qquad (5.3)$$

The function of $F(\varepsilon)$ shall be considered as the macroscopic expression for particle-loaded filter media. Figure 5.7 shows the value of $F(\varepsilon)$ as a function of test particle loading rate for two test filter media loaded with two test dusts. It is found that the microstructure of dust cake is a function of particle loading rate (i.e., the test particle mass concentration times the total flowrate) for the cases with ARD and the effect of loading rate is more significant in the low loading rate range. The above observed was also found in the cases with the cakes built up by ultrafine dust, even though it was less obvious. It may be because of the narrow particle loading rate range tested in our study. Notice that the value of $F(\varepsilon)$ for the cases with ultrafine dust (Fig. 5.7 c and d) is much lower than those obtained in the cases with ARD (Fig. 5.7 a and b). The reason for the above $F(\varepsilon)$ value change is primarily because of the particle size.

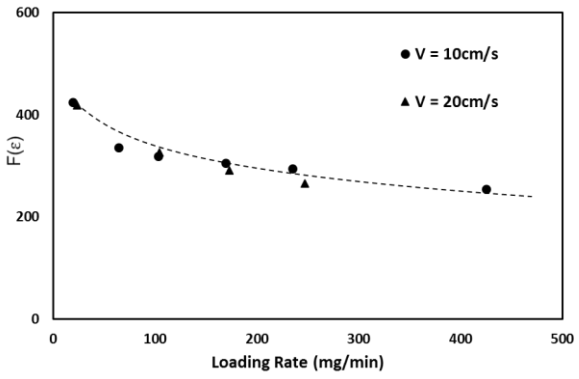

(a) Testing on filter media A with ARD

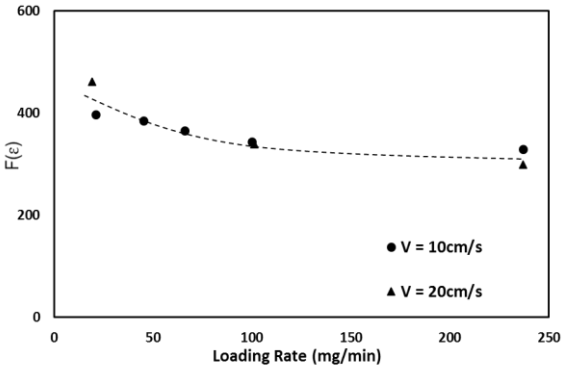

(b) Testing on filter media B with ARD

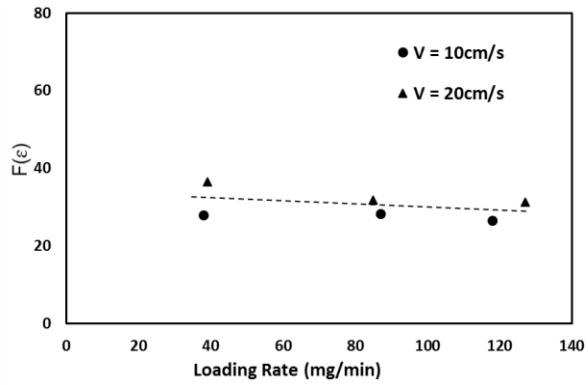

(c) Testing on filter media A with ultrafine dust

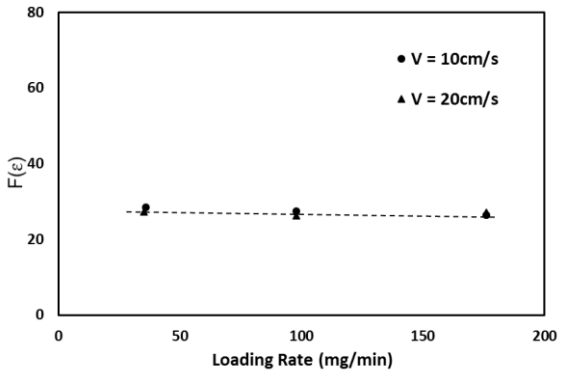

(d) Testing on filter media B with ultrafine dust

Figure 5.7 The relationship of F(ε), defined in this work, as a function of particle loading rate for the cases of (a) Filter A loaded with ARD; (b) Filter B loaded with ARD; (c) Filter A loaded with ultrafine dust; (d) Filter B loaded with ultrafine dust.

5.3.4.2 For the dust loading curve

To describe the entire loading curves obtained in this study, we proposed the following empirical equation (i.e., *Eq. 5.4*) to fit the experimental data collected. *Eq. (5.4)* assumes that the pressure drop across the loaded filter media is attributed by two parts; one part is from the clean filter and the other from the loaded particles:

$$P_{total} = \Delta P_{clean} + \Delta P_{loaded\ particles} \tag{5.4}$$

By assuming that $\frac{\Delta P_{cake}}{\Delta P_{clean}} = C_1 \bar{M}^{C_2}$, where $\bar{M}$ is mass deposited per unit area, *Eq. (5.4)* can be written as

$$\frac{\Delta P_{total}}{\Delta P_{clean}} = 1 + C_1 \bar{M}^{C_2} \tag{5.5}$$

The result of best-fitted C_1 and C_2 values are listed in Table 5.2. Figure 5.8 shows the C_1 and C_2 as a function of test particle loading rate. In the cases of loading with ARD, the C_1 value slightly decreases as the test particle mass concentration increases, and the value of C_2 remains nearly constant for a given face velocity. Both C_1 and C_2 values are influenced by the face velocity, even though the effect is not considered to be significant. In the case of loading with ultrafine dust, the values of C_1 and C_2 seem to keep constant on both filter medium cases. Similar to cases of ARD, the effect of face velocity is apparently unimportant when ultrafine dust used.

Table 5-2 Summary of fitted curve parameters for entire loading curves

(a) ARD particle loading on filter A

Face velocity (cm/s)	Mass Conc. (μg/cm³)	C1	C2	Std Error C1	Std Error C2
10	0.32	0.1168	1.3125	0.0022	0.0084
	1.07	0.1179	1.2190	0.0051	0.0169
	1.72	0.0834	1.3098	0.0047	0.0214
	2.82	0.0982	1.2317	0.0073	0.0262
	3.92	0.0586	1.3706	0.0045	0.0257
	7.08	0.0537	1.3344	0.0043	0.0251
20	0.19	0.0854	1.5423	0.0034	0.0232
	0.87	0.0637	1.5092	0.0018	0.0146
	1.44	0.0649	1.4459	0.0024	0.0179
	2.06	0.0294	1.6885	0.0027	0.0390

(b) ARD particle loading on filter B

Face velocity (cm/s)	Mass Conc. (μg/cm³)	C1	C2	Std Error C1	Std Error C2
10	0.35	3.3696	1.5124	0.2166	0.0295
	0.75	2.0660	1.5913	0.2053	0.0416
	1.10	1.8304	1.6595	0.1673	0.0369
	1.67	2.2500	1.5588	0.2061	0.0363
	3.95	1.8048	1.5159	0.1924	0.0398
20	0.16	0.4570	2.2368	0.0406	0.0494
	0.84	0.2563	2.2391	0.0386	0.0724
	1.98	0.7223	1.7549	0.1367	0.0902

(c) Ultrafine particle loading on filter A

Face velocity (cm/s)	Mass Conc. (μg/cm³)	C1	C2	Std Error C1	Std Error C2
10	0.63	0.1173	1.2323	0.0038	0.0143
	1.45	0.0954	1.2961	0.0018	0.0078
	1.63	0.0952	1.2819	0.003	0.0133
	1.97	0.1286	1.1663	0.009	0.0283
20	0.33	0.0922	1.4728	0.0029	0.018
	0.71	0.1047	1.3417	0.0035	0.0175
	1.06	0.0624	1.5478	0.0041	0.0321

(d) Ultrafine particle loading on filter B

Face velocity (cm/s)	Mass Conc. (μg/cm³)	C1	C2	Std Error C1	Std Error C2
10	0.60	3.2678	1.3735	0.1894	0.0245
	1.63	2.9330	1.4179	0.1045	0.0154
	2.93	2.3766	1.4540	0.2517	0.0440
20	0.29	1.4071	1.5542	0.0425	0.0157
	0.82	1.2037	1.5909	0.0351	0.0157
	1.47	0.9344	1.6881	0.0530	0.0271

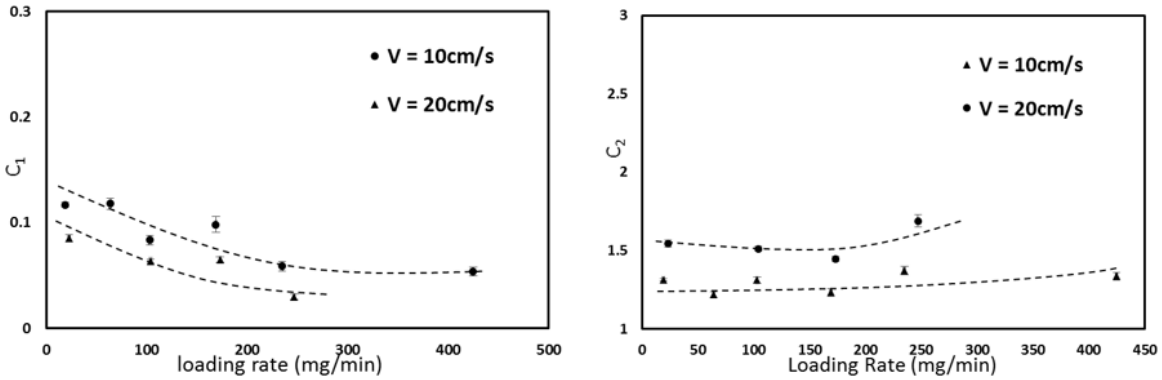

(a) ARD particle loading behavior on filter A.

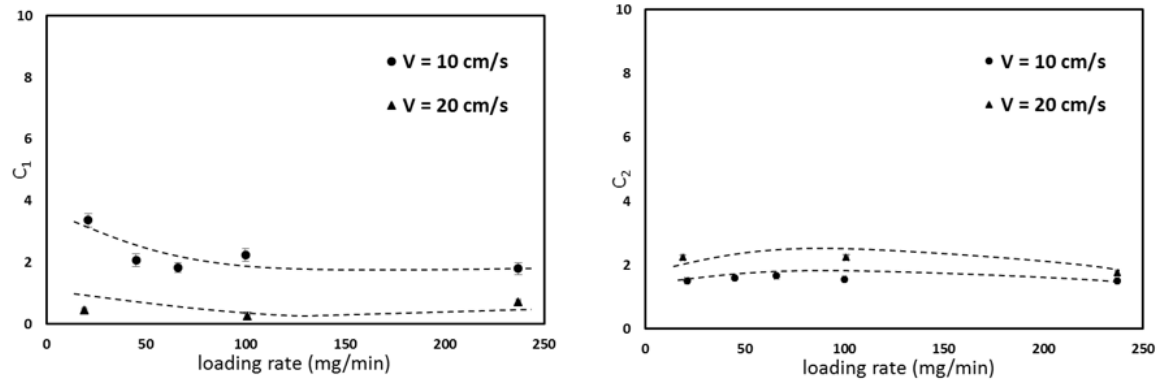

(b) ARD particle loading behavior on filter A.

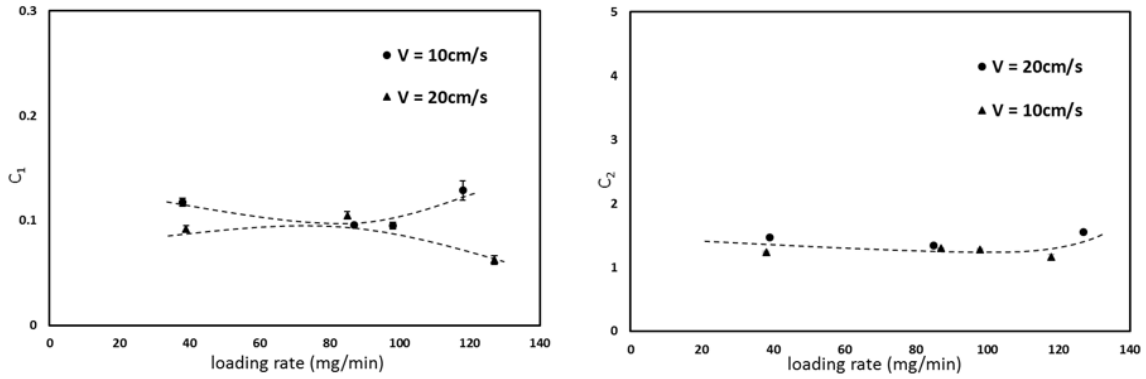

(c) Ultrafine particle loading behavior on filter A.

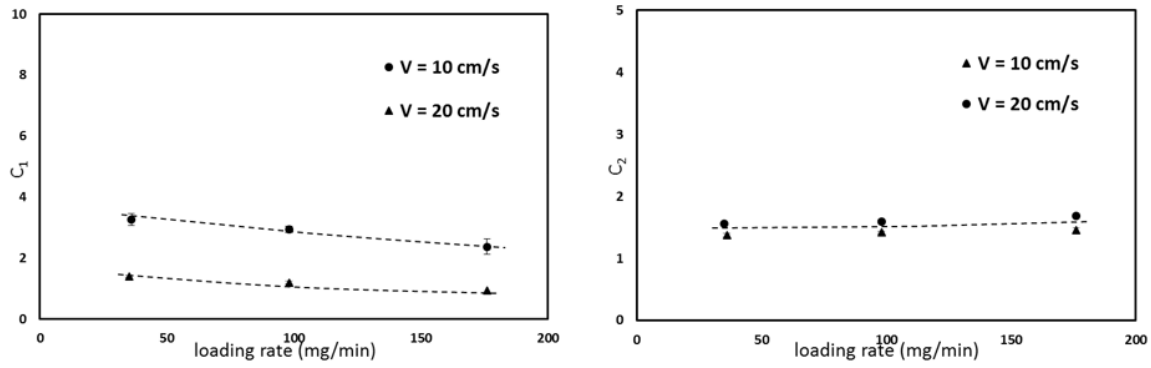

(d) Ultrafine particle loading behavior on filter B.

Figure 5.8 The values of fitted parameters as a function of mass particle loading rate for the cases: (a) Filter A loaded with ARD; (b) Filter B loaded with ARD; (c) Filter A loaded with ultrafine dust; (d) Filter B loaded with ultrafine dust.

5.4 Summary

In this study, we systematically investigated the effect of dust loading rate (i.e., test particle mass concentration and total flowrate) on the particle loading curves of high efficiency filter media (i.e., the filter pressured drop as a function of particle mass loaded on

unit filter medium area). To the authors' knowledge this is the first study focused on this subject. Two high efficiency filter media, i.e., glass fiber and electret filters, were selected for this study. Filter media were loaded with two different dusts: one is *ISO 12103-1*, A3 Medium test dust (Arizona road dust) and the other is *ISO 12103-1*, A1 Ultrafine test dust. Both dusts were obtained from Powder Technology Inc.. The particle loading curves of the test filters were experimentally collected under various loading rates and two face velocities (10 and 20 cm/sec). Because of the selection of high efficiency filter media, the filtration status of the test filter media under the particle loading was primarily in the dust cake filtration regime (after a short period of time staying in the initial, depth and transitional filtration).

Based on the collected data, it is evidenced that the dust loading rate indeed has its effect on the filter pressure drop during the particle loading, especially in the low loading rate region. Under a given face velocity, the filter pressure drop decreases as the test particle mass concentration increases for the cases loaded with ARD. The above observation is less obvious when filters were loaded with ultrafine particles. It is because at low particle mass concentration particles collected on the filter surface had more time and space to reach a stable status (without much interference from later incoming particles). At high mass concentration, loading particles collected had less chance to achieve a stable status, thus resulting in more porous dust cake. The above hypothesis was further supported by the SEM images of the cutoff view of loaded filter media. Our study also shows the minor effect of face velocity on the filter loading curves. The effect of the particle loading rate on the filter

loading curves was further quantified via data analysis. An empirical model was at last proposed to best fit the experimental particle loading data collected under various test conditions.

CHAPTER 6 Performance of HVAC Entrance Filter Panel under Non-uniform Particle Loading

6.1 Introduction

HVAC filter medium is playing a paramount role in determining the efficiency of a HVAC system which is used to control and main indoor air quality. HVAC filter device are broadly used in aircraft to keep proper air quality in the passenger cabin. Fig. 6.1 shows an example of a mix manifold of cargo area in an aircraft. The air in the surrounding space is sucked into these mix manifolds through HVAC filter panels, then the air pass through the main distribution ducts and is delivered into the passenger cabin. The pleated HVAC filters installed here are to remove particles from the surrounding air. As particle are deposited on the HVAC filter panel, the pressure drop cross the filter element will gradually increase, which will increase the pump load and operational cost.

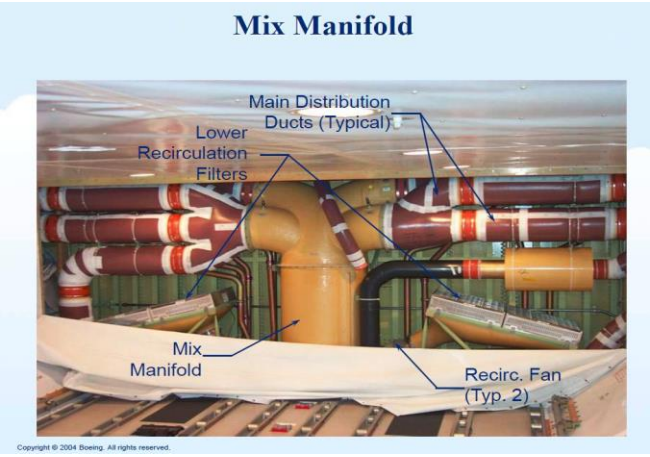

Figure 6.1 An example of a mix manifold in an aircraft

In practical applications, the HVAC filters need to be replaced after a certain period of time. It has been reported that under some circumstance particles are not uniformly deposited on the filter panel (see Fig. 6.2). These non-uniform deposition patterns will not only reduce the usage of HVAC filter panels, but also bring heavy loss to airline companies due to maintenance of aircraft. The most possible reasons are because of the limited space of aircraft which causes non-uniform velocity profile around HVAC filter panels that resulting in non-uniform spatial distribution of particles.

Figure 6.2 An example of particle non-uniform deposition

Therefore, it would be so meaningful and essential to study particle motion and deposition on the panel filters at the HVAC channel entrance. And the research is aimed to deliver effective solutions to deal with the serious issue about the reduction of filter panels' lifetime which were installed in HVAC systems of aircrafts, also for the purpose of avoiding the huge loss of "Aircraft on Ground" and cutting down the cost of HVAC filter panel

replacement. There are many practical issues to operate experiments for this work. A typical HVAC system commonly takes large space that is not possible to fulfill based on university laboratory situations, as well as the actual layout in the cargo area of an aircraft. Thus, modeling and simulation (CFD) were employed to deal with this problem instead of experiments.

6.2 2-D Model for Calculating the Loading Curves

To study the behavior of non-uniform particle loading on HVAC filter panels, we started from 2-D numerical models as a simple way to establish a reliable method which can simulate the processing of particle deposition on filter media and calculate the pressure drop across filter panels under the non-uniform particle loading. FLUENT ANSYS has been chosen as our computational fluid dynamic (CFD) tool for this work. We applied Navier-Stokes equations to solve the flow field in the model as following:

Continuity equation is, $$\frac{\partial u}{\partial x}+\frac{\partial v}{\partial y}+\frac{\partial w}{\partial z}=0$$

Momentum equation is, $$\rho\left(u\frac{\partial u}{\partial x}+v\frac{\partial u}{\partial y}+w\frac{\partial u}{\partial z}\right)=-\frac{\partial P}{\partial x}+\mu\left(\frac{\partial^2 u}{\partial x^2}+\frac{\partial^2 u}{\partial y^2}+\frac{\partial^2 u}{\partial z^2}\right)$$

$$\rho\left(u\frac{\partial v}{\partial x}+v\frac{\partial v}{\partial y}+w\frac{\partial v}{\partial z}\right)=-\frac{\partial P}{\partial y}+\mu\left(\frac{\partial^2 v}{\partial x^2}+\frac{\partial^2 v}{\partial y^2}+\frac{\partial^2 v}{\partial z^2}\right)$$

$$\rho\left(u\frac{\partial w}{\partial x}+v\frac{\partial w}{\partial y}+w\frac{\partial w}{\partial z}\right)=-\frac{\partial P}{\partial x}+\mu\left(\frac{\partial^2 w}{\partial x^2}+\frac{\partial^2 w}{\partial y^2}+\frac{\partial^2 w}{\partial z^2}\right)$$

Laminar flow was assumed to simplify the model at the beginning. For the model of filter media, the porous media was enabled, meanwhile an addition momentum sink term was added to the standard fluid flow equations. And the source term consists of two parts:

one is viscous loss term (the first term of right-hand side of following equation) and an inertial loss term (the second term of the right-hand side of equation)

$$S_i = -\left(\sum_{j=1}^{3} D_{ij}\mu v_j + \sum_{j=1}^{3} C_{ij}\frac{1}{2}\rho|v|v_j\right)$$

where S_i is the source term for the ith (x, y or z) momentum equation, $|v|$ is the magnitude of the velocity and D and C are prescribed matrices. This momentum sink term would contribute to the pressure gradient in the porous cell, creating a pressure drop that is proportional to the fluid velocity in the cell. For the particle trajectory part, Fluent predicts the trajectory of a discrete phase particle by integrating the force balance on the particle with Lagrangian method. The force balance equates the particle inertia with the force acting on the particle, and can be expressed as (in x direction),

$$\frac{du_p}{dt} = F_D(u - u_p) + \frac{g_x(\rho_p - \rho)}{\rho_p} + F_x$$

where $F_D(u - u_p)$ is the drag force per unit particle mass and $F_D = \frac{18\mu}{\rho_p d_p^2}\frac{C_D Re}{24}$, u is the fluid phase velocity, u_p is the particle velocity, μ is the molecular viscosity of fluid, ρ_p is the density of the particle, and d_p is the diameter of particle. R_e is the relative Reynolds number. However, the effect of gravity is ignored just for simplifying the case, and there is also no other force acting on particle except drag force. Therefore, the equation of particle trajectory can be simplified as,

$$\frac{du_p}{dt} = F_D(u - u_p)$$

One approach used to account for particle collection by filter media is described by Bergman et al. (1978) who assumed that the filter as a medium with two sorts of fibres during the deposit of particles. The first sort is composed of the clean fibres, the second is dendrites formed by the collected particles. This approach was mentioned in the review section above. In ANSYS FLUENT, relative viscous resistance (VR) is the reciprocal of permeability for porous media. Combine with Darcy's Law, we could get equation of VR as,

$$\Delta P_0 = 64\pi\mu U\left(\frac{\alpha_f}{d_f}+\frac{\alpha_p}{p}\right)\left(\frac{\alpha_f}{d_f^2}+\frac{\alpha_p}{d_p^2}\right)^{0.5}$$

$$\frac{dP}{dz}=\frac{\mu}{k}V, \qquad \frac{1}{k}=\frac{\Delta P}{\mu VZ}$$

$$\text{VR} = 64\left(\frac{\alpha_f}{d_f}+\frac{\alpha_p}{p}\right)\left(\frac{\alpha_f}{d_f^2}+\frac{\alpha_p}{d_p^2}\right)^{0.5}$$

The value of VR would be the instantaneous relative viscous resistance of filter media during the particle loading processing. Because it is known that the permeability of filter media would decrease due to the deposition of particle loaded on fibers, as a result that the flow field around HVAC filter panel would be changed. Therefore, the flow filed is needed to be updated after a short period of particle loading on filter panel to predicate and provide much accurate flow field for particle tracking. In ANSYS FLUENT, there is user define function (UDF) where we can customize ANSYS FLUENT and enhance its capabilities by coding. For the return status PATH_ABORT in UDF, the particle will be

stopped and considered to be aborted. User define memory (UDM) is also available that can store global variables. With the help of UDF and UDM, we could update the permeability of each cell on filter media during particle loading process. For the update of flow filed, Fluent Journal file was built to enable this function automatically. The detailed process of modeling methodology is shown in bellowing flow chart:

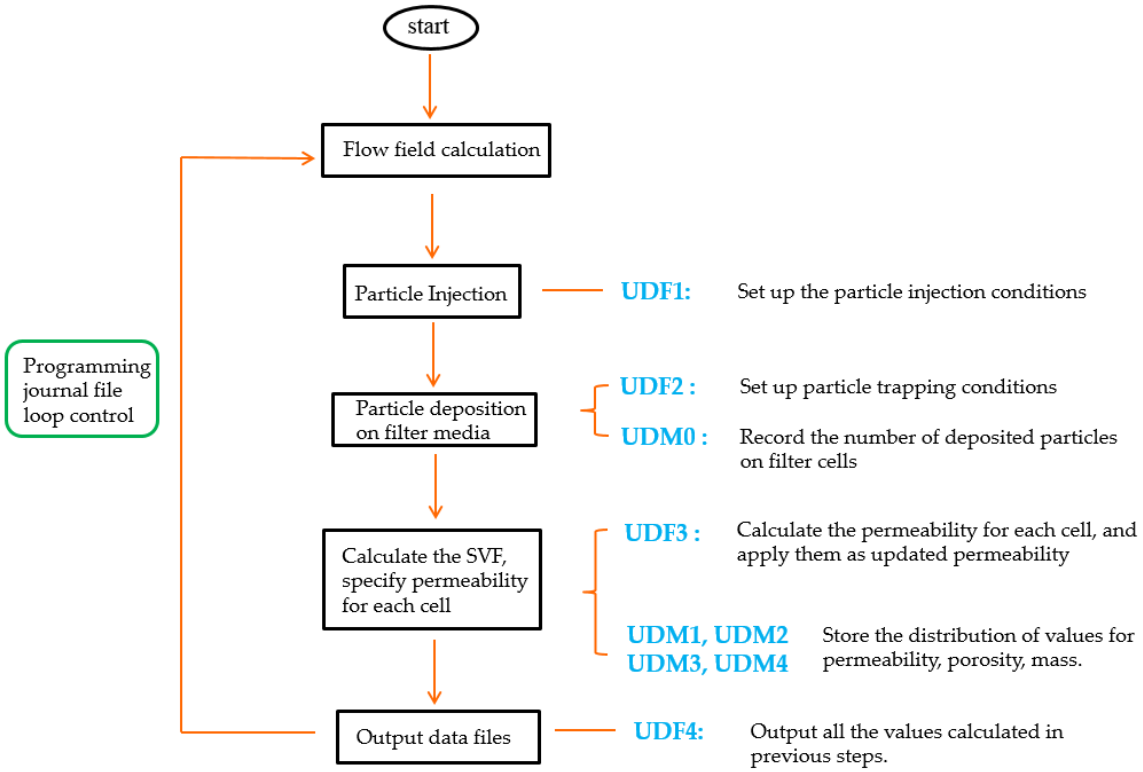

Figure 6.3 Flow chart of particle continuous loading calculation

Two models of pipe entrance filter panel were selected to calculate the loading curve based on the developed methodology above. Fig. 6.4(a) is a model of filter panel with flat medium with thickness of 0.4 mm and length L of 60 mm, where the length of the upstream

channel is 5L and downstream 8L. Fig. 6.4(a) shows half of the geometry model, which is symmetry about the dash centerline. Besides, Fig. 6.4(a) was also serving as the reference model. The other model Fig. 6.4(b) is a filter panel with pleated filter medium installed in the same pipeline as Fig. 6.4(a).

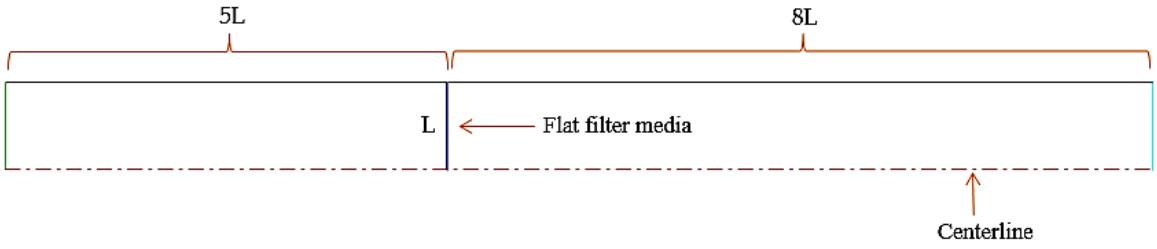

(a) Filter Panel with Flat medium (Reference)

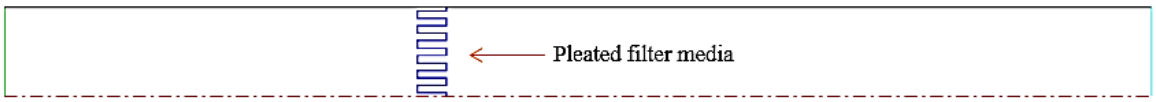

(b) Filter panel with pleated medium

Figure 6.4 The geometry model of filter panels

To have good mesh quality for our models, the mesh was specifically treated around wall and filter that high density grid was set at the wall and filter media. The density of mesh was decreasing as the location getting far from wall and media. One example of the mesh distribution was given around the pleated filter media as shown in Fig. 6.5. All the boundaries setup were also indicated in Fig. 6.5, including the Inlet, Outlet, Wall, Symmetry, and Media zone.

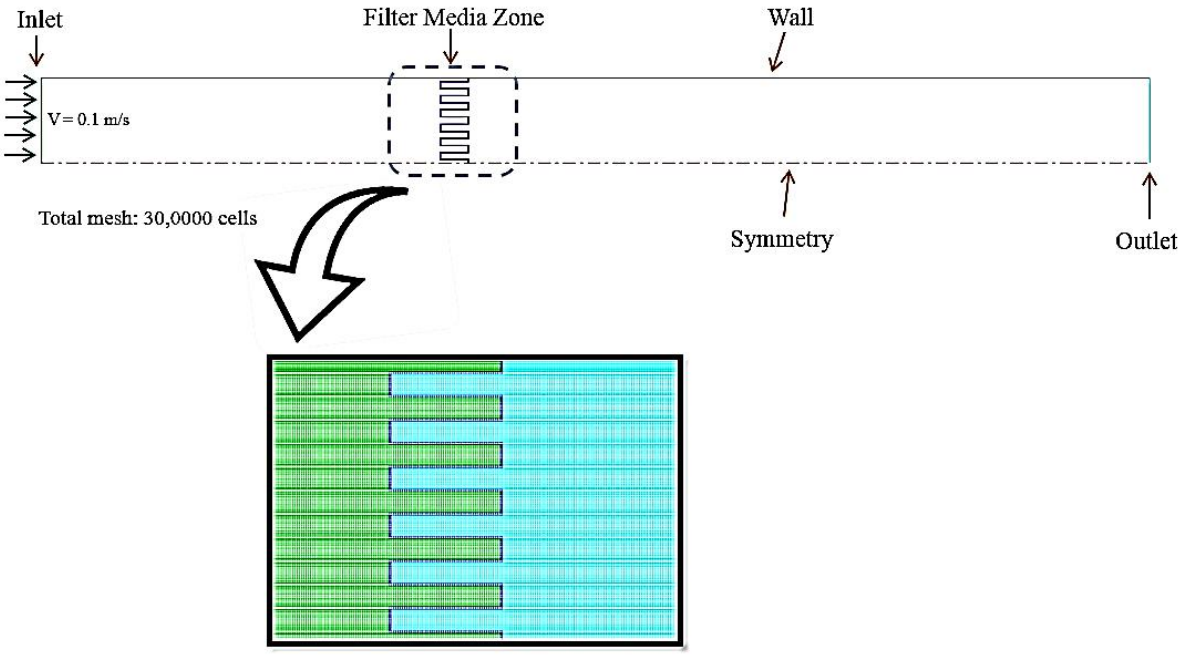

Figure 6.5 The mesh distribution around filter

In addition, the detailed parameters of initial boundaries conditions for the modeling were listed in Table. 6.1, both cases have exactly same initial boundary conditions. The viscous resistance is 2.02E+12 ($1/m^2$) in each direction. It is necessary to clarify that three zones were created including porous zone for filter media, upstream and downstream fluid zones.

Table 6-1 Boundaries conditions

PHYSICAL BOUNDARY/ZONE	BOUNDARY/ZONE CONDITIONS
Velocity Inlet	V = 0.1 m/s
Pressure Outlet	Zero gauge pressure (Pascal)
Interior-L	Porous jump, face permeability=1E+10 (m^2)
Wall	Stationary wall, no slip condition
Symmetry	Mirror symmetry
Filter Media Zone	Porous zone, viscous resistance in direction of x, y = 2.02E+12 ($1/m^2$)
Flow-1 & 2 Zone	Standard fluid conditions, pressure=1atm

For the particle release method: the particles used here were monodisperse with diameter of 0.5μm; the number of particle was 5,000 for each injection in all cases; all particles were released from one third of the opening from the centerline as shown in Fig. 6.6, and the initial velocity of u, v, w direction were null for every particle; the particle type was defined as inert particle with density of 1000 kg/m^3; ANSYS Fluent Discrete phase model (DPM) and One-way coupled model were enabled for particle tracking.

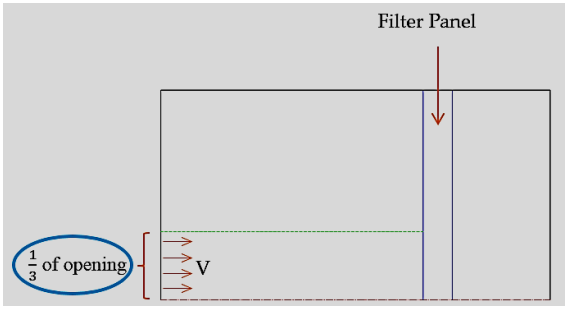

Figure 6.6 Diagram of particles injection location

Results and Discussion for Flat Filter Media Case

Fig. 6.7 shows the evolution of flow field for flat filter media during the particle continuously loading process. Since all particles were released from the center part of the pipe channel (1/3 area of channel width), all particles should follow the flow field calculated and start the deposition from the center part on filter panel, then spread to wall side as particle continuous loading.

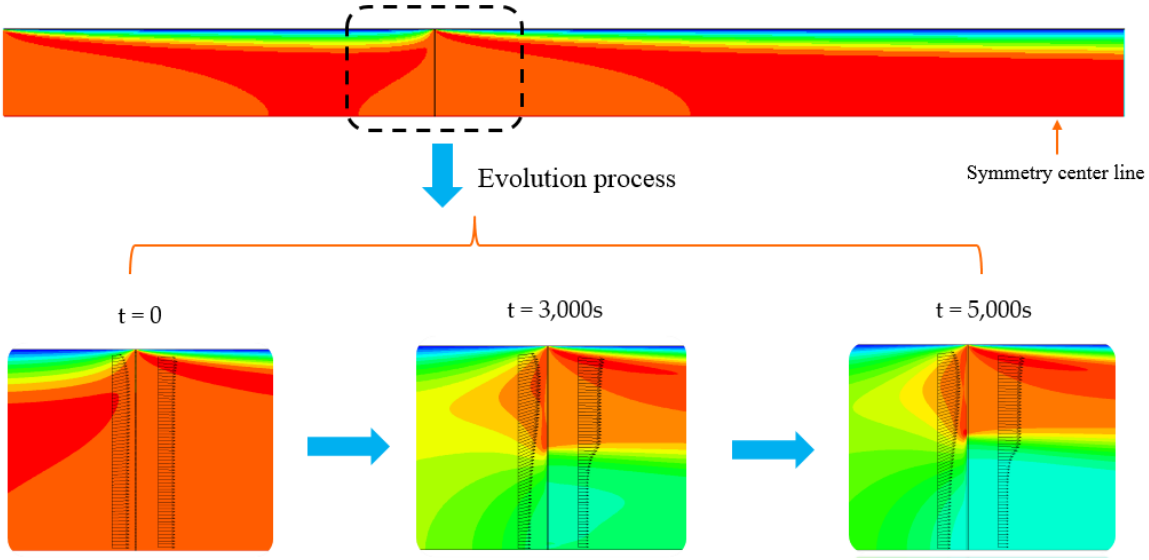

Figure 6.7 Flow evolution as particle loading on filter medium

The permeability of each cells on filter media were also plotted. In Fig. 6.8, the ratio of instant permeability divided by initial permeability is shown in y-axis, the distance from the centerline of filter media is x axis. It is clear to see the distribution and evolution of permeability on filter media panel in the particle loading process. At initial stage, the permeability of filter media is 4.94E-13 m^2, it decreases along with particle loading time.

The flow field will be affected by the evolution of permeability, the flow field will spread to the wall, as a result the particles can deposit to broader region.

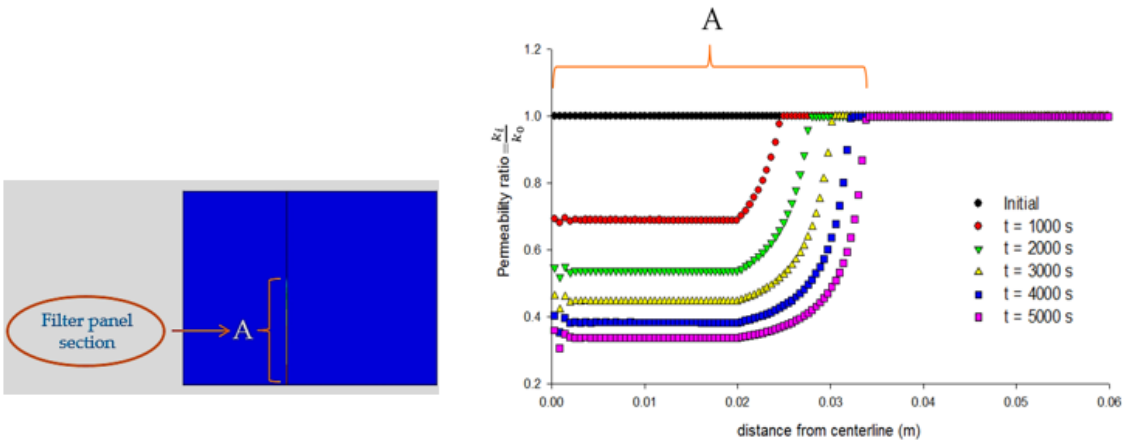

Figure 6.8 The evolution of filter media permeability

Fig 6.9(a) gives us the relationship of pressure drop ratio to mass loaded per unit filter area as non-uniform particle depositing on flat filter media case in pipeline model. The pressure drop is increasing as mass loaded per unit area increases. Initially, the ratio of permeability is 1 due to no particle loaded on filter media, and the ratio is around 1.5 when mass per unit increased to 0.2. Comparison between non-uniform and uniform particle loading was also plotted in Fig 6.9(b). The symbol of the orange Square is standing for the permeability ratio due to uniform particle deposition, the blue square is for non-uniform loading permeability ratio. It is concluded that the permeability ratio of uniform particle loading is continuously higher than the case with non-uniform particle loading at same mass deposited per unit filter area.

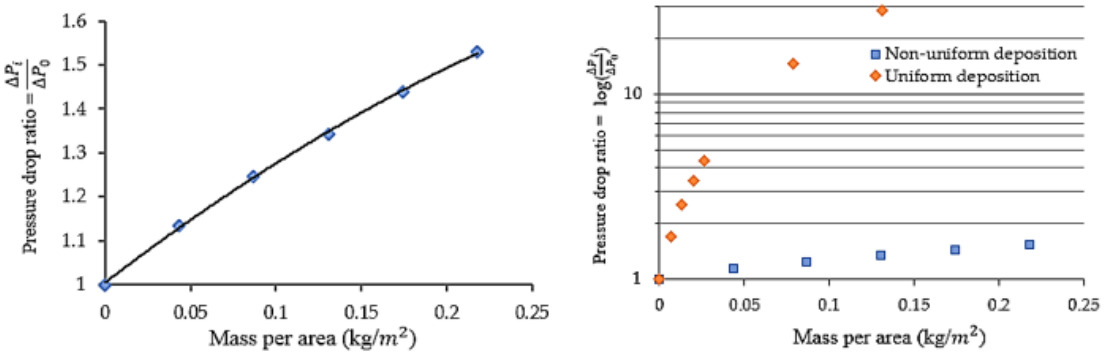

(a) Non-uniform particle loading **(b) Non-uniform vs Uniform particle loading**

Figure 6.9 Results of calculation for flat media

Results and Discussion for Pleated Filter Media Case

For the other model, pleated filter media was installed in the pipeline. Fig. 6.10 shows the evolution of flow field for pleated filter media during the particle continuously loading process. We also obtained the similar results as flat media case. When pleated filters installed, the surface area for collecting particle was much increased on filter media, but less pressure drop was generated under same conditions as flat filter case. It is also observed from Fig. 6.10 that the flow field is almost uniform distributed in the front and at the back of filter media at initial stage. Due to deposition of particles, resulting the decrease of permeability on particle loaded filter media, more flow trends to pass through filter area with higher permeability which is closer to the wall.

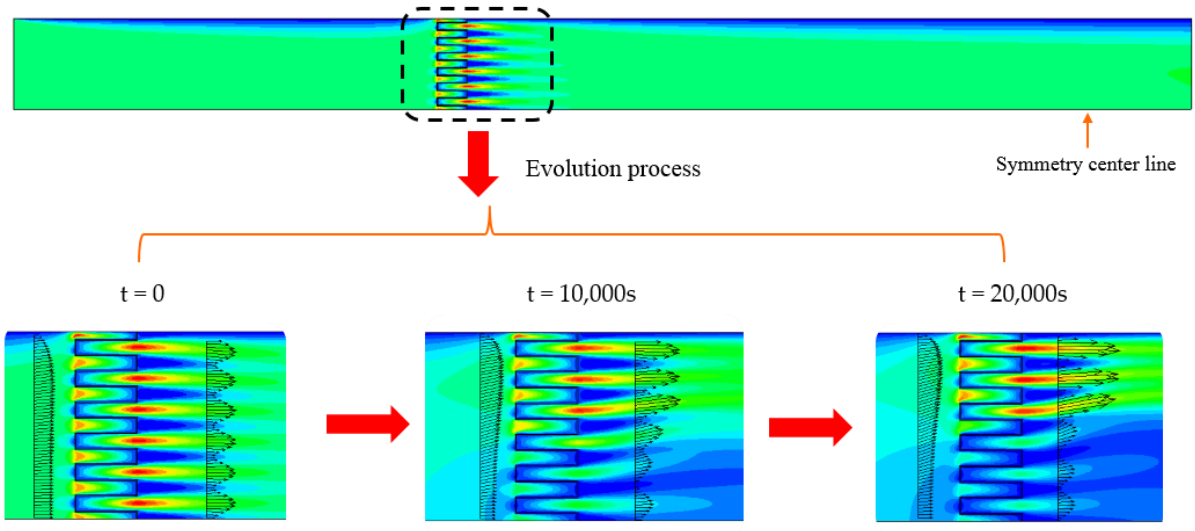

Figure 6.10 Evolution of flow field as pleated filter medium installed

Fig. 6.11 (a) gives us more sense about the distribution of permeability on pleated filter panel. The permeability ratio keep decreasing as particle loaded. The permeability ratio around the corners was changing much. As the filter area close to the wall, the permeability ratio is increasing because of less particles' deposition. The pressure drop ratio was plotted as particle mass deposited per unit filter area as shown in Fig. 6.11 (b). It is concluded that the pressure drop ratio is increasing as more particle deposited, however, to get same pressure drop ratio much more mass needed to be deposited compared with flat filter media case. Thus, pleated filter media have higher capacity for collecting dust particle compared with flat filter media.

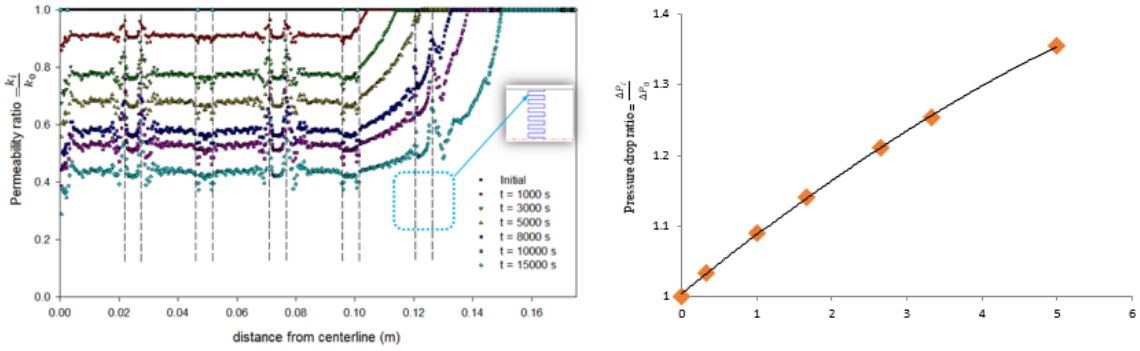

(a) Permeability **(b) Loading curve**

Fig. 6.11 Results of calculation as pleated filter installed

In order to understand the effect of pleating on filter media, we did comparison between our two models mentioned above. It is obviously that both particle deposition area increases with time increases, but the spreading length on pleated filter is much longer than that on flat filter media from bellowing Fig. 6.12. This tells us that pleating design facilitates the spreading of particle deposition on filter surface. As a conclusion, a 2-D modeling was developed to calculate the filter loading curves under the loading of monodisperse particles via ANSYS FLUENT. The effect of media pleating facilitates the spread of particle deposition area on filter surface, resulting in lower pressure drop (as compared with that for flat filter panels).

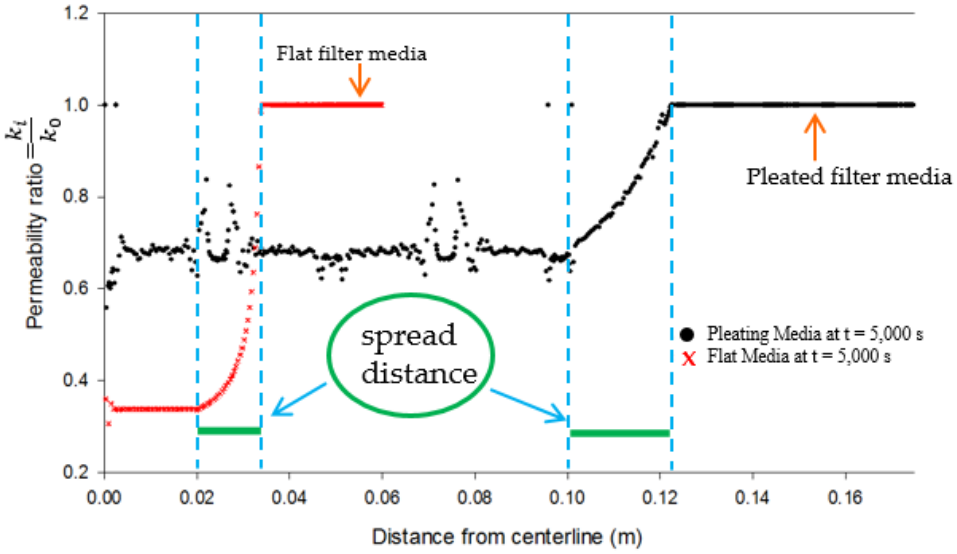

Fig. 6.12 Comparison of flat and pleated filter

6.3 The Effect of Pleat Geometry and Point-release Locations on HVAC Filter Performance under Non-uniform Loading

In this section, we extent our model from 2-D pipe to 2-D open space to study the effect of pleat geometry and point-released locations on HVAC filter performance under non-uniform loading with developed methodology (as Fig. 6.3). The flow field around HVAC filter panel was assumed as turbulent flow field in the whole process. RNG $k-\epsilon$ turbulent model was selected to solve the flow filed here, and the equations used are written as,

$$\frac{\partial}{\partial t}(\rho k)+\frac{\partial}{\partial x_i}(\rho k u_i)=\frac{\partial}{\partial x_j}\left(\alpha_k \mu_{eff}\frac{\partial k}{\partial x_j}\right)+G_k+G_b-\rho\epsilon-Y_M+S_k$$

$$\frac{\partial}{\partial t}(\rho\epsilon) + \frac{\partial}{\partial x_i}(\rho\epsilon u_i) = \frac{\partial}{\partial x_j}\left(\alpha_k \mu_{eff} \frac{\partial \epsilon}{\partial x_j}\right) + G_{1\epsilon}\frac{\epsilon}{k}(G_k + G_{3\epsilon}G_b) - G_{2\epsilon}\rho\frac{\epsilon^2}{k} - R_\epsilon + S_\epsilon$$

where G_k is the generation of turbulence kinetic energy due to the mean velocity gradient, G_b is the generation of turbulence kinetic energy due to buoyancy. Y_M represents the contribution of the fluctuating dilatation in compressible turbulence to the overall dissipation rate, and the equations α_k and α_ϵ are the inverse effective Prandtl numbers for k and ϵ, respectively. S_k and S_ϵ are user-defined source terms. The momentum sink term is also included for filter medium. For the particle trajectory part, ANSYS FLUENT predict the trajectories of particles applying the mean fluid phase velocity when flow is turbulent. We also can include the instantaneous value of the fluctuating gas flow velocity to predict the dispersion of the particles for this study. The discrete random walk model (DRW) is written as,

$$u = \bar{u} + u', \quad u' = \zeta\sqrt{\overline{u'^2}}$$

where ζ is a normally distributed random number.

Again, the model of Bergman *et al.* (1978) was utilized here to estimate filter permeability changed under the particle loading process, and the expression for the relative viscous resistance which is the reciprocal of permeability combined with Darcy's law is as following, where $\alpha_f = 0.02$, $d_f = 1\ um$, $d_p = 0.5\ um$,

$$VR = 64\left(\frac{\alpha_f}{d_f} + \frac{\alpha_p}{d_p}\right)^2 \sqrt{\left(\frac{\alpha_f}{{d_f}^2} + \frac{\alpha_p}{{d_p}^2}\right)}$$

Four types of pleated filter with different pleating geometry were established. The dimension of the computational domain is same for all four cases. The length of HVAC channel is 600 mm, and the entrance filter width is 12 mm. We defined the external space as sphere with diameter d of 2000 mm. We have two types of pleating density and two kinds of pleating height. The pleating density of first pleated filter panel is 3.175/inch with 50 mm pleating height. The second one has the same pleating density but 30 mm pleating height. The third pleated filter model has 1.27/inch of pleating density with pleating height of 50 mm. And the last one is 1.27/inch pleating density with 30 mm pleating height as shown in Fig. 6.13.

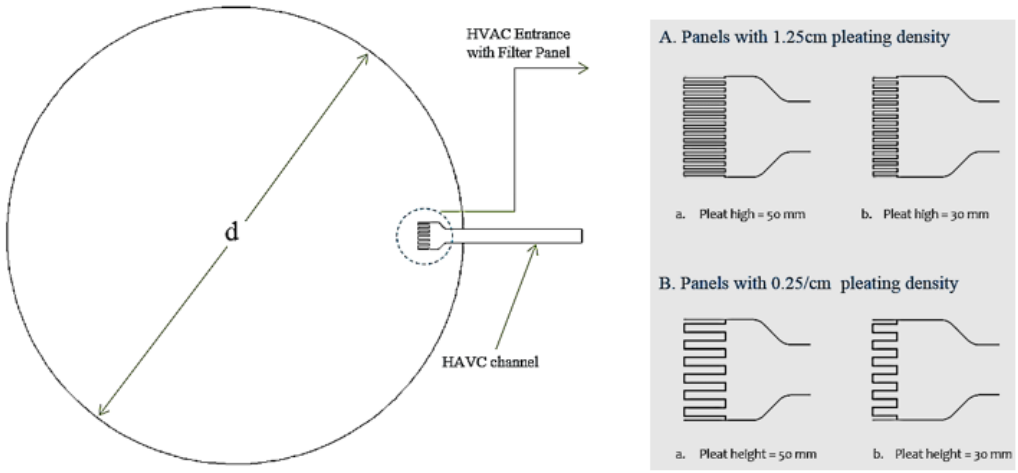

Figure 6.13 Geometry models and typical mesh size distribution

Fig. 6.14 shows how we defined the boundary conditions for the models. The whole sphere was treated as open space and set as inlet, from which air fluid comes from. The right end of the pipe channel was outlet where the fluid would be sucked in. The pleated filter media part was defined as porous zone. An example of mesh was given to show how we generate mesh for the whole model, the typical mesh distribution around filter panel was also shown in an enlarged view.

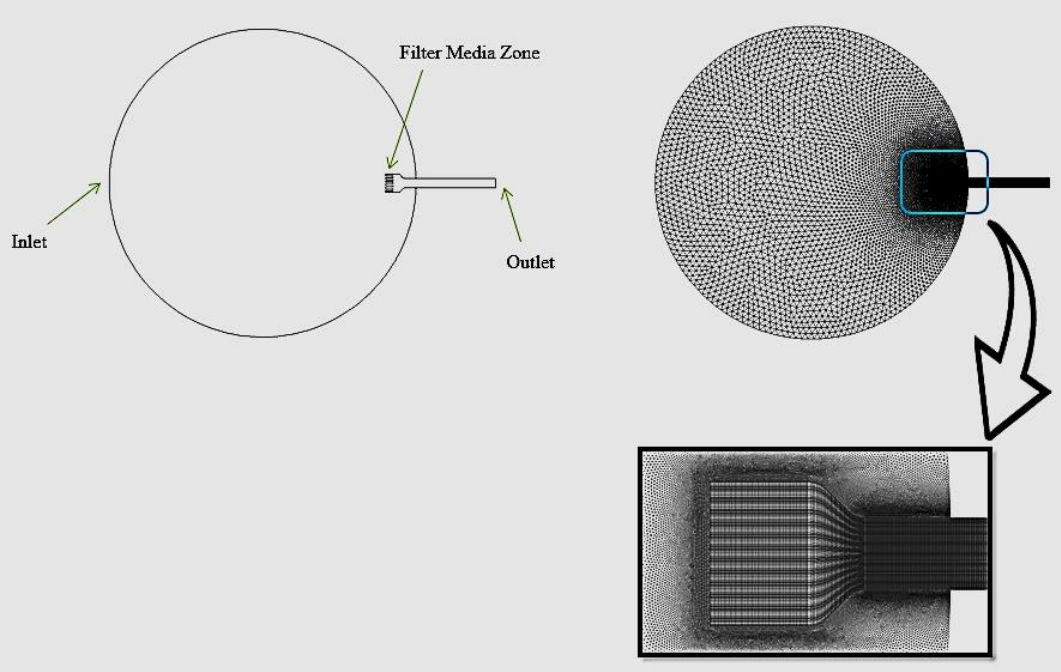

Figure 6.14 Diagram of Boundary Setup and Typical Mesh Distribution

Additionally, Table. 6.2 lists the detailed parameters for initial boundaries conditions used in the calculations, all cases with different pleating geometry have exactly same initial boundary conditions. The viscous resistance is 1.81E+12 ($1/m^2$) in each direction. The face

velocity was kept as 0.1 m/s passing through filter media. Three zones were created including porous zone for filter media, upstream open space and downstream fluid zones.

Table 6.2 Boundaries conditions for pleated filter cases

PHYSICAL BOUNDARY/ZONE	BOUNDARY/ZONE CONDITIONS
Filter Face Velocity	V = 0.1 m/s
Pressure inlet	Zero gauge pressure (Pascal)
Interior-L	Porous jump, face permeability=1E+10 (m^2)
Wall	Standard wall function
Filter Media Zone	Porous zone, viscous resistance in direction of x, y = 1.81E+12 ($1/m^2$)
Flow-1 & 2 Zone	Standard fluid conditions, pressure=1atm

Table 6.3 gives all the flow parameters for four cases with different pleating geometry situations investigated in this study. Because the face velocity was constant as V = 0.1 m/s through HVAC panel filter medium in all cases, as a result the other relevant parameters are all different in this table, i.e., outlet velocity, Reynolds number, total flow rate.

Table 6.3 Flow parameters for each case

	1.25/cm pleat density 50 mm pleat height	1.25/cm pleat density 30 mm pleat height	0.5/cm pleat density 50 mm pleat height	0.5/cm pleat density 30 mm pleat height
Outlet Velocity (m/s)	2.66	1.66	1.184	0.784
Reynolds number	105,336	65,736	46,886	31,046
I (turbulent flow intensity)	0.038	0.040	0.042	0.044
Hydraulic Diameter (mm)	60	60	60	60
2D_Filtetr Surface (mm^2)	1,596	996	710.4	470.4
Q, total flow rate (m^3/s)	0.1596	0.0996	0.07104	0.04704

For the locations of particles injecting, five point locations were selected that they were located on half circle of the external space (see Fig. 6.14) to be the particles releasing sources. Because the external space is symmetrical to the centerline of HVAC channel, we only need to study the upper half point locations. It is still a question about the particles releasing source location in the external space, and how these locations affect the distribution of particle deposition on filter panel. Thus, we aim to understand the effect of particles' release locations on the deposition distribution of particles on filter medium.

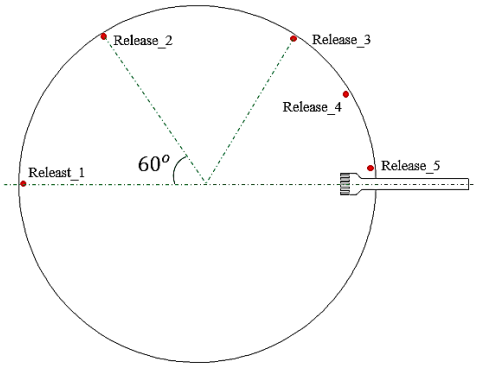

Figure 6.14 Point-release locations on the model

The general correlation to calculate the pressure drop across filter panels with rectangular pleat shape can be expressed as:

$$\frac{\Delta P}{\Delta P_m} = 1 + 1.85 \frac{8}{K} \frac{L^2}{(W-t)^3}$$

where ΔP_m is the pressure drop of filter media, L is pleat height, W is pleat space, t is the thickness of filter media, K is the constant of filter media, defined as the pressure drop per unit media face velocity. Combine with the VR previously derived, the pressure drop over pleated filter panel under uniform particle deposition can be obtained as,

$$\Delta P = \Delta P_m \left(1 + 1.85 \frac{8}{K} \frac{L^2}{(W-t)^3} \right)$$

With the implement of the method developed in previously section, we are able to simulate the process of particle loading on filter medium for each designed case. In the following part, some of important results will be given. The filter constant ratio, $R = \frac{k_0}{k_i}$, is

defined, where k_0 is the permeability of clean filter media and k_i is the permeability at the time of $t = t_i$. Fig. 6.15 is the plot of relationship between filter constant ratio and distance from filter panel top for the model with 1.25/cm pleat density and 50mm pleat height. It is found that the filter constant ratio R increases as particles loaded. Due to the location of particle releasing source, Location_1, it is noticed that the permeability distribution is almost symmetrical on filter panel. We also can observe that more particles were deposited on the front of panel in the pleated filter media, and less particle deposited the deeper part of the pleated channel.

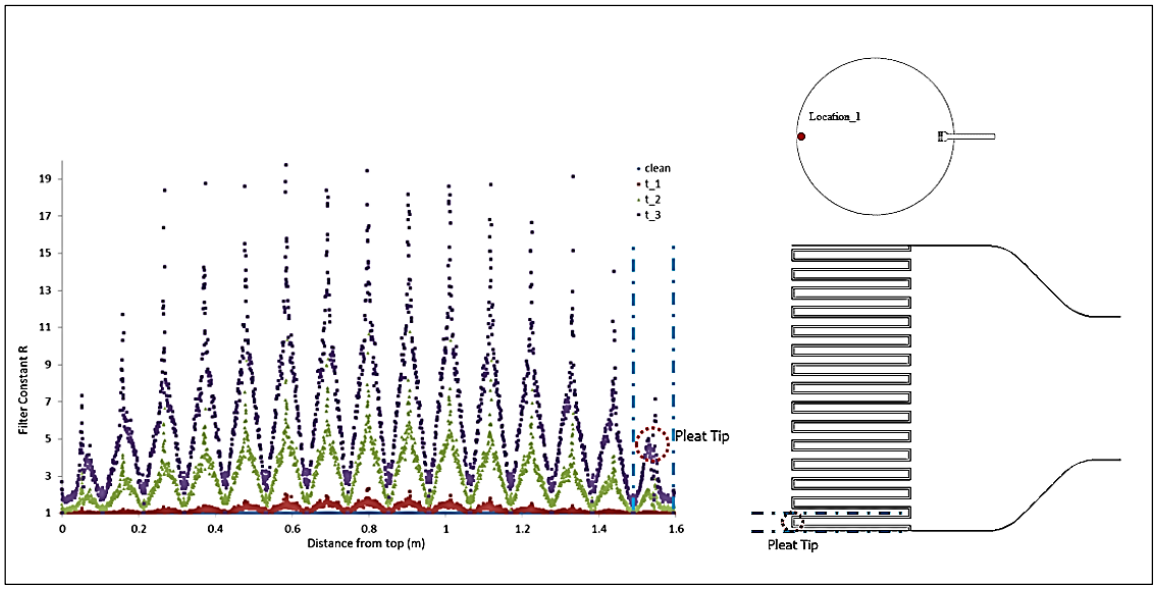

Figure 6.15 The evolution of constant R on pleated filter medium at different time step

For the same pleating geometry of filter media condition, we also calculated and concluded other cases with particles released from different locations as shown in Fig. 6.16 (a), from which it is not hard to find the difference among them. As the particles releasing

source get close to HVAC filter panel, the non-uniform distribution of particles on filter panel becomes more obvious. Fig. 6.16 (b) shows the evolution of solidity on filter media in the process of particle loading. Apparently, similar observation was found that the non-uniform distribution of particles is becoming obvious as the point release location moving to closer to head of HVAC pleated filter panel.

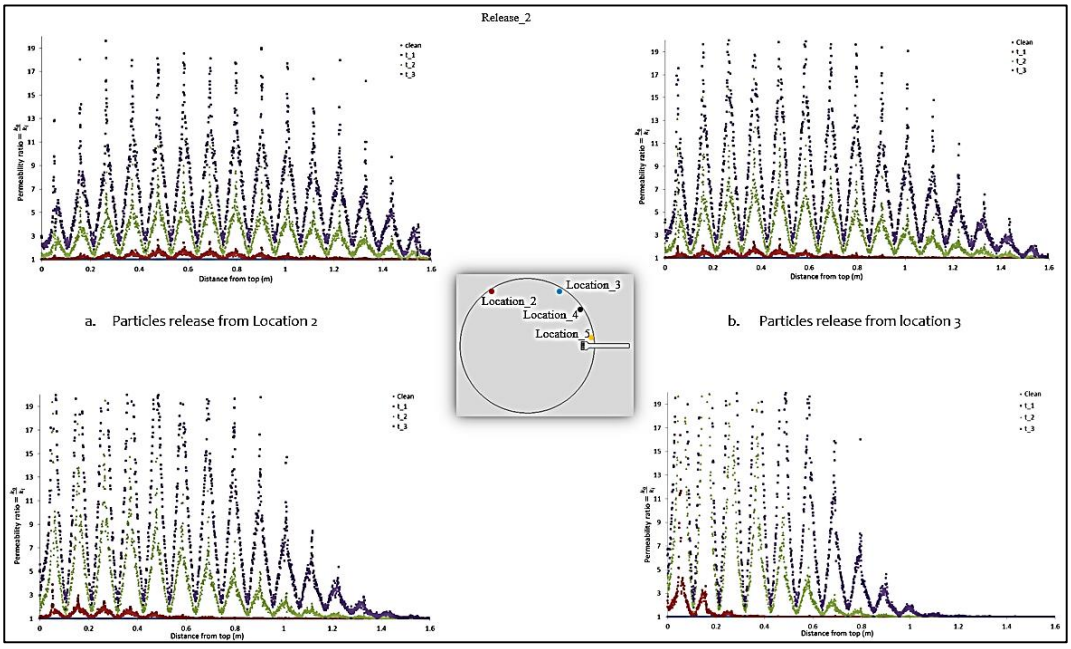

(a) Permeability change under point-released particle loading

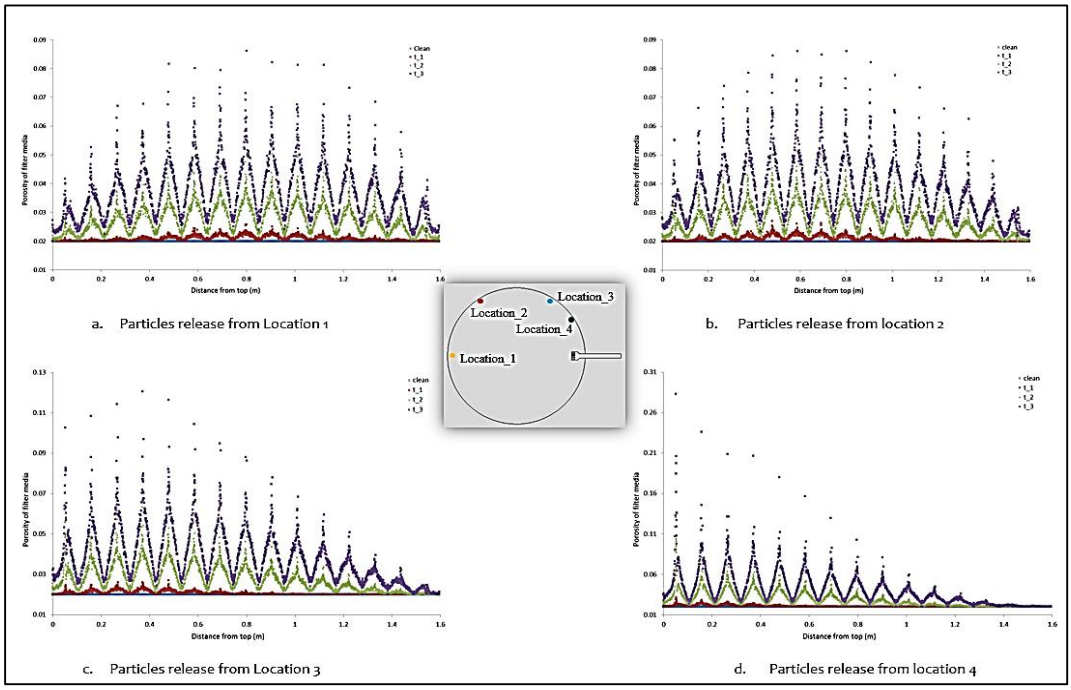

(b) Solidity change under point-released particle loading

Figure 6.16 Results for pleated filter media loading

The pressure drop under point-released particle loading was calculated and plotted in Fig. 6.17, as well as uniform particle loading. In Fig. 6.17, the entrance filter media with pleat density of 1.25/cm and pleat height of 50mm was studied. We noticed that the pressure drop of filter panels in general increases under the point-released particle loading condition, the pressure drop ratio can reach high to 5 as particle loaded. Based on the comparison, it is found that the particle release location has its effect on the pressure drop of filter panels: the filter panel pressure drop decreases as the particle release location moves to the back of entrance filter panels. In the case, the filter panel pressure drop under the point-released particle loading is in general lower that that under the uniform particle loading condition.

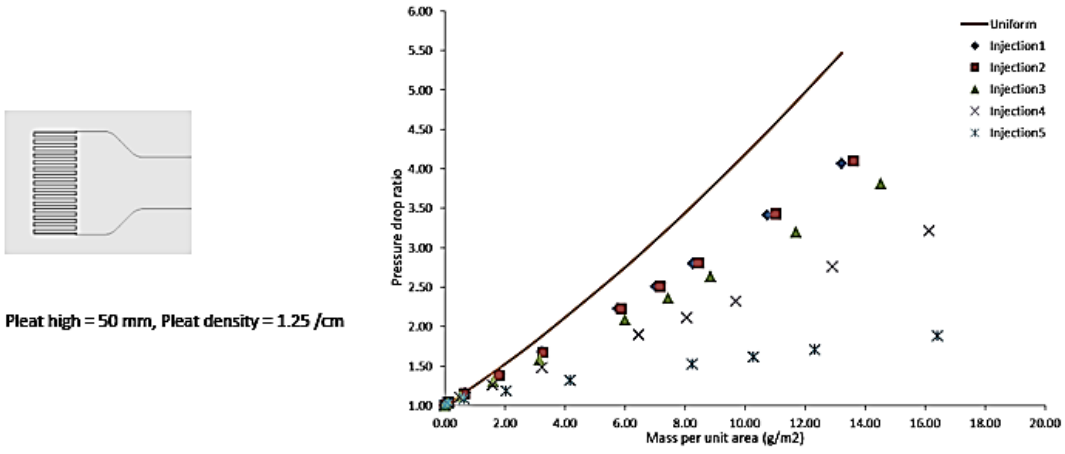

Figure 6.17 Pressure drop under point-released particle loading for flat media

For pleat filter media with pleat density of 0.5/cm and same pleat height of 50 mm, the pressure drop under point-release particle loading was also calculated to determine if there is any effect of pleating geometry. Fig. 6.18 plots the curves to show the relationship between pressure drop ratio and mass deposited per unit area, where the pressure drop of filter panels increases under the point-release particle loading condition. In general, the particle release loactions affect the pressure drop of filter panels. For the case with pleat density of 0.5/cm and pleat height of 50mm, the filter panel pressure drop under uniforma particle loading is between two injections' curves under non-uniform particle loading.

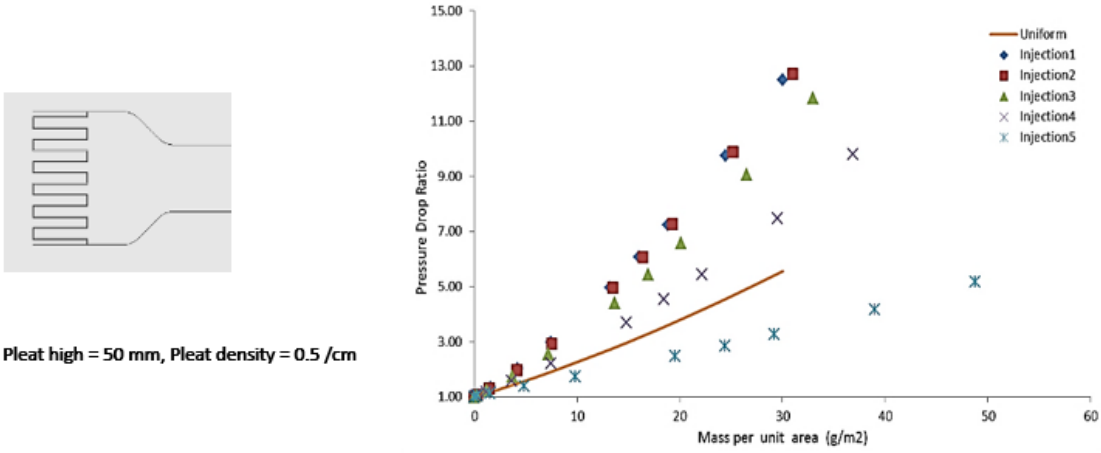

Figure 6.18 Pressure drop under point-released particle loading for pleated filter

Results and Discussion – Pleat Height

Four types of HVAC entrance filter panel with different pleating geometry were created to investigate the influence of pleating geometry on the pressure drop due to loaded particles. The pressure drop ratio to mass deposited per unit area were plotted together for comparing the effect of pleat height when filter model have same pleat density. In Fig. 6.19 (a), two pleat filter models both having pleat density of 1.25/cm were compared including pleating height of 50mm and 30mm. From the plot of pressure drop ratio to mass deposited per unit filter area, we could see that the pressure drop ratio with pleat height of 50 mm is slightly lower compare to that with pleat height of 30 mm. However, in Fig. 6.19 (b), both filter models have pleat density of 0.5 /cm, two pressure drop ratio lines are almost overlapped to each other. As a conclusion here, it is found that the pleat height doesn't have much effect on the pressure drop ratio.

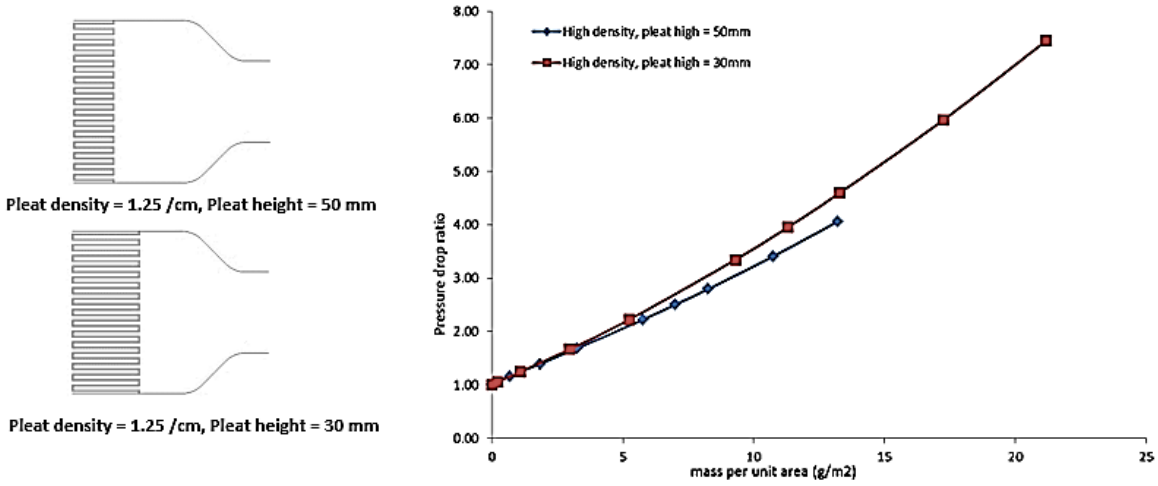

(a) Pleat density =1.25/cm

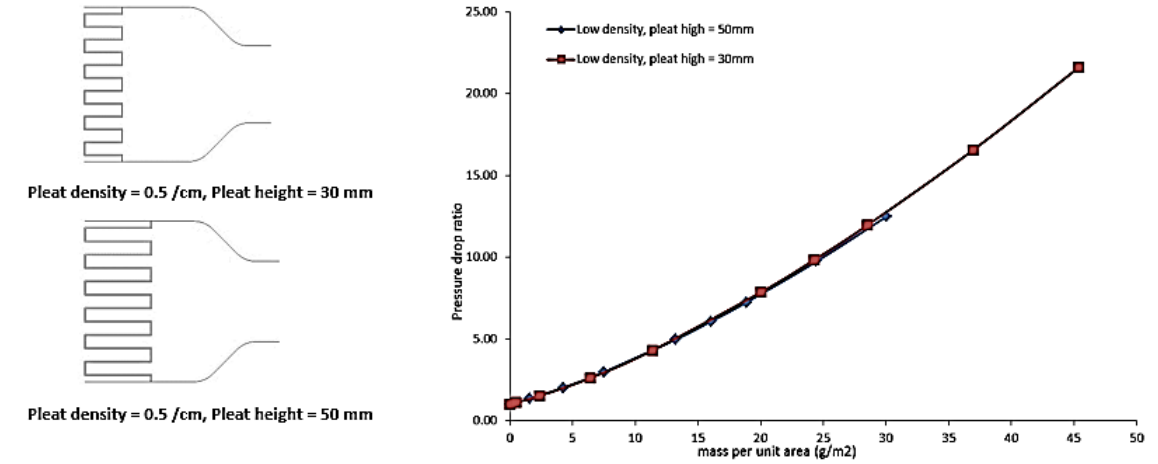

(b) Pleat density =1.25/cm

Figure 6.19 Pressure drop comparison between different pleat heights

Results and Discussion – Pleat Density

To compare the influence of pleat density on the pressure drop raito curves, we compared the filter models with pleat density of 1.25/cm and 0.5/cm at same pleat height conditions. Fig. 6.20 (a) shows the comparison of pressure drop ratio of two pleat density models when both pleat height are 50mm, in which the pressure drop ratio is keeping lower for the case with pleat density of 1.25/cm compared to the other case with pleat density of 0.5/cm. When pleat height equal to 30 mm, it is also noticed that for the filter media model with pleat density of 0.5/cm, the pressure drop ratio is higher than that with pleat density of 1.25/cm.

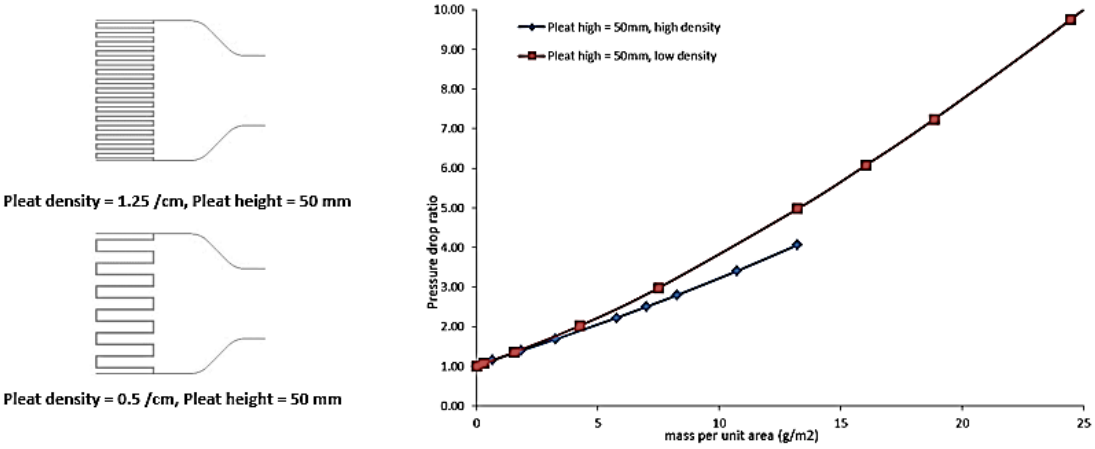

(a) Pleat height = 50 mm

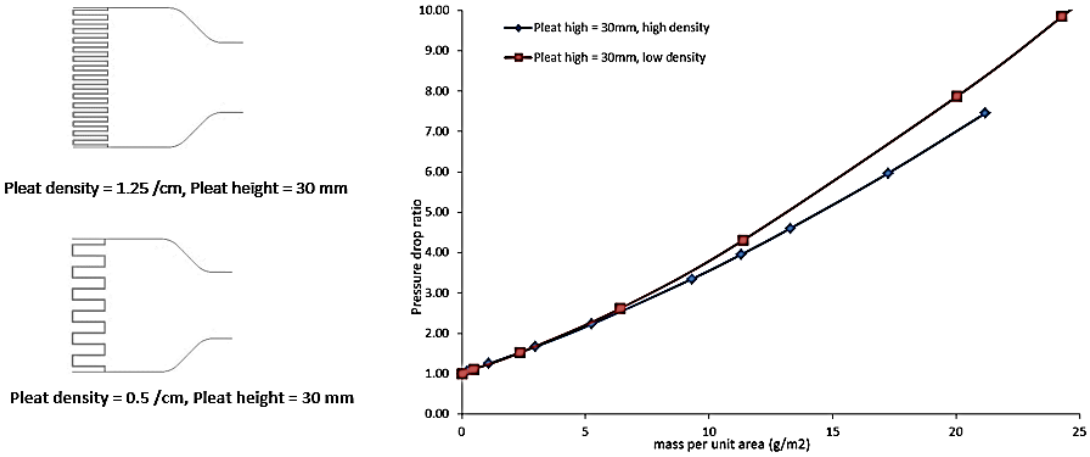

(b) Pleat height = 30 mm

Figure 6.20 Pressure drop comparison between different pleat densities

6.4 The Performance of Filter Panels in the Presence of Flow Obstruction near the HVAC Entrance

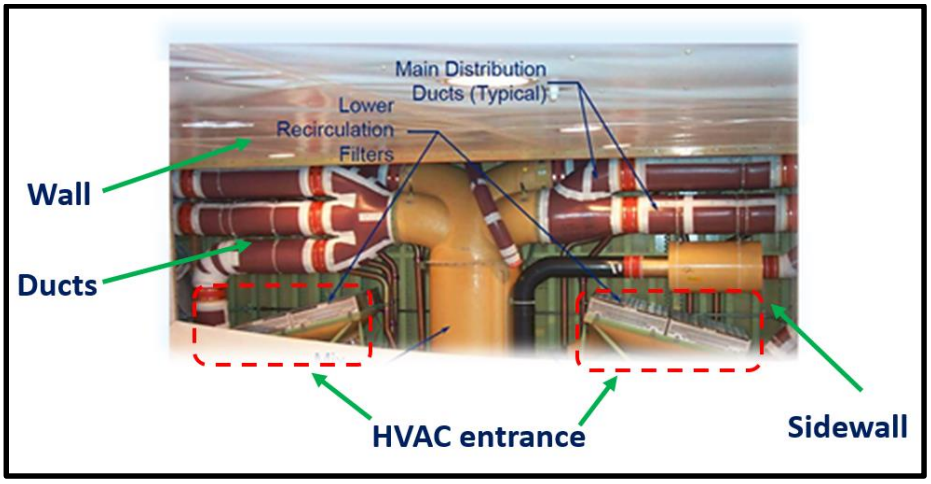

Figure 6.21 Diagram of aircraft HVAC entrance filter panel

In the real world application for HVAC entrance filter panel, there are existing many possible obstacles around filter panels that could bring flow field obstruction or distortion. For example, as shown in Fig. 6.21, it's a HVAC filter entrance panel which is installed in cargo area on an aircraft. The filter panels are indicated by the dashed red rectangle, as well as the wall and mix manifold. In this study, we focus on the investigation of wall effect on the particle loading of HVAC entrance pleated panel filters. Three different possible relative positions were considered between the wall and HVAC entrance panels: the first category was vertical front wall that exists in the front of filter entrance panel; second type was back vertical wall which was located behind the pleated entrance panel; and the last one was inclined wall placed in front of the filter entrance panels. The example diagram of three walls has been plotted in Fig. 6.22.

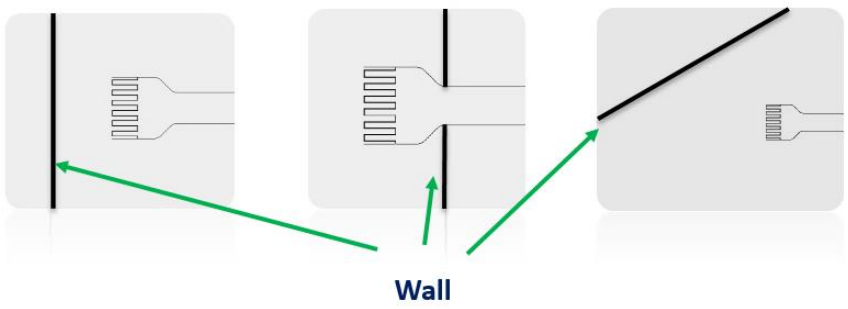

Figure 6.22 Diagram of wall positions

The four types of pleated filter with different pleating geometry were used to study the wall effect. The length of HVAC channel is 600 mm, and the entrance filter width is L = 120 mm. The distance between wall and pleat filter panels was defined in the ratio of L. Six types of distance were set for the front vertical wall away from pleated filter panel,

including 1L, 3L, 5L, 10L, 20L, and 20L. For the back vertical wall away from pleated filter panel, four types of distances were chosen as 1L, 3L, 5L and 10L. For the inclined wall case, two angles between the wall and HAVC entrance centerline were defined.

Two types of pleating density, as well as two types of pleating height were applied here for the HVAC entrance filter panel. The pleating density of first pleated filter panel is 1.25/cm/ with 50 mm pleating height. The second one has the same pleating density but 30 mm pleating height. The third pleated filter model has 0.5/cm of pleating density with pleating height of 50 mm. And the last one is 0.5/cm pleating density with 30 mm pleating height. Fig. 6.23 gives all the geometry models as show in the following.

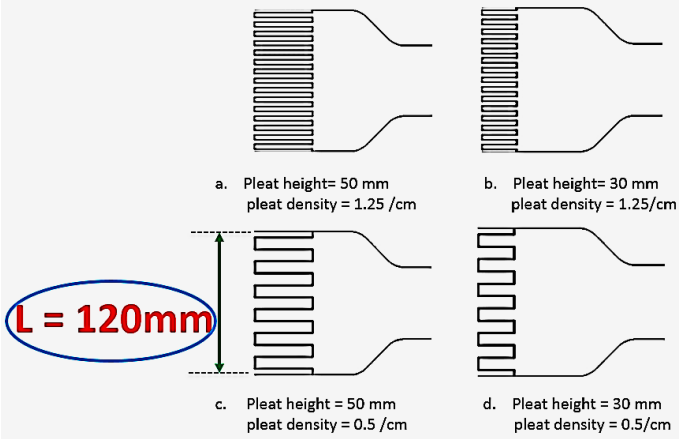

Figure 6.23 Diagram of pleat filter panels

The flow field was assumed as turbulence flow. RNG k-ε model was utilized for calculate the flow field. There was a momentum sink term included in the filter media. For the particle trajectory part, stochastic tracking and DRW model were enabled. All the

detailed information about the governing equations for the study could be referred to Chapter 6.3.

All the particles were released uniformly from the locations close to the open-space as show in Fig. 6.24, in which the outlet was indicated as two red curves and all particles were uniformly distributed along the outlet before particle injection process. The front vertical wall was also pointed out in the plot, as well as the HVAC channel. The particles were mono-size of 5 μm diameter, and the number of particles was set as 10,000 for each injection. There was no initial velocity for each direction.

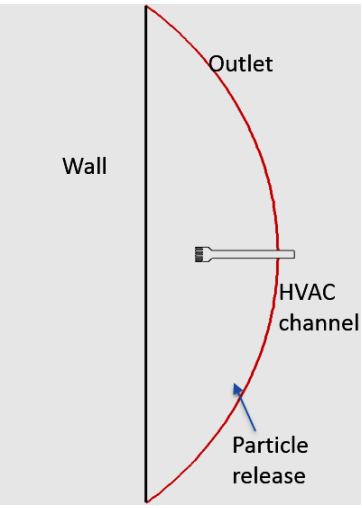

Figure 6.24 Diagram of model

Results and Discussion – Wall Effect

Effect of the Front Vertical Wall

Fig. 6.25 show the pressure drop ratio evolution as particles deposited on pleated filter media in the presence of different front walls. The left two diagrams gives an example of the relative locations for walls and pleated filter media, and six types of wall were applied. The filter media studied here has pleat density of 0.5/cm and pleat height of 50 mm. It is noticed that the pressure drop ratios are keeping nearly constant as long as the distance is greater than 10L between the wall and pleated filter media at different time step. As the distance is less than 10L, it is found that the pressure drop ratio were constant almost for different wall cases before time step T = 15, while sharp change of pressure drop ratio occurred as particle deposited after T = 15. As front wall moves close to the pleated filter media, the pressure drop ratio across filter is getting higher which illustrates that the front vertical wall have its effect on particle deposition on filter panels.

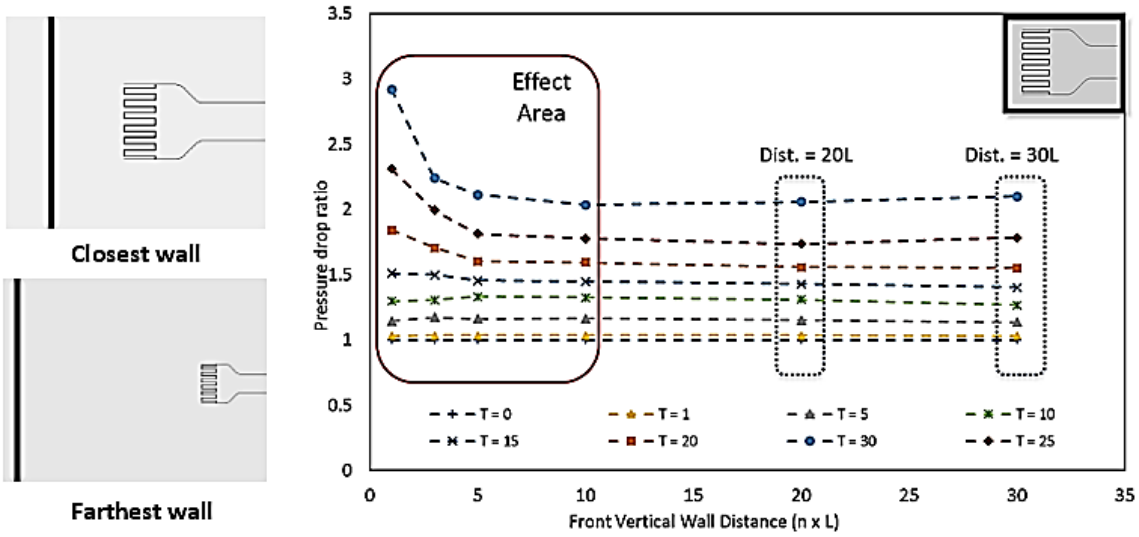

Figure 6.25 Pressure drop ratio evolution for various front vertical walls

The local permeability distribution on filter panel was also plotted under particle loading conditions as shown in Fig. 6.26. I only plotted the distribution of initial and final steps when the front vertical wall was placed at L and 30L apart from pleated filter panel. In this figure, X axis is location position of filter panel; Y axis is permeability ratio equal to instant permeability divided by initial permeability. The particle started to deposit from the center part of pleated filter medium. We also defined the filter cell is blocked when solidity higher than 0.6. The statistical summary was listed for four different wall distance cases in table 6.4, where we can find that the particle deposited area is highest when wall distance = L, and the clogged area on filter is also highest. As a result, the pressure drop ratio is highest when the front vertical wall was placed at distance of L away from pleated filter panel.

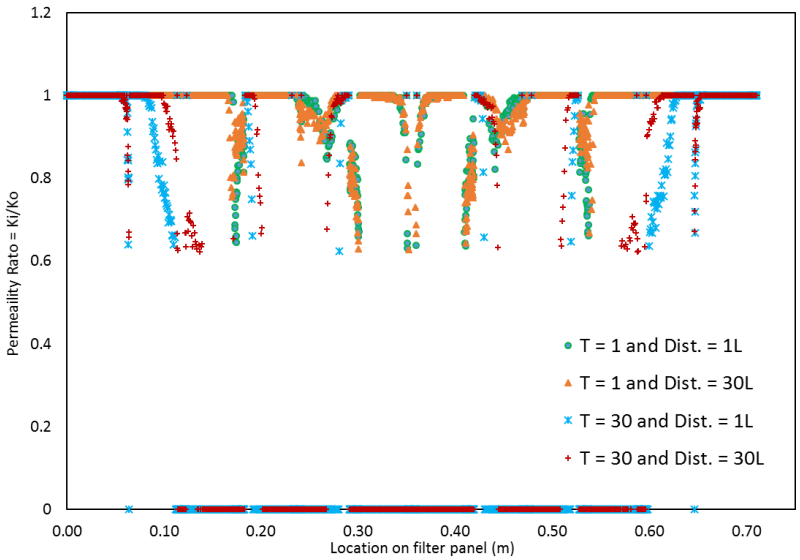

Figure 6.26 Local permeability distributions on filter panel when front wall placed

Table 6.4 Statistical summary for front vertical wall case

	Initial particle deposited area ratio (T = 1)	Final particle deposited area ratio (T = 30)	Blocked area ratio
Dist.= L	0.30	**0.77**	**0.66**
Dist.= 5L	0.31	0.70	0.57
Dist.= 10L	0.31	0.70	0.55
Dist.= 30L	0.32	0.71	0.57

Effect of the Back Vertical Wall

For the back vertical wall effect, the curves of pressure drop ratio were plotted for different distance cases. As seen from Fig. 6.27, two diagrams show the relative locations between the back vertical wall and pleated filter. Overall, the pressure drop across filter panel increases as particle loading process for all cases. The effect area was circled out by the rad square when the distance is less than 5L between back vertical wall and pleated filter panel, the pressure drop ratio decrease as the back wall getting close to the filter panel.

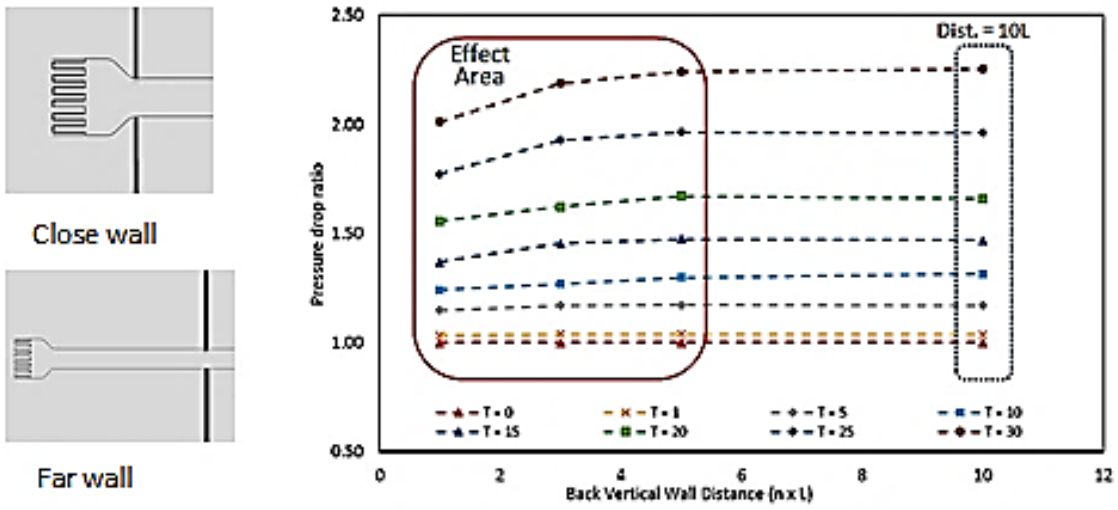

Figure 6.27 Pressure drop ratio evolution for various back vertical walls

The distributions of local permeability ratio was also plotted for each cell on the filter panel. In Fig. 6.28, it is found that all particles were trending to deposit on the middle part of the filter media panel, and then spreading to other two ends. The statistical summary was also concluded in Table. 6.5 for the initial and final area ratio of particle deposited area and clean filter area, as well as the blocked area ratio. We can find that the initial particle deposition area ratio is higher when the back vertical wall was getting close to filter panel. But the clogged area ratio on filter panel is lowest when the distance is smallest between filter panel and the back vertical wall. More clogged area on filter panel could cause higher pressure drop across filter media.

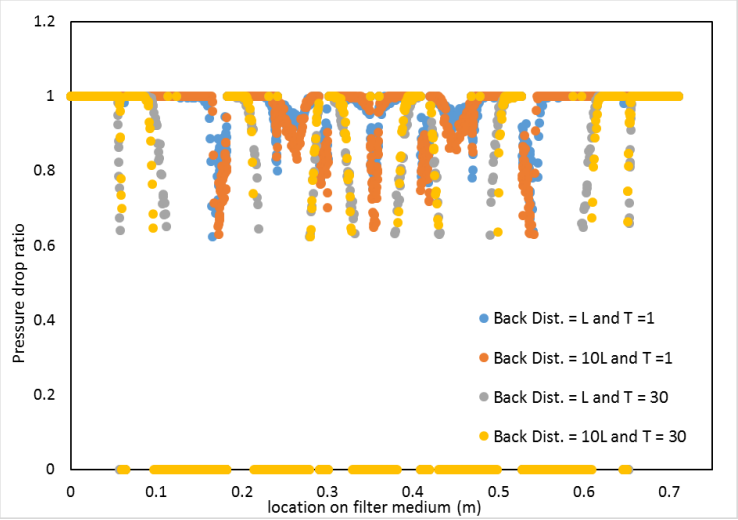

Figure 6.28 Local permeability distributions on filter panel when back wall placed

Table 6.5 Statistical summary for back vertical wall case

	Initial particle deposited area ratio (T = 1)	Final particle deposited area ratio (T = 30)	Clogged area fraction
Dist.= L	0.40	0.76	**0.57**
Dist.= 3L	0.36	0.76	0.60
Dist.= 5L	0.36	0.75	0.61
Dist.= 10L	0.33	0.74	0.61

Effect of the Inclined Wall

The effect of inclined wall on the particle deposition on filter panels was also investigated. Fig. 6.29 shows the diagram of two types inclined wall studied here, one is 30 degree between the inclined wall and centerline of pleat filter panel and the other one is 60 degree. In both cases, the distances are 5L from the pleat filter panel to inclined wall. In the right plot of Fig. 6.29, the pressure drop ratio to mass deposited per unit area were plotted for two inclined walls and vertical wall. It is found that three loading curves were almost overlapped to each other which means the effect of inclined wall doesn't have much effect on the loading of particles when the walls are 5L away from pleated filter panels.

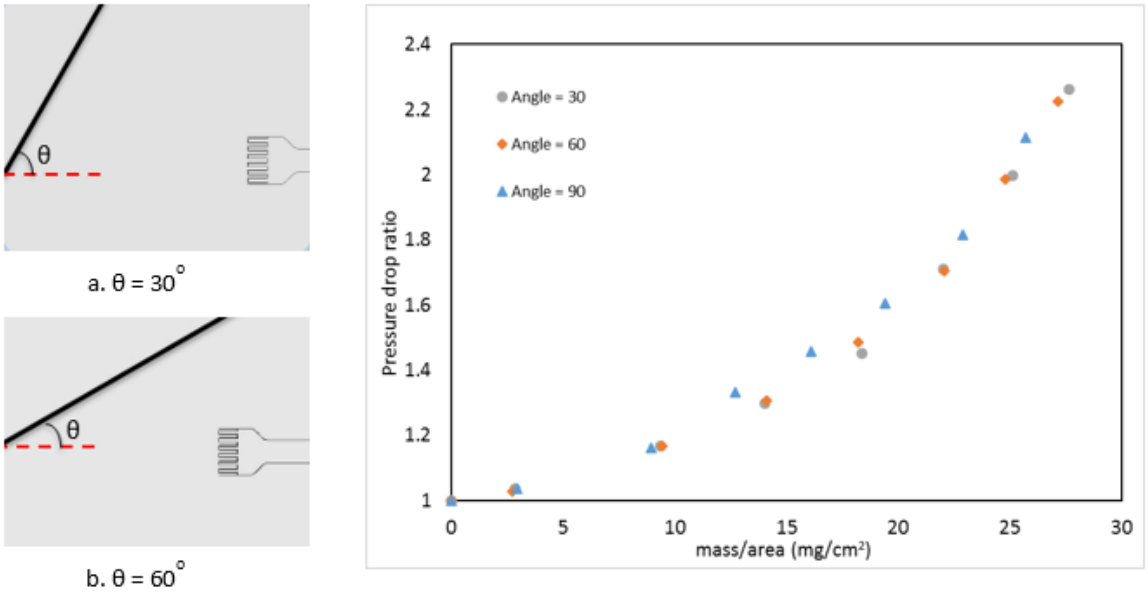

Figure 6.29 Effect of inclined wall

Effect of the pleating geometry

Four types of pleated filter media model were applied for studying the effect of pleating geometry on the particle loading curves. Fig. 6.30 gives the loading curves for different front vertical walls when the HVAC filter entrance with pleat density of 1.25/cm and pleat height of 30mm. The pressure drop ratio is increasing as particles collected on filter panels. All the loading curves are very close to each other at different value of X (mass deposited per unit filter area).

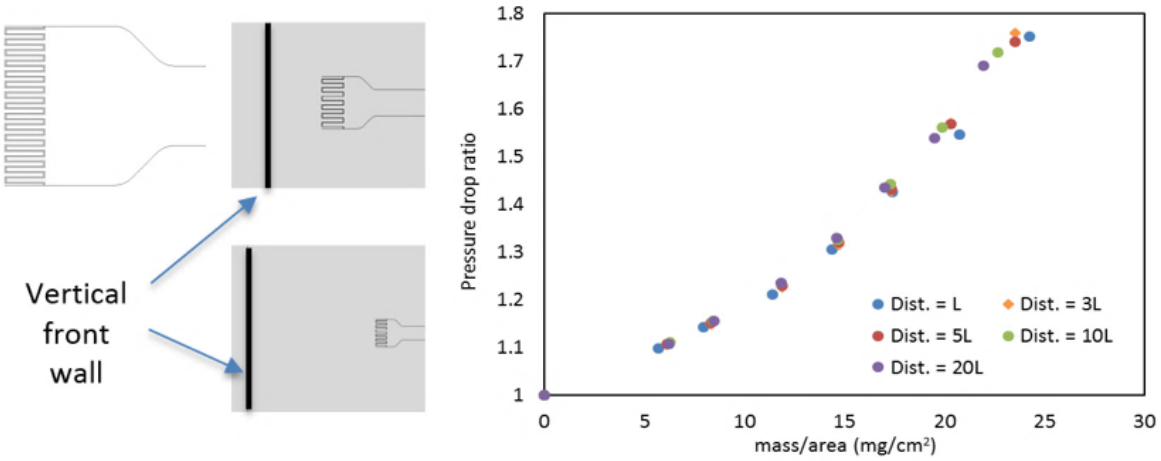

Figure 6.30 Effect of pleating geometry, pleat height=30mm pleat density=1.25/cm

Fig. 6.31 is showing the loading curves when filter entrance model with pleat density of 1.5/cm and pleat height of 50mm. The pressure drop ratio is keeping increase as dust particles collected by the filter panels. The similar situations could be observed that all loading curves with different wall locations to filter panel are overlapped.

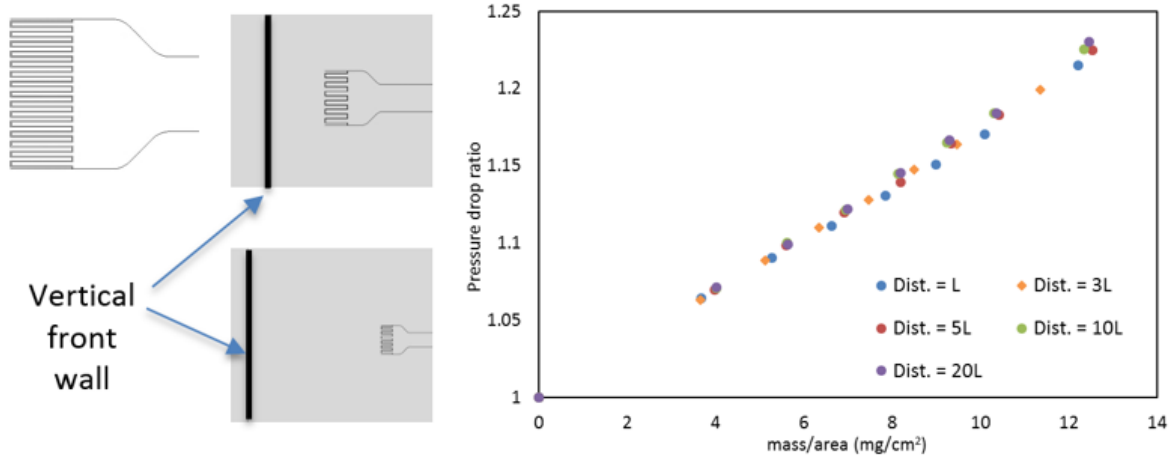

Figure 6.31 Effect of pleating geometry, pleat height=50mm pleat density=1.25/cm

Fig. 6.32 is giving other two types of pleat filter entrance models that were placed in the front of wall. Fig. 6.32(a) is the case for filter entrance model with pleat density of 0.5/cm and 50mm, Fig. 6.32(a) is for pleat filter model with pleat density of 0.5/cm and pleat height of 30mm. In both plots, the pressure drop ratios are increasing as particles filtered by the filter panels. We also notice that all the loading curves are overlapped to each other. Therefore, the loading curves are not affected by the pleating geometry of HVAC filter entrance models when the front vertical walls were placed at different distance apart from the filter panel.

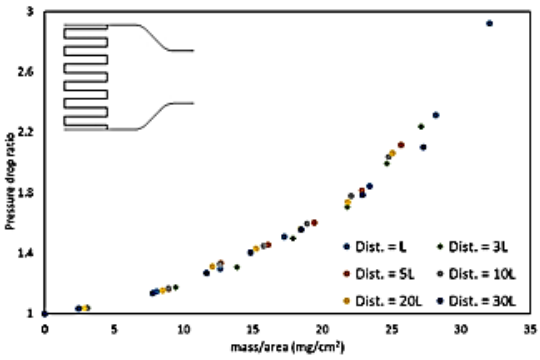

Figure 6.32(a)

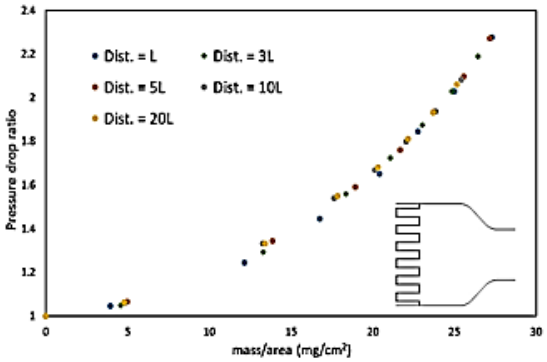

Figure 6.32(b)

Figure 6.32 Effect of pleating geometry, pleat density=0.5/cm, pleat height (a) 50mm (b) 30mm

When the vertical wall was placed on the back of HVAC filter panels, four distances were determined as previous. We also studied the effect of pleating geometry for filter entrance panels. The same four types of filter panel models were utilized again. In Fig. 6.33, the loading curves are plotted as mass collect per unit filter area for the four filter entrance models at different distance away from back vertical walls. In all figures, we could see that

the loading curves increase as particle deposited, but for each case all loading curves are very close under the condition that the distances are different between the back vertical wall and pleat filter panels. It can be concluded that the effect of filter pleat geometry is not affecting the loading curves when the back vertical is presented.

We also investigated the effect of pleating geometry for different inclined walls, including 30 and 60 degree as mentioned above. The similar summary was obtained as front and back vertical wall. For the loading curves, the pleating geometry would not affect.

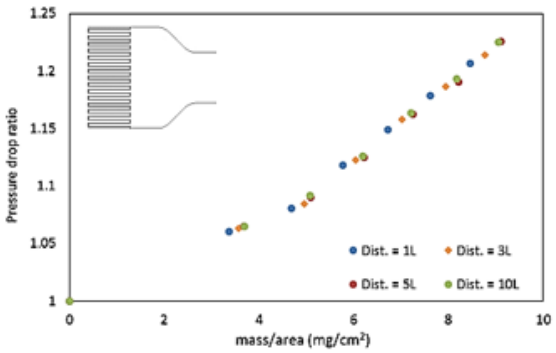

Figure 6.33(a)

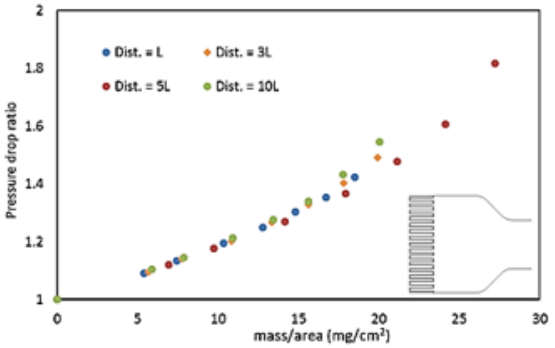

Figure 6.33(b)

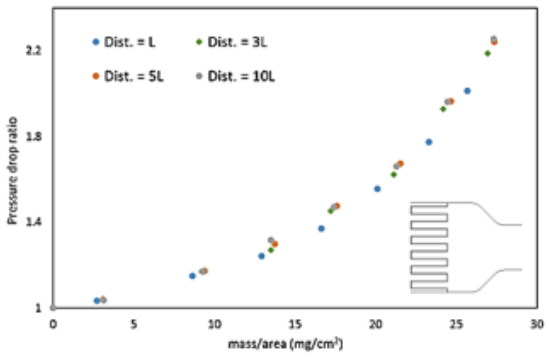

Figure 6.33(c)

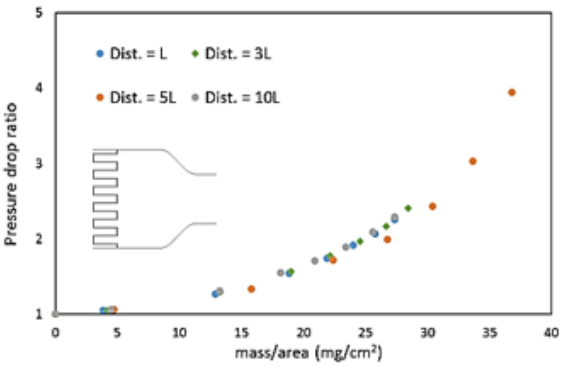

Figure 6.33(d)

Figure 6.33 Effect of pleating geometry, (a) pleat density=1.25/cm, pleat height=50mm (b) pleat density=1.25/cm, pleat height=30mm (c) pleat density=0.5/cm, pleat height=50mm (4) pleat density=0.5/cm, pleat height=30mm

6.5 Summary

A 2-D modeling has been developed to calculate the filter loading curve under the loading of monodisperse particles via ANSYS FLUENT. When filter panels were installed in the pipeline, the effect of media pleating facilitates the spread of particle deposition area on filter surface, resulting in lower pressure drop as compared with that for flat filter panels. Besides, a 2-D numerical open-space model for pleated entrance HVAC filter panels under the point-release particle loading was also developed. It is noticed that particles release location affect the pressure drop across entrance filter panels under the point-release particle loading. Within the studied the cases, filter pleat density has more influence than pleat height for lowering the pressure drop of loaded entrance filter panels. Besides, the 2-D open-space modeling for HVAC filter panel has been developed and studied in the presence of flow obstruction. The wall does have effect on the performance of HVAC filter panel. The total pressure drop increases as the front vertical wall getting close to filter panel. But, as back vertical wall getting close to filter panel, the pressure drop decreases. The effect of oblique wall is relative small on the loading curve of filter panel. Furthermore, this study investigated the effect of presence of wall at the HVAC entrance on the loading characteristics of HVAC panel filters with different pleating geometry. (i.e., pleat height: 50mm, 30mm; pleat density: 1.25/cm, 0.5/cm.) For the cases of vertical front wall, the wall effect on the overall filter

pressure drop was negligible when the distance was greater than 1L (L is the width of pleated filter panel) for the loading curves. For the cases of vertical back wall, the result similar to that for the cases with front wall was obtained when the distance was greater than 1L. The result implies two possibilities: (1) the wall effect on the filter loading curves should be observable within 1L; or (2) the wall effect is 3-D and could not be demonstrated in a 2-D model. The effect of wall presence on panel filters should be observed locally (i.e., in the pressure drop distribution along the panel filter surface).

CHAPTER 7 3-D Modeling for HVAC Filter Panels

7.1 Introduction

As known, 3-D modeling is becoming more and more popular for researchers to do the numerical simulating as the development of computer capability. It matches the real world conditions as much as possible, providing us more realistic and accurate information about the problem. It would be very helpful for us to study the effect of non-uniform particle deposition on HVAC pleated filter entrance panels. One objective of this section is to develop a 3-D numerical model which can describe the flow field around HVAC channel and particle deposition on the panel, the other purpose is to investigate the effect of panel pleating density on the initial deposition pattern of particles on an entrance filter panel.

We employed the similar pleated filter entrance model developed in last chapter, extended it from 2-D to 3-D geometry model with open space situation. To understand the effect of pleating geometry on the particle deposition, various types of pleated filter panel have been created, containing four levels of pleating density for filter panels, which includes low pleating density (0.4/inch, 0.5/inch), moderate pleating density (1/inch), high pleating density (3/inch), and flat panel as the reference pleating panel. Most of them have two types of pleating height (5” and 10”). The detail study have been described in the following part.

7.2 3-D Numerical Model for Investigating the Flow Filed and Particle Behavior around Clean HVAC Entrance Filter Panels

Fig. 7.1 shows a typical example of 3-D geometry model for pleated filter entrance built in an open space and the front view of the HVAC channel. The sphere is standing for the exterior space where particles can move free in the model, the HVAC entrance with filter panel and HVAC channel are indicated as well. The front area of filter media panel is 20" × 20". The dimension of the filter media panel head are (a) 20"× 20"× 5" (b) 20"× 20"× 10", thus we have two pleat heights.

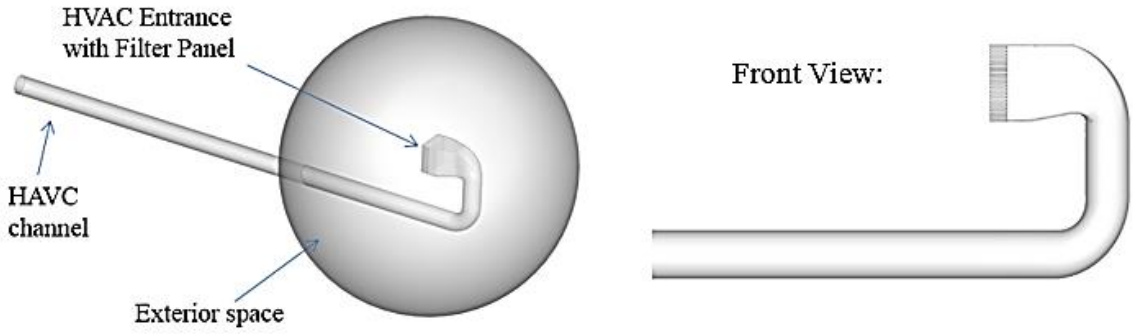

Figure 7.1 3-D view of panel model and computational domain

All the filter panels studied are listed in Fig. 7.2, and four levels of filter pleating density were established. Before introducing the detail about the models, the parameters should be defined: *N* is the pleating number, *H* is the pleating height, and *D* is the pleating number per inch. For the filter panels with low pleating densities, one model has *N* of 5, *H* of 10", and *D* of 0.25; the other with *N* of 10, *H* of 5", and *D* of 0.5. For the two moderate

pleating density models, both of which have pleating number of 20, resulting pleating density of 1.0. One has pleating height of 5", the other 10". We also build two high pleating density models, the pleating number of them are 40, pleating density of 2.0. The pleating height of one is 5" and the other is 10". The last filter panel is flat media which was used as the reference.

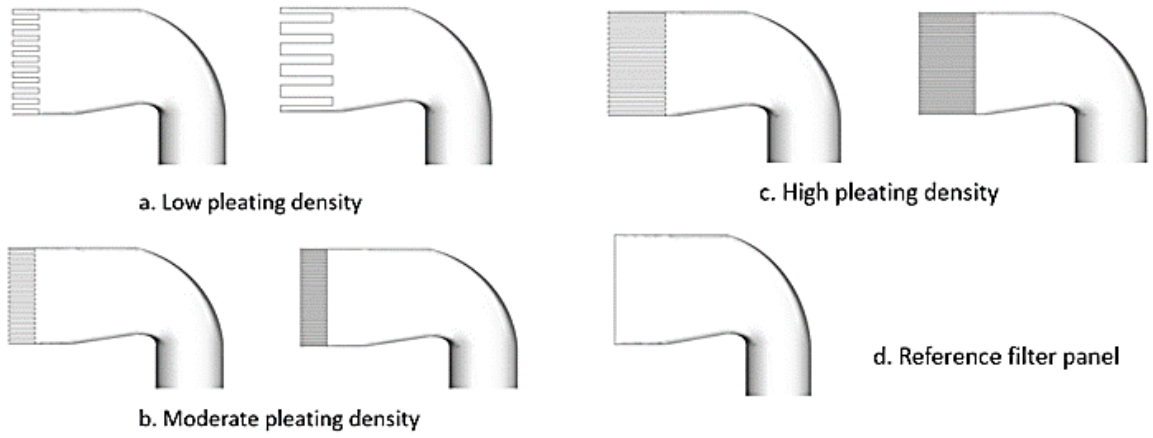

Figure 7.2 Geometry models of filter panel studied

The model of laminar flow was assumed and activated for solving the flow field. We still applied FLUENT build-in Navier-Stokes equations to calculate the flow field or the 3-D models. Fluent predicts the trajectory of a discrete phase particle by integrating the force balance on the particle with Lagrangian method. The force balance equates the particle inertia with the force acting on the particle. ANSYS FLUENT Discrete phase model (DPM) was enabled for tracking particles. The permeability of filter media was set as 1E-10 (m^2) for each pleating case. The total flow rate was controlled as constant, and the initial boundaries/zone conditions were kept same for each case. In Fig. 7.3, the filter media zone,

inlet and outlet of the computational domain were indicated in the geometry model; at the right side, Gambit was utilized to generate mesh for the computational domain and a typical mesh distribution was also given.

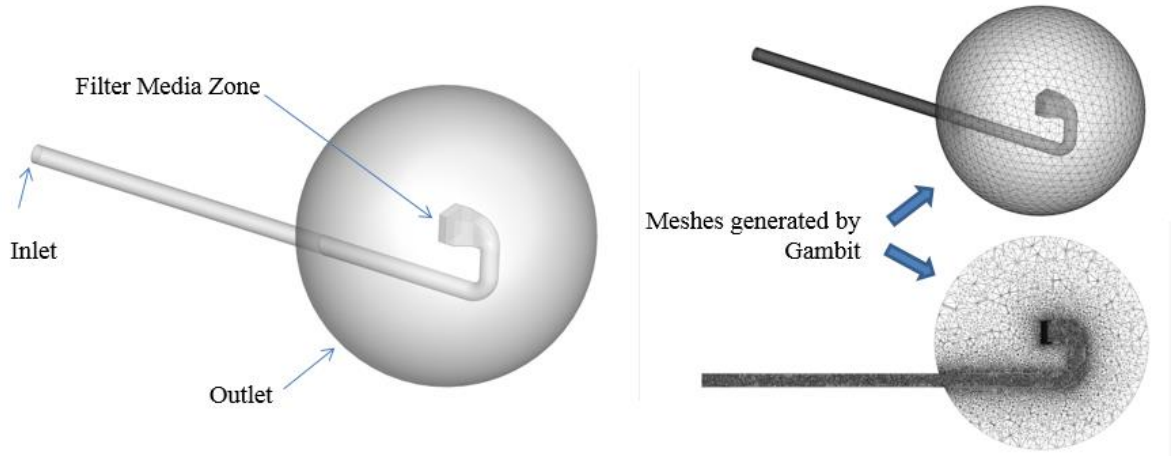

Figure 7.3 Model boundary conditions setup

Table 7.1 lists the detailed information about the parameters that were applied for the flow field calculations. Parabolic velocity profile was enabled by UDF to control the flow inlet velocity profile, the maximum velocity was set as -1.0 m/s. For the flow outlet, zero velocity gradient and standard pressure were defined.

Table 7.1 Initial boundary and cell zone conditions

PHYSICAL BOUNDARY/ZONE	BOUNDARY/ZONE CONDITIONS
Flow Inlet	Parabolic Velocity Profile (UDF), V_{max}= -1.0m/s
Flow Outlet	Zero velocity gradient, pressure=1atm
Interior-L	Porous jump, face permeability=1E-10 (m^2)
Channel Wall (Inside & outside)	Stationary wall, no slip condition
Filter Media Zone	Porous zone, viscous resistance u,v,w= 1E10($1/m^2$)
Flow-1 & 2 Zone	Standard fluid conditions, pressure=1atm

For the particles release method, 9000 particles with mono diameter of 5 um were initialed. All these particles' release source is from the same location that is indicated in Fig. 7.4 from a sphere plate which is in the front of HVAC filter panel. We calculated flow fields of all cases with various pleating geometry. In the presence of calculated flow fields, particles were released and deposited on filter panels.

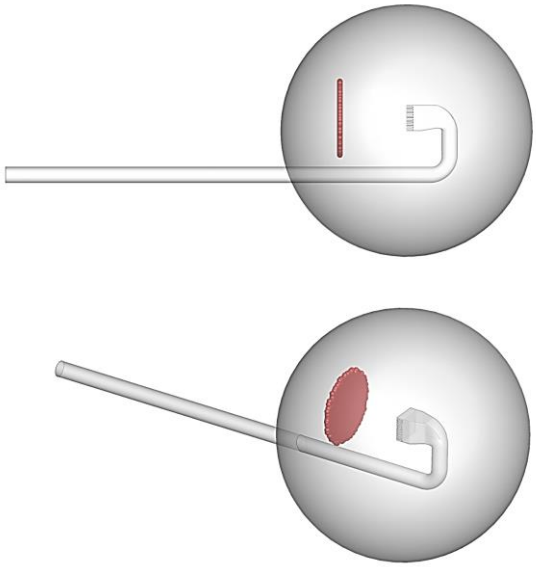

Figure 7.4 3-D view of particle release location

Results and Discussion

First of all, all the flow fields should be calculated properly within their computational domain. Fig. 7.5 only gives us four plots describing the flow field around different pleat filter panels, containing the cases of moderate pleating density and high pleating density. Comparing Fig. 7.5(a) and (b), both have filter pleat height of 5" but the pleat densities are 1.0 and 2.0, two flow fields are very similar. Fig. 7.5(c) and (d) have the pleat height of 10", one has pleat density of 1.0 and the other 2.0. It is noticed that the profile of flow velocity is uniformly distributed near the filter panel for the case with pleat density of 2.0 compared with 1.0 pleat density condition. For Fig. 7.5(a) and (c), (b) and (d), it is found that the velocity near to pleat panel is lower for cases with pleat height of 10" from the velocity fields.

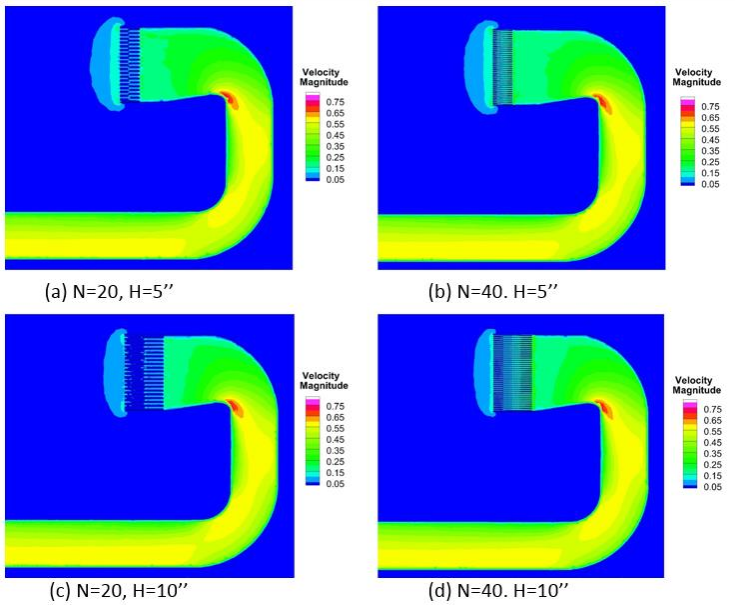

Figure 7.5 Calculated flow filed for four pleat filter models

After the calculation for all flow fields, the particles were injected from the designed location. All the particles would be following the flow field, it was defined that the particles would be collected by filter media once touching filter media. (Ultra-high collection efficiency filter assumed) Based on the deposition pattern and locations of dust particles on filter media, it would be able to find how the pleat geometry of filter panel affect the initial deposition of dust particles.

Fig. 7.6 shows the particle deposition pattern at the case of low pleat density models. The front-view and side-view of the particle deposition pattern were given in Fig. 7.6(a). The deposition shape is like a balloon on flat panel, as well as low pleat density filter panels. Fig. 7.6(b) are the plots of velocity vector profile for low pleat density cases, where the velocity vector on the lower part is higher than that on the upper part and this could be the reason cause the balloon shape of particle deposition.

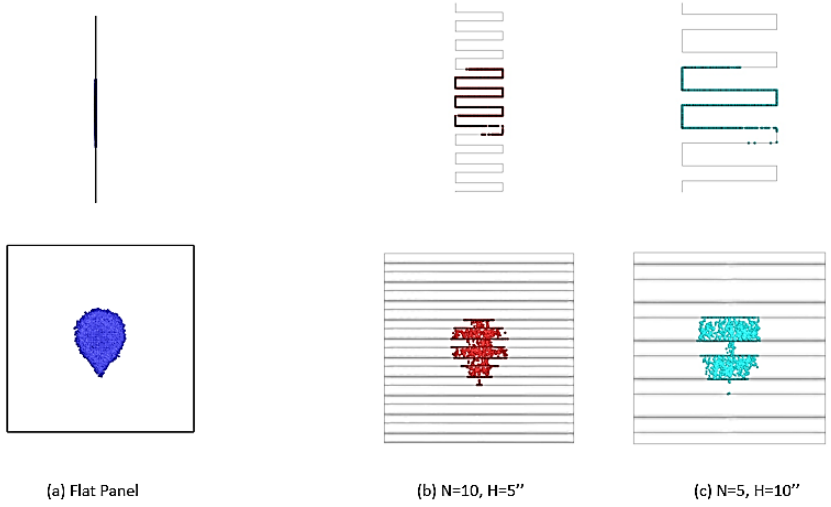

(a) Particle deposition pattern

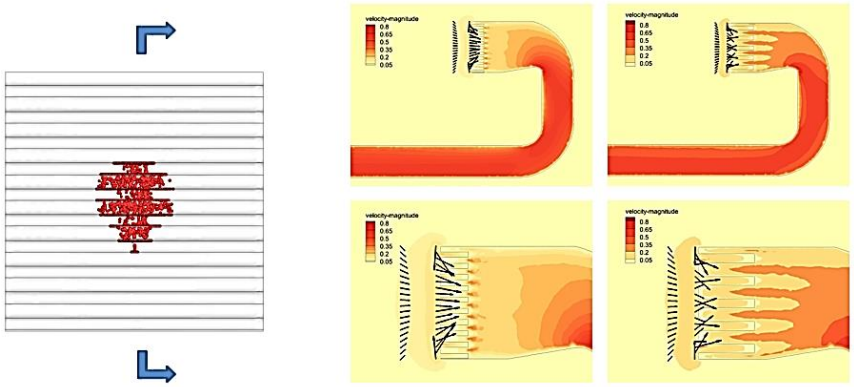

(b) Approaching velocity around filter panel

Figure 7.6 Particle deposition pattern at case of low pleat density model

The particle deposition pattern at the case of moderate pleat density models is given at Fig. 7.7. Similar particle deposition pattern were obtained, but there is difference among these plots. The deposition area is smallest for flat panel case, the biggest deposition are could be found for the model with pleat density of 1.0 and pleat height of 10". The velocity vector plot was also given near to the pleat panels. The velocity vectors at lower part are higher than those at upper part, explaining the reason for the balloon shape pattern of particle deposition.

(a) Particle deposition pattern

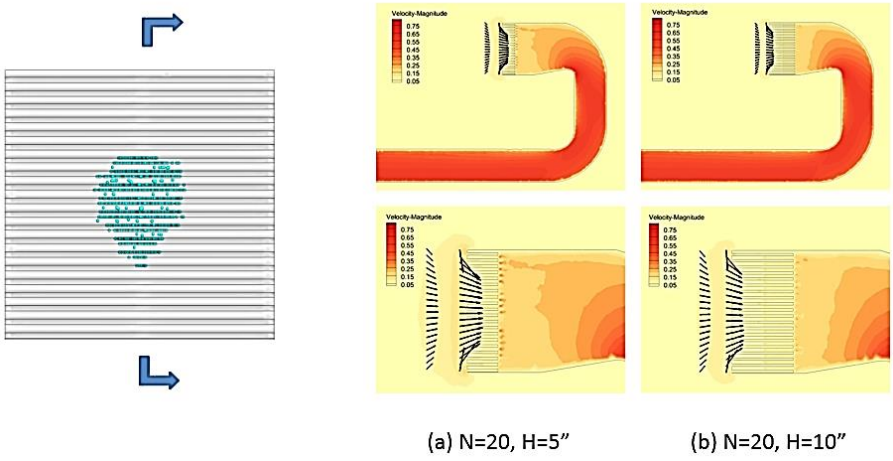

(b) Approaching velocity around filter panel

Figure 7.7 Particle deposition pattern at case of moderate pleat density model

For the results of high pleat density models from Fig. 7.8, the similar observation could be identified that all the deposition patters are balloon shape. The deposition area is

biggest for the model with pleat height of 10". Besides, the vector plot also illustrates the cause of deposition pattern.

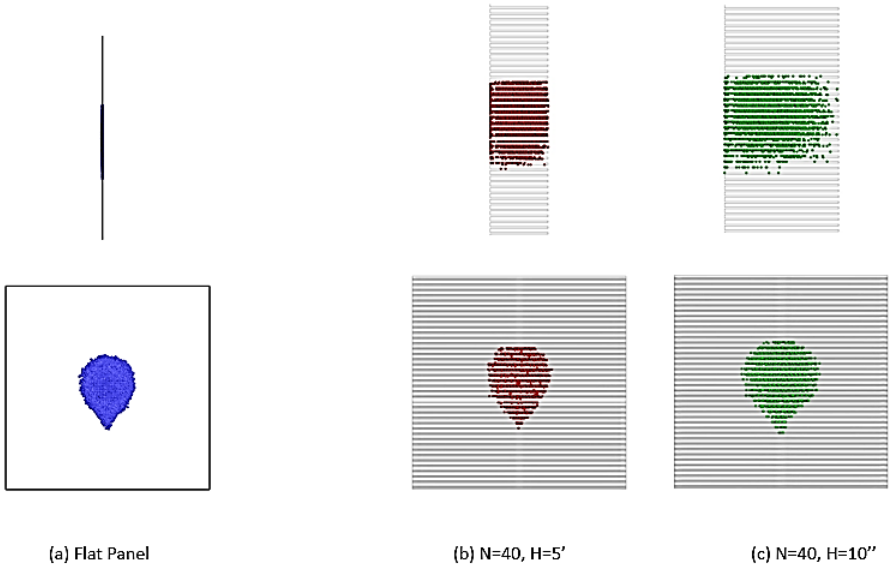

(a) Particle deposition pattern

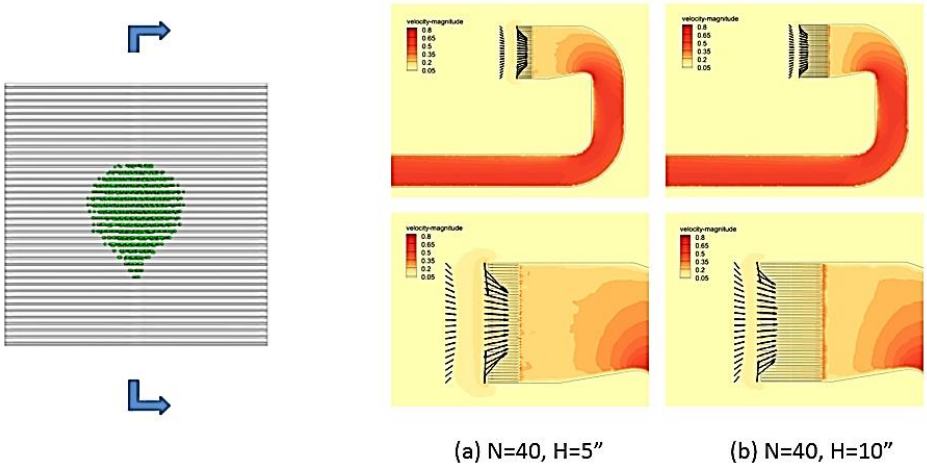

(b) Approaching velocity around filter panel

Figure 7.8 Particle deposition pattern at case of high pleat density model

Based on the observation shown above, the particle deposition pattern could be concluded that all particle trend to deposit on the front center part of the filter panel because the laminar flow model was enabled. It is also noticed that all the cases have similar shape of pattern as balloon, the reason is mostly due to the non-uniform flow field in the front of filter panel. The side view of flow field velocity vector was plotted, where the velocity vectors are not symmetrical, the vectors at lower part are bigger than those at upper part. It should be the reason causing the balloon shape of particle deposition. The deposition area of particle does not change much from reference case to high pleating density case, but the pleating height does have some effect, especially in case of high pleating density, on the spreading of particle deposition area.

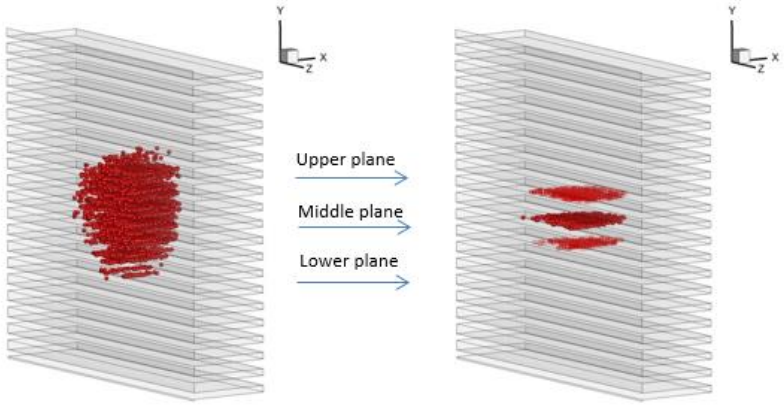

Figure 7.9 (a)

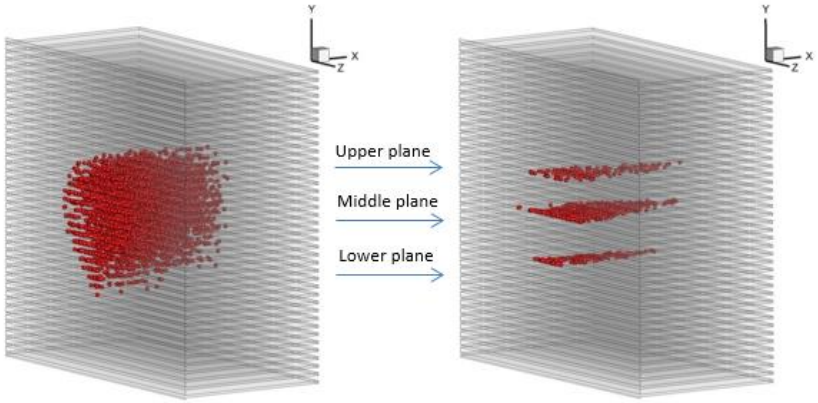

Figure 7.9 (b)

Figure 7.9 3-D view of translucent diagram (a) H = 5'' (b) H = 10''

The 3-D translucent view of particles deposition on pleat filter panels are shown in Fig. 7.9, in which two examples of pleat filter panels were selected. The idea is to figure out where and how these particle deposited on filter media within the filter pleat channel, there layers were picked up from the upper, middle and lower part in the deposition area. On the right side of Fig. 7.9, the selected slices from pleat filter media were given. Based on the 3-D view, it is observed that most particles trend to deposit on the front area within the pleat channel, and the deposition pattern on the surface of pleat filter is parabolic shape. The possible reason for explaining this phenomenon could attribute to the flow field developed within the pleat filter channel that the velocity is getting smaller as move deeper in the pleat channel.

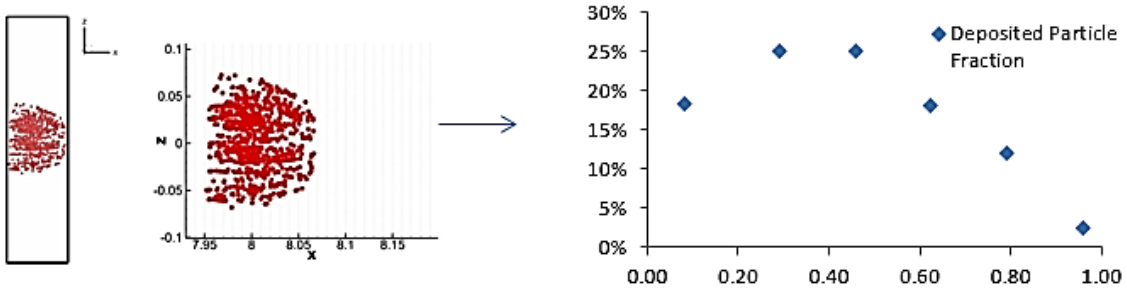

(a) Upper Plane

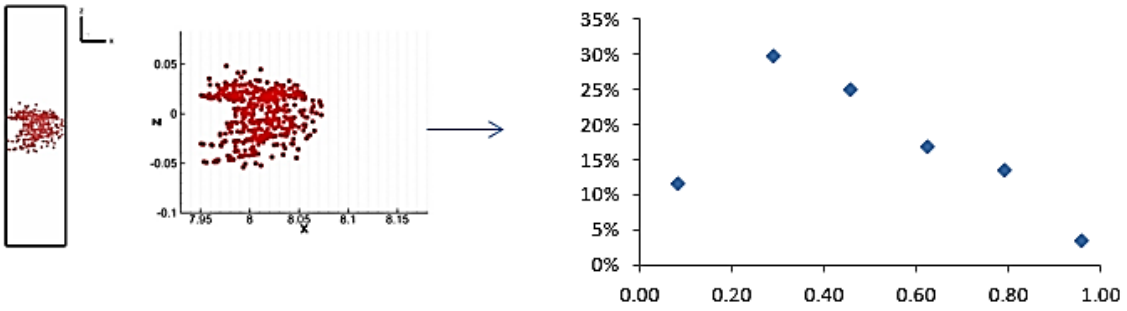

(b) Middle Plane

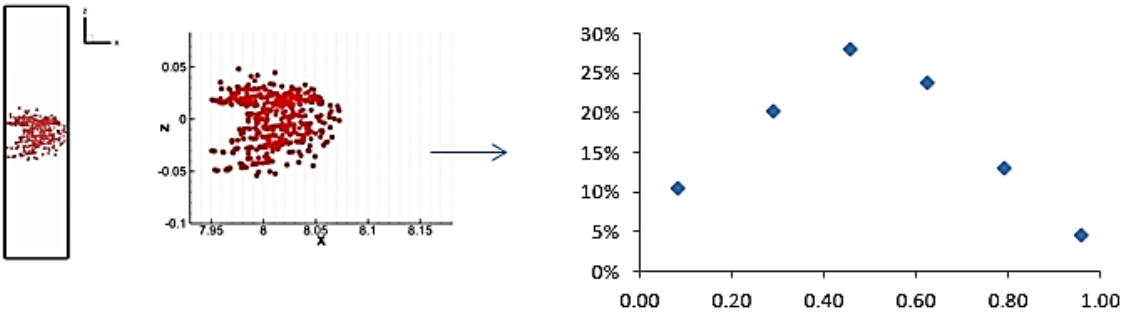

(c) Lower Plane

Figure 7.10 Statistics of particle deposition at case of N=20, H=5''

The statistical analysis was used to count the particle distribution along the selected slices of filter side planes for filter pleat panels with moderate and high pleat density. Fig. 7.10 shows the statistics of particle deposition for three slices of filter media at case of *N*=20, *H*=5". The x-axis is the distance from the left to right on the pleat filter panel, y-axis is for the percentage of particles deposited on that location. In Fig. 7.10, most particles were deposited on the front part of pleat filter panels, less and less particles were collected in the deep area of filter plane.

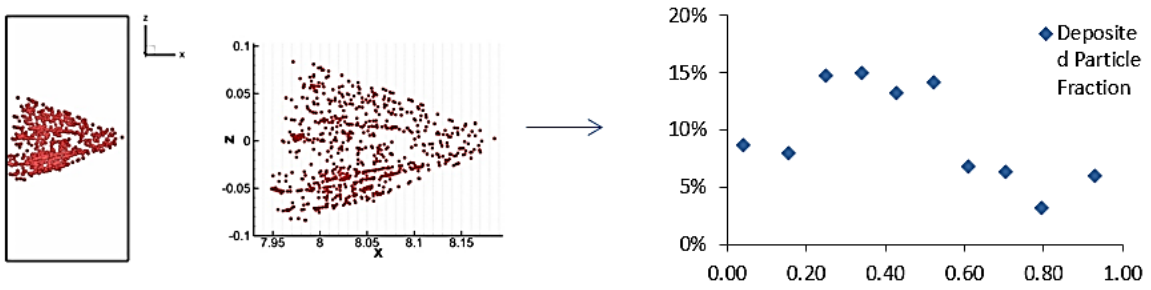

(a) Upper Plane

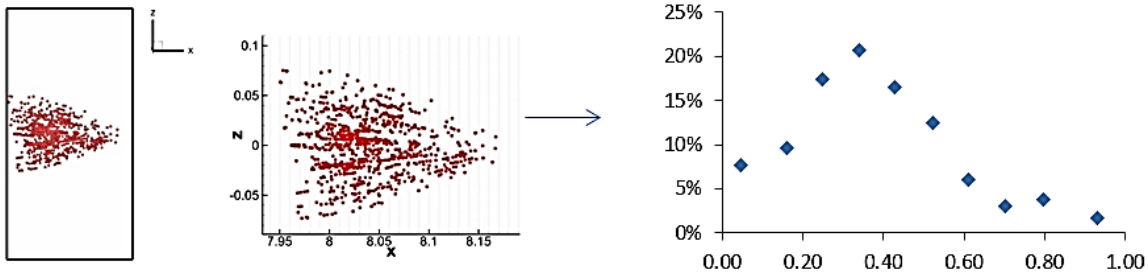

(b) Middle Plane

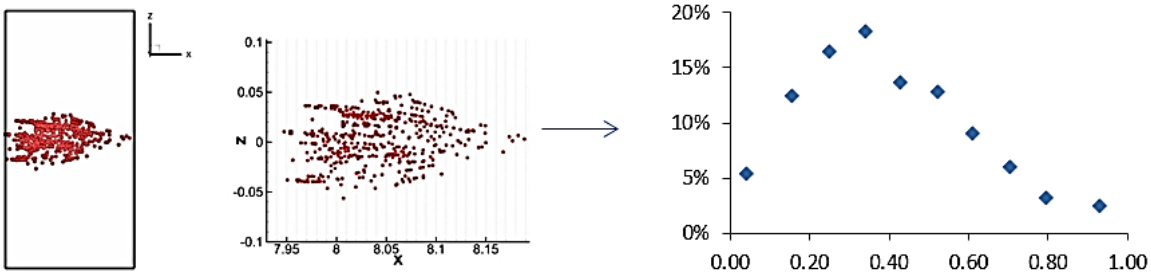

(c) Lower Plane

Figure 7.11 Statistics of particle deposition at case of N=20, H=10''

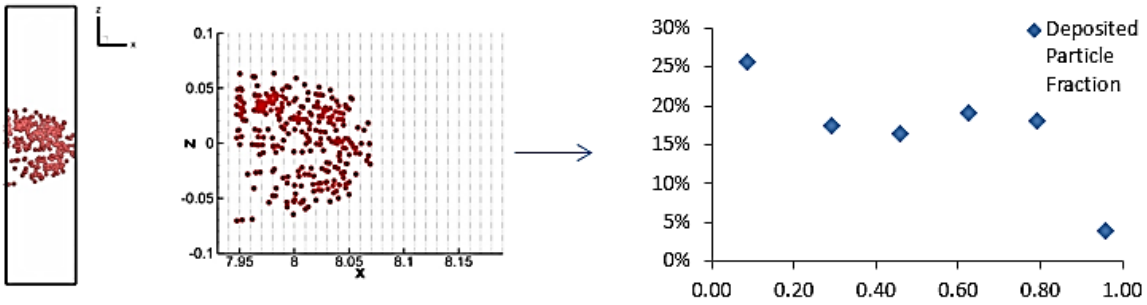

(a) Upper Plane

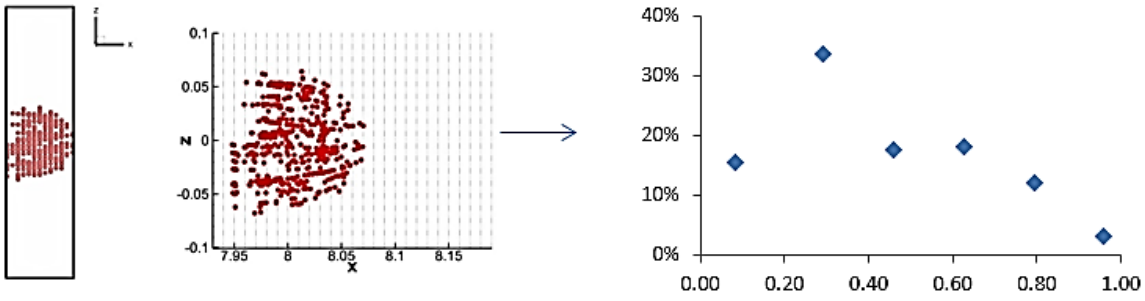

(b) Middle Plane

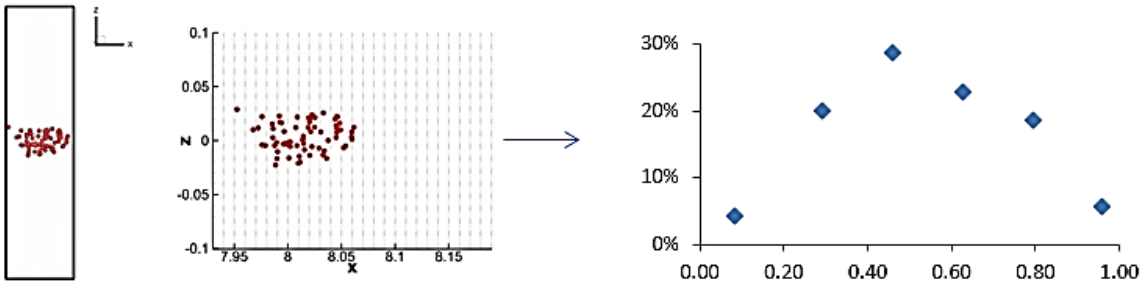

(c) Lower Plane

Figure 7.12 Statistics of particle deposition at case of N=40, H=5''

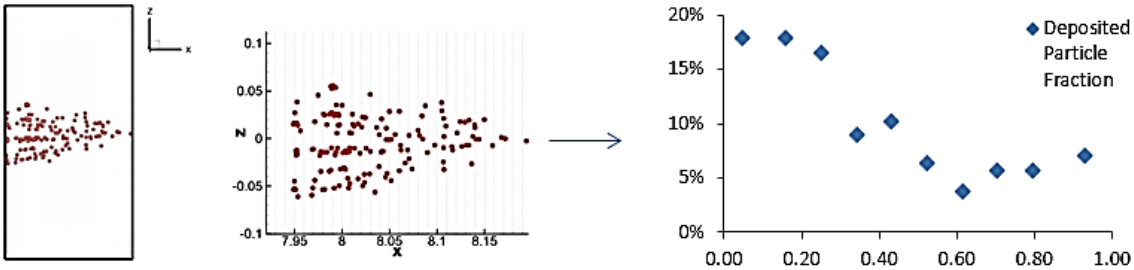

(a) Upper Plane

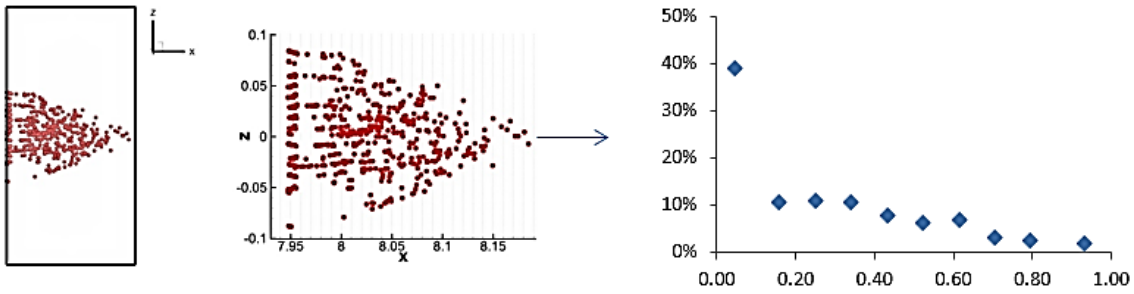

(b) Middle Plane

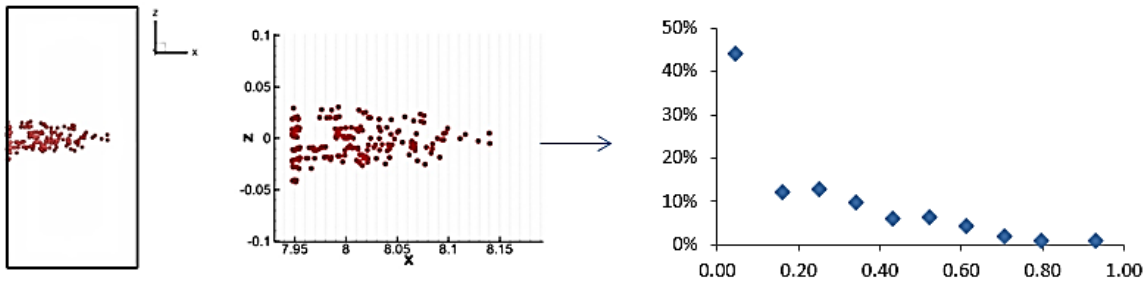

(c) Lower Plane

Figure 7.13 Statistics of particle deposition at case of N=40, H=10''

All the statistics results are shown above for different pleat filter models. All of them share the same observation that particles are likely to deposit in the front part of filter panels. As particles move into deeper and deeper to the filter pleat channel, less and less particle would be collected by filter media. Especially when the pleat filter panels have high pleat density and pleat height.

7.3 Summary

As a short conclusion here, a 3-D model of HVAC was established to investigate the flow filed and particle behavior around clean pleated HVAC entrance filter panels. The pleat filter panels with three levels of pleat density were built up: (1) Low pleat density, i.e., *D*=0.25, 0.5/inch, *H*=5", 10"; (2) Moderate pleat density, i.e., *D*=1.0/inch, *H*=5", 10"; (3) high pleat density, i.e., *D*=2.0/inch, *H*=5", 10". The effect of filter pleat density on the spreading of particle deposition on HVAC filter panels is observable but not that significant.

Much effect on the spreading of particle deposition was found for panels with high pleat height. In general, particle deposition on pleated filter media is not uniform. The deposition non-uniformity is more pronounced for panels with high pleat height and pleat density.

CHAPTER 8 Dissertation Accomplishments and Future Work

8.1 Summary of Accomplishments

In this dissertation, the filter media performance under simulated real-world conditions have been investigated. This research has been accomplished by both experimental methods and computer modeling. For the experimental part, an advanced respirator filter media testing setup was developed, it is capable of evaluating the performance of various respirator media preciously. Based on the proposed experimental method, seven types of respirator filter media were systematically studied. Novel conclusions were discovered for the performance of media under cyclic flow conditions compared with previous findings. In addition, a flat filter test apparatus was built to study the dust loading rate behavior on filter media, the testing flow rate (or face velocity) and mass concentration of challenge particles can be adjusted under the controlled flow patterns. For the computer modeling part, 2-D model was successfully established to calculate the filter loading curve under non-uniform loading of monodisperse particles via ANSYS FLUENT. The effect of filter pleat geometry and point-release locations on HVAC filter performance were investigated under non-uniform particle loading. Besides, the performance of filter panels in the presence of flow obstruction near the HVAC entrance was also studied. A 3-D Numerical Model was further developed to investigate the flow filed and particle behavior around clean HVAC entrance filter panels. The detailed accomplishments of each section are summarized as follows.

8.1.1 Development of Advanced Respirator Testing Method

An advanced method is developed to evaluate the performance of respirator filter media under cyclic flow conditions. Respirator filter media were tested using DMA-classified particles with the size having the maximal penetration. Two CPCs were applied in this method to monitor the up- and down- stream concentrations of classified particles, the particle penetration could be derived by taking the ratio of the two concentrations. With 0.1-second sampling time of CPCs, the close-to-instantaneous particle penetration through respirator filter media could be measured by the new testing method. The individual effects of BF and PIFR on the performance of respirator filter media can accurately be studied from the new testing method.

Prior to the series testing, a pilot study was performed to validate the new testing method. In the study, the penetration of a selected respirator filter media was measured under cyclic flow conditions. Cyclic flows with the sinusoidal wave patterns were applied. Two breathing frequencies, i.e., 6 and 25 BPM and two different peak inhalation flow rates, i.e., 9.42 and 18.14 L/min were selected. The inhalation-only condition was considered. The results measured by the new testing method were compared with the results obtained using SMPSs as the particle sizers. Due to the relatively long measuring cycle time of SMPS to measure the entire particle size distribution, the smoothing effect of breathing frequency (i.e. lowering the average values) on the peak particle penetration of filters was observed. Different from what reported in the previous work, the effect of BF on the particle penetration of respirator filters was in fact significant. The significant selection of CPC

sampling frequency and test particle size were also illustrated. Additionally, the effect of BF on the filter penetration under cyclic flow conditions was further confirmed when applying the new testing method to a HEPA membrane filter.

8.1.2 Investigation of Respirator Performance under Cyclic Flow Condition

The performance of different types of respirator filter media, including two single-layer fibrous media, one charged fibrous media and two composite media, have been investigated with the developed advanced testing method under the worse scenario in this study, by testing the filter media with the most penetrating particle size. With the advanced method, the individual effect of BF and PIFR on the performance of respirator filter media could be determined.

Cyclic flow with sinusoidal wave patterns simulating human breathing patterns were applied and only inhalation part was considered in the experiments. Three breathing frequencies, i.e., 6, 12 and 25 BPM and three different peak inhalation flow rates i.e., 9.42, 13.6 and 18.14 L/min were selected. The penetration of respirator filter media were also tested under constant flow condition, i.e., equivalent mean inhalation flow rate (MIFR) for each peak inhalation flow rate (PIFR) conditions. The effect of BF and PIFR were confirmed that the peak penetration increases by increasing of BF or PIFR. Peak penetration ratio, defined as the ratio of peak penetration and the penetration from corresponding MIFR, was also discussed. It is concluded that the peak penetration ratio increases as BF increases, while

the value does not significantly change at various PIFRs within the conditions considered in this study.

Furthermore, a semi-theoretical model was developed to predict the peak penetration of respirator filter media under cyclic flow with various BFs. It consists of two parts: one is the fitting function of peak penetration ratio, and the other is the penetration calculated by single-fiber theory. Two sample examples were given to assess the proposed model. Due to the good match between the peak penetrations measured by the semi-theoretical model and by the experiments, this semi-theoretical model was thus confirmed and validated. Therefore, the semi-theoretical numerical model could be used to predict the peak penetration of respirator filter media under cyclic flow conditions.

8.1.3 Effect of Particle Loading Rate on the Performance of Filter Media

In this study, the effect of dust loading rate (i.e., test particle mass concentration and total flowrate) on the particle loading curves of high efficiency filter media (i.e., the filter pressured drop as a function of particle mass loaded on unit filter medium area) have been systematically investigated. This is the first research focused on this subject to the authors' knowledge. Two high efficiency filter media, i.e., glass fiber and electret filters, were chosen in this study. Filter media were loaded with two different dusts: one is *ISO 12103-1*, A3 Medium test dust (Arizona road dust) and the other is *ISO 12103-1*, A1 Ultrafine test dust. Both dusts were provided by Powder Technology Inc.. The particle loading curves of the test filters were experimentally collected under various loading rates and two face velocities

(10 and 20 cm/sec). Due to the selection of high efficiency filter media, the filtration status of the test filter media under the particle loading was primarily in the dust cake filtration regime (after a short period of time staying in the initial, depth and transitional filtration).

Based on the results, the effect on the filter pressure drop during the particle loading was verified, especially within the low loading rate region. The filter pressure drop decreases as the test particle mass concentration increases for the cases loaded with ARD at a given face velocity. This observation is not obvious when filters were loaded with ultrafine particles. The reason is that at low particle mass concentration particles deposited on the media surface had more time and space to reach a balance status without much interference from later incoming particles. Particles had less chance to achieve a stable status under high mass concentration, resulting in more porous dust cake. The hypothesis was further supported by the SEM images of the cutoff view of loaded filter media. Our study also shows the minor effect of face velocity on the filter loading curves. The effect of the particle loading rate on the filter loading curves was further quantified via data analysis. An empirical model was at last proposed to best fit the experimental particle loading data collected under various test conditions.

8.1.4 Performance of HVAC entrance filter panel under non-uniform particle loading

The numerical methodology to study the performance of HVAC entrance filter panel under non-uniform particle loading have been established. At first, a 2-D modeling was developed to calculate the media loading curves through ANSYS FLUENT. Various filter

pleat filter panels were built up, it is found that the effect of media pleating facilitates the spread of particle deposition area on filter surface, resulting in lower pressure drop as compared with that for flat filter panels. Within the studied cases, filter pleat density has more influence than pleat height for lowering the pressure drop of loaded entrance filter panels. The effect of point-release locations has been identified that the pressure drop across filter panels decreases as the particle release location moves to the back of entrance filter panels. Besides, the performance of filter panels in the presence of flow obstruction near HVAC filter entrance was studied. The total pressure drop increases as the front vertical wall getting close to filter panel. But, as back vertical wall getting close to filter panel, the pressure drop decreases. The effect of oblique wall is relative small on the loading curve of filter panel. For the influence of pleating geometry. (i.e., pleat height: 50mm, 30mm; pleat density: 1.25/cm, 0.5/cm.), the wall effect on the overall filter pressure drop was negligible when the distance was greater than 1L (L is the width of pleated filter panel) for the loading curves when the vertical front wall is present. Similar observation was obtained for the presence of vertical back and inclined wall. The possible reasons are: (1) the wall effect on the filter loading curves should be observable within 1L; or (2) the wall effect is 3-D and could not be demonstrated in a 2-D model. The effect of wall presence on panel filters should be observed locally (i.e., in the pressure drop distribution along the panel filter surface).

Additionally, to study the flow filed and particle behavior around clean pleated HVAC entrance filter panels a 3-D model of HVAC was developed. Different pleat filter panels were built up. Based on the results, it is concluded that the effect of filter pleat density

on the spreading of particle deposition on HVAC filter panels is observable but not important. High pleat height could bring much effect on the spreading of particle deposition. Generally, particle deposition on pleated filter media is not uniform, and high pleat height and pleat density increase the deposition non-uniformity.

8.2 Recommendations for Future Research

The study of filter performance under real-world conditions is a new and challenge field in filtration research, and there are still much work needs to be done to understand the actual performance of media. The detailed recommendations for future research is described as follows.

The advanced method was developed to study the performance of respirator filter media, and the individual contribution of breathing frequency and peak inhalation flow rate on performance of various respirator filter have been investigated. The challenge particle used in the study was neutralized as Boltzmann charge distribution by Kr-85 neutralizer before all the tests, thus it is needed to evaluate performance of respirator filter under charged particles, i.e., particles with mono positive or negative charge. The upstream concentration of aerosol was varied under the cyclic flow condition due to limit vessel volume in the upstream testing system, however the concentration of particles in the real environment is nearly constant in real-world. Thus, the second recommendation is to modify the current experimental setup to keep the concentration of upstream particle as constant under cyclic flow rate test. To achieve the object, one can build up a larger testing chamber for the

upstream system and generate high concentration particles for the experiments. In addition, it would be interesting to compare the proposed model with measured instantaneous penetration, and this requiring the data reduction scheme to recover true particle penetration of test filter media from the raw data. Furthermore, it is necessary to set up the experiment for evaluating respirator filter under inhalation-and-exhalation flow conditions.

A flat filter testing apparatus was established to study the performance of other general purpose filter media. Because of my research schedule, it is a pity that to evaluate the performance of filter media under non-uniform dust concentration is not accomplished. It is significant to understand the actual performance of filter media under their exposure conditions of applications to insure filter function would not fail. Either the flow rate or the mass concentration of test dust could be controlled by programming as unsteady conditions to simulate the actual conditions.

For the modeling of HVAC filter panels under non-uniform particle loading, there are a few recommendations for this research. First, the complete filtration model could be developed for filter media, i.e., depth filtration, transient regime of filtration, surface filtration. Then the complete filtration model could substitute current filtration model with surface filtration-only to calculate the loading curves of HVAC filter media under non-uniform particle deposition. Second, we have started to work on 3-D model to study the flow field and particle behavior around clean HVAC filter panels, but this is only related to initial loading. It is significant to understand the flow field and particle behavior around filter panels under the dust loading process. With the help of the developed filtration model

implanted on the 3-D model for HVAC filter panels, it would be able to study the flow field, particle behavior and performance of HVAC filter panel at the dust loading conditions.

Literature Cited

Brown, Richard Colin. Air filtration: an integrated approach to the theory and applications of fibrous filters. Pergamon, 1993.

Hinds, William C. Aerosol technology: properties, behavior, and measurement of airborne particles. John Wiley & Sons, 2012.

Howard, J. "Guidance for filtration an air-cleaning systems to protect building environments from airborne chemical, biological, or radiological attacks."Available from:(accessed 21.4. 2005) (2003).

Chuanfang, Y. A. N. G. "Aerosol Filtration Application Using Fibrous Media—An Industrial Perspective." Chinese Journal of Chemical Engineering 20.1 (2012): 1-9.

Endo, Yoshiyuki, Da-Ren Chen, and David YH Pui. "Effects of particle polydispersity and shape factor during dust cake loading on air filters." Powder Technology 98.3 (1998): 241-249.

Brown, Richard Colin. Air filtration: an integrated approach to the theory and applications of fibrous filters. Pergamon, 1993.

Leung, Wallace Woon-Fong, Chi-Ho Hung, and Ping-Tang Yuen. "Effect of face velocity, nanofiber packing density and thickness on filtration performance of filters with nanofibers coated on a substrate." Separation and purification technology 71.1 (2010): 30-37.

Hajra, M. G., K. Mehta, and G. G. Chase. "Effects of humidity, temperature, and nanofibers on drop coalescence in glass fiber media." Separation and purification technology 30.1 (2003): 79-88.

Ji, J. H., et al. "Effect of particle loading on the collection performance of an electret cabin air filter for submicron aerosols." Journal of aerosol science 34.11 (2003): 1493-1504.

Japuntich, Daniel A., et al. "A comparison of two nano-sized particle air filtration tests in the diameter range of 10 to 400 nanometers." Journal of Nanoparticle Research 9.1 (2007): 93-107.

Ergüdenler, Ali, et al. "Performance of high-temperature fabric filters under gasification and combustion conditions." Separation and purification technology 11.1 (1997): 1-16.

Saleem, Mahmood, and Gernot Krammer. "Effect of filtration velocity and dust concentration on cake formation and filter operation in a pilot scale jet pulsed bag filter." Journal of hazardous materials 144.3 (2007): 677-681.

Schmidt, E., and F. Löffeler. "Preparation of dust cakes for microscopic examination." Powder technology 60.2 (1990): 173-177.

Schmidt, Eberhard, and Friedrich Löffeler. "The analysis of dust cake structures." Particle & Particle Systems Characterization 8.1-4 (1991): 105-109.

Cheng, Yu-Hsiang, and Chuen-Jinn Tsai. "Factors influencing pressure drop through a dust cake during filtration." Aerosol Science and Technology 29.4 (1998): 315-328.

Stamatakis, K., and Chi Tien. "Cake formation and growth in cake filtration."Chemical Engineering Science 46.8 (1991): 1917-1933.

Aguiar, M. L., and J. R. Coury. "Cake formation in fabric filtration of gases."Industrial & engineering chemistry research 35.10 (1996): 3673-3679.

Choi, Joo-Hong, Soon-Jong Ha, and Young-Ok Park. "The effect of particle shape on the pressure drop across the dust cake." Korean Journal of Chemical Engineering 19.4 (2002): 711-717.

Neiva, Antonio CB, and Leonardo Goldstein. "A procedure for calculating pressure drop during the build-up of dust filter cakes." Chemical Engineering and Processing: Process Intensification 42.6 (2003): 495-501.

Rocha, Sandra Mara Santana, et al. "The Influence of the Velocity of Filtration in the Formation and Removal the Dust Cake." Materials Science Forum. Vol. 660. 2010.

Cheng, Yu-Hsiang, and Chuen-Jinn Tsai. "Factors influencing pressure drop through a dust cake during filtration." Aerosol Science and Technology 29.4 (1998): 315-328.

Jaganathan, S., H. Vahedi Tafreshi, and B. Pourdeyhimi. "A realistic approach for modeling permeability of fibrous media: 3-D imaging coupled with CFD simulation." Chemical Engineering Science 63.1 (2008): 244-252.

Maze, B., et al. "A simulation of unsteady-state filtration via nanofiber media at reduced operating pressures." Journal of aerosol science 38.5 (2007): 550-571.

Tahir, M. A., and H. Vahedi Tafreshi. "Influence of fiber orientation on the transverse permeability of fibrous media." Physics of Fluids (1994-present) 21.8 (2009): 083604.

Hosseini, S. A., and H. Vahedi Tafreshi. "Modeling particle filtration in disordered 2-D domains: A comparison with cell models." Separation and Purification Technology 74.2 (2010): 160-169.

Hosseini, S. A., and H. Vahedi Tafreshi. "Modeling permeability of 3-D nanofiber media in slip flow regime." Chemical Engineering Science 65.6 (2010): 2249-2254.

Hosseini, S. A., and H. Vahedi Tafreshi. "3-D simulation of particle filtration in electrospun nanofibrous filters." Powder Technology 201.2 (2010): 153-160.

Fotovati, S., et al. "Modeling instantaneous pressure drop of pleated thin filter media during dust loading." Chemical Engineering Science 66.18 (2011): 4036-4046.

Kanaoka, Chikao, Hitoshi Emi, and Toshihiko Myojo. "Simulation of the growing process of a particle dendrite and evaluation of a single fiber collection efficiency with dust load." Journal of Aerosol Science 11.4 (1980): 377-389.

Kanaoka, Chikao, Hitoshi Emi, and Wiwut Tanthapanichakoon. "Convective diffusional deposition and collection efficiency of aerosol on a dust-loaded fiber."AIChE journal 29.6 (1983): 895-902.

Kanaoka, C., Emi, H., Otani, Y., & Iiyama, T. (1987). Effect of charging state of particles on electret filtration. Aerosol Science and Technology, 7(1), 1-13.

Myojo, Toshihiko, Chikao Kanaoka, and Hitoshi Emi. "Experimental observation of collection efficiency of a dust-loaded fiber." Journal of aerosol science 15.4 (1984): 483-489.

Kanaoka, Chikao, and Sotoji Hiragi. "Pressure drop of air filter with dust load."Journal of aerosol science 21.1 (1990): 127-137.

Tanthapanichakoon, W., Maneeintr, K., Charinpanitkul, T., & Kanaoka, C. (2003). Estimation of collection efficiency enhancement factor for an electret fiber with dust load. Journal of aerosol science, 34(11), 1505-1522.

Emi, Hitoshi, Chikao Kanaoka, and Yuji Kuwabara. "The diffusion collection efficiency of fibers for aerosol over a wide range of Reynolds numbers." Journal of Aerosol Science 13.5 (1982): 403-413.

Novick, V. J., P. R. Monson, and P. E. Ellison. "The effect of solid particle mass loading on the pressure drop of HEPA filters." Journal of aerosol science 23.6 (1992): 657-665.

Gupta, A., Novick, V. J., Biswas, P., & Monson, P. R. (1993). Effect of humidity and particle hygroscopicity on the mass loading capacity of high efficiency particulate air (HEPA) filters. Aerosol Science and Technology, 19(1), 94-107.

Japuntich, D. A., J. I. T. Stenhouse, and B. Y. H. Liu. "Experimental results of solid monodisperse particle clogging of fibrous filters." Journal of aerosol science 25.2 (1994): 385-393.

Japuntich, D. A., J. I. T. Stenhouse, and B. Y. H. Liu. "Effective pore diameter and monodisperse particle clogging of fibrous filters." Journal of aerosol science28.1 (1997): 147-158.

Walsh, D. C., and J. I. T. Stenhouse. "The effect of particle size, charge, and composition on the loading characteristics of an electrically active fibrous filter material." Journal of aerosol science 28.2 (1997): 307-321.

Walsh, Declan C. "Recent advances in the understanding of fibrous filter behaviour under solid particle load." Filtration & separation 33.6 (1996): 501-506.

Brown, R. C., and D. Wake. "Loading filters with monodisperse aerosols: macroscopic treatment." Journal of aerosol science 30.2 (1999): 227-234.

Chen, C. C., Chen, W. Y., Huang, S. H., Lin, W. Y., Kuo, Y. M., & Jeng, F. T. (2001). Experimental study on the loading characteristics of needlefelt filters with micrometer-sized monodisperse aerosols. Aerosol Science & Technology,34(3), 262-273.

Thomas, D., Penicot, P., Contal, P., Leclerc, D., & Vendel, J. (2001). Clogging of fibrous filters by solid aerosol particles experimental and modelling study.Chemical Engineering Science, 56(11), 3549-3561.

Lawrence, C. A., & Liu, P. (2006). Relation of structure, properties and performance of fibrous media for gas filtration. Chemical engineering & technology, 29(8), 957-967.

Contal, P., Simao, J., Thomas, D., Frising, T., Callé, S., Appert-Collin, J. C., & Bémer, D. (2004). Clogging of fibre filters by submicron droplets. Phenomena and influence of operating conditions. Journal of Aerosol Science, 35(2), 263-278.

Kuwabara, S. (1959). The forces experienced by randomly distributed parallel circular cylinders or spheres in a viscous flow at small Reynolds numbers.Journal of the physical society of Japan, 14(4), 527-532.

Stechkina, I. B., & Fuchs, N. A. (1966). Studies on fibrous aerosol filters—I. Calculation of diffusional deposition of aerosols in fibrous filters. Annals of occupational Hygiene, 9(2), 59-64.

Fuchs, N. A., & Stechkina, I. B. (1963). A note on the theory of fibrous aerosol filters. Annals of Occupational Hygiene, 6(1), 27-30.

Yeh, H. C., & Liu, B. Y. (1974). Aerosol filtration by fibrous filters—I. Theoretical. Journal of aerosol science, 5(2), 191-204.

Lee, K. W., & Liu, B. Y. H. (1982). Theoretical study of aerosol filtration by fibrous filters. Aerosol Science and Technology, 1(2), 147-161.

Kirsch, A. A., Stechkina, I. B., & Fuchs, N. A. (1974). Gas flow in aerosol filters made of polydisperse ultrafine fibres. Journal of Aerosol Science, 5(1), 39-45.

Kirsch, A. A., & Fuchs, N. A. (1968). Studies on fibrous aerosol filters—III diffusional deposition of aerosols in fibrous filters. Annals of Occupational Hygiene, 11(4), 299-304.

Fuchs, N. A., Kirsch, A. A., & Stechkina, I. B. (1973). A contribution to the theory of fibrous aerosol filters. In Faraday Symposia of the Chemical Society (Vol. 7, pp. 143-156). Royal Society of Chemistry.

Davies, C. N. (1950). The Separation of Airborne Dust and Particles. Arhiv za Higijenu Rada, 1(4), 393-427.

Werner, R. M., & Clarenburg, L. A. (1965). Aerosol filters. Pressure drop across single-component glass fiber filters. Industrial & Engineering Chemistry Process Design and Development, 4(3), 288-293.

Jackson, G. W., & James, D. F. (1986). The permeability of fibrous porous media. The Canadian Journal of Chemical Engineering, 64(3), 364-374.

Kanaoka, C., Emi, H., Hiragi, S., & Myojo, T. (1986). Morphology of particulate agglomerates on a cylindrical fiber and collection efficiency of a dust loaded fiber. In 2nd International Aerosol Conference (pp. 674-677).

Bhutra, S., & Payatakes, A. C. (1979). Experimental investigation of dendritic deposition of aerosol particles. Journal of Aerosol Science, 10(5), 445-464.

Payatakes, A. C., & Tien, C. (1976). Particle deposition in fibrous media with dendrite-like pattern: a preliminary model. Journal of Aerosol Science, 7(2), 85-100.

Tien, C., & Payatakes, A. C. (1979). Advances in deep bed filtration. AIChE Journal, 25(5), 737-759.

El-Shobokshy, M. S., Al-Sanea, S. A., & Adnan, A. M. (1994). Computer simulation of monodisperse aerosol collection in fibrous filters. Aerosol science and technology, 20(2), 149-160.

Werner, R. M., & Clarenburg, L. A. (1965). Aerosol filters. Pressure drop across single-component glass fiber filters. Industrial & Engineering Chemistry Process Design and Development, 4(3), 288-293.

Chen, Da-Ren, David YH Pui, and Benjamin YH Liu. "Optimization of pleated filter designs using a finite-element numerical model." Aerosol Science and Technology 23.4 (1995): 579-590

Mackley, M. R., and N. E. Sherman. "Cake filtration mechanisms in steady and unsteady flows." Journal of membrane science 77.1 (1993): 113-121.

Qian, Yinge, et al. "Performance of N95 respirators: filtration efficiency for airborne microbial and inert particles." American Industrial Hygiene Association 59.2 (1998): 128-132.

Rengasamy, Samy, and Benjamin C. Eimer. "Total inward leakage of nanoparticles through filtering facepiece respirators." Annals of occupational hygiene 55.3 (2011): 253-263.

Rengasamy, Samy, and Benjamin C. Eimer. "Nanoparticle penetration through filter media and leakage through face seal interface of N95 filtering facepiece respirators." Annals of occupational hygiene 56.5 (2012): 568-580.

Wang, Anbo, Aaron W. Richardson, and Kent C. Hofacre. "The effect of flow pattern on collection efficiency of respirator filters." Journal of the International Society of Respiratory Protection 29.1 (2012): 41.

Martin Jr, Stephen B., and Ernest S. Moyer. "Electrostatic respirator filter media: filter efficiency and most penetrating particle size effects." Applied occupational and environmental hygiene 15.8 (2000): 609-617.

Mostofi, Reza, et al. "Investigation of potential affecting factors on performance of N95 respirator." Journal of the International Society for Respiratory Protection 28.1 (2011): 26-39.

Mostofi, Reza, et al. "Performance of mechanical filters and respirators for capturing nanoparticles-limitations and future direction." Industrial health 48.3 (2010): 296-304.

"Respirator Protection," *Code of Federal Regulations Title 42*, Part 84. 1995. pp. 30382-30383).

Jordan, Harry S., and L. Silverman. Effect of Pulsating Air Flow on Fiber Filter Efficiency. No. NYO-4814. Harvard Univ., Boston. School of Public Health, 1961.

Stafford, Ronald G., Harry J. Ettinger, and Thomas J. Rowland. "Respirator cartridge filter efficiency under cyclic-and steady-flow conditions." The American Industrial Hygiene Association Journal 34.5 (1973): 182-192.

Brosseau, Lisa M., Michael J. Ellenbecker, and J. S. Evans. "Collection of silica and asbestos aerosols by respirators at steady and cyclic flow." The American Industrial Hygiene Association Journal 51.8 (1990): 420-426.

Wang, Anbo, Aaron W. Richardson, and Kent C. Hofacre. "The effect of flow pattern on collection efficiency of respirator filters." *Journal of the International Society of Respiratory Protection* 29.1 (2012): 41.

Eshbaugh, Jonathan P., et al. "N95 and P100 respirator filter efficiency under high constant and cyclic flow." *Journal of occupational and environmental hygiene* 6.1 (2008): 52-61.

Haruta, H., et al. "Experimental and theoretical investigation of the performance of N95 respirator filters against ultrafine aerosol particles tested at constant and cyclic flows." *J Int Soc Res Prot* 25 (2008): 75-88.

Mahdavi, Alireza, et al. "Contribution of breathing frequency and inhalation flow rate on performance of N95 filtering facepiece respirators." *Annals of occupational hygiene* 58.2 (2014): 195-205.

Wang, Qiang, Xiuli Lin, and Da-Ren Chen. "Effect of dust loading rate on the loading characteristics of high efficiency filter media." Powder Technology 287 (2016): 20-28.

Wang, Qiang, Laleh Golshahi, and Da-Ren Chen. "Advanced Testing Method to Evaluate the Performance of Respirator Filter Media." Journal of Occupational and Environmental Hygiene just-accepted (2016): 00-00.

Romay, Francisco J., Benjamin YH Liu, and Soo-Jae Chae. "Experimental study of electrostatic capture mechanisms in commercial electret filters." *Aerosol Science and Technology* 28.3 (1998): 224-234.

Chen, Chih-Chieh, and Sheng-Hsiu Huang. "The effects of particle charge on the performance of a filtering facepiece." *American Industrial Hygiene Association* 59.4 (1998): 227-233.

Benchetrit, Gila. "Breathing pattern in humans: diversity and individuality." Respiration physiology 122.2 (2000): 123-129.

Lee, K. W., and M. U. K. U. N. D. Ramamurthi. "Filter collection." Aerosol measurement: Principles, techniques and applications (1993): 179-205.

Davies, Charles Norman. "Air filtration." (1973).

Stechkina, I. B., and N. A. Fuchs. "Studies on fibrous aerosol filters—I. Calculation of diffusional deposition of aerosols in fibrous filters." Annals of occupational Hygiene 9.2 (1966): 59-64.

Hinds, William C. "Aerosol technology: properties, behavior, and measurement of airborne particles." New York, Wiley-Interscience, 1982. 442 p. 1 (1982).

Mostofi, Reza, et al. "Impact of two particle measurement techniques on the determination of N95 class respirator filtration performance against ultrafine particles." *Journal of hazardous materials* 217 (2012): 51-57.

APPENDIX A

SEM images of Filter media

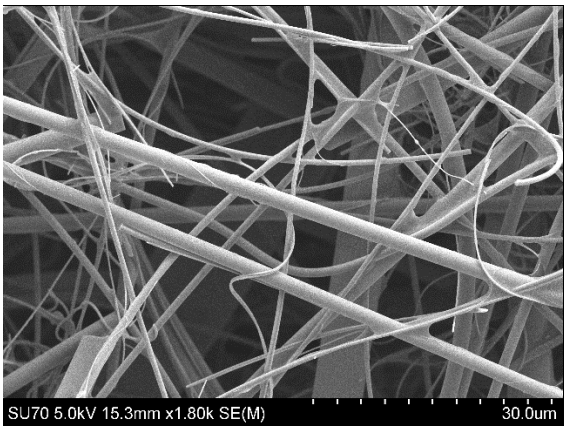

(a) Respirator filter media type-1

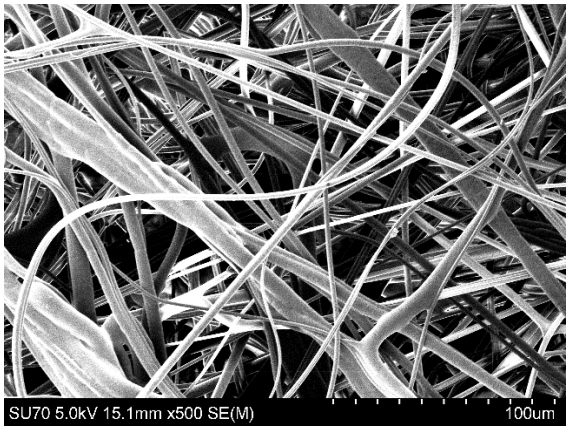

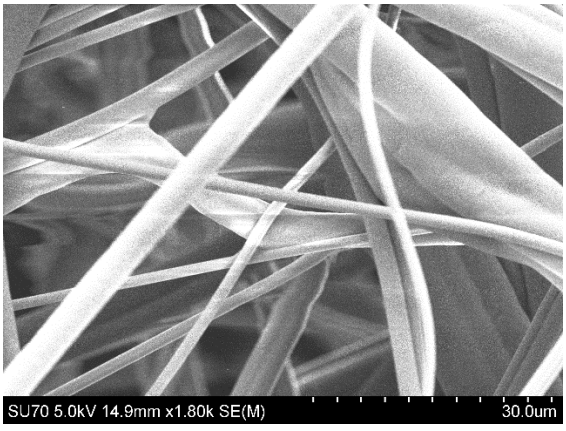

(b) Respirator filter media type-2

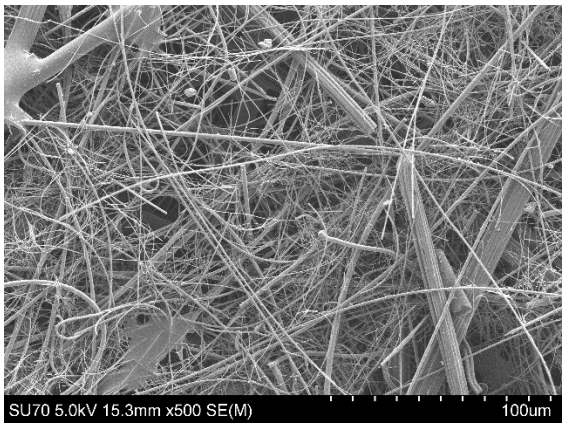

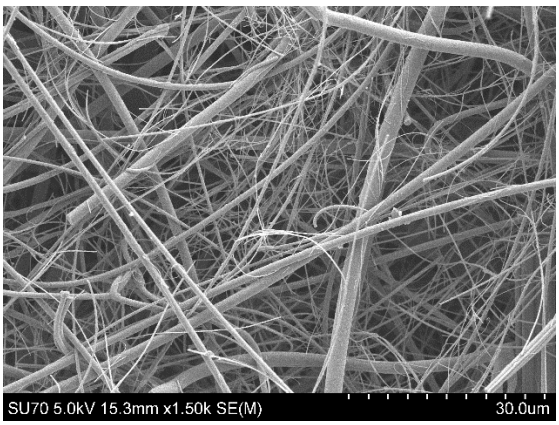

(c) Respirator filter media type-3

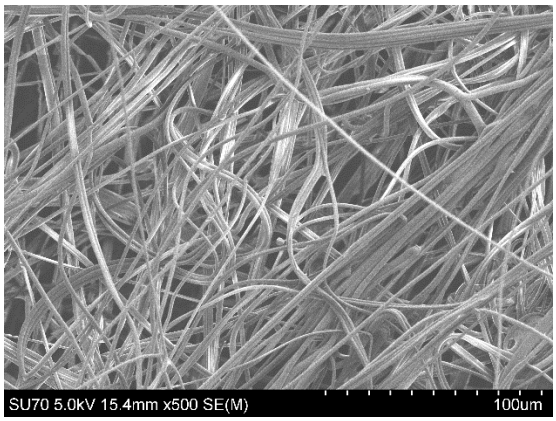

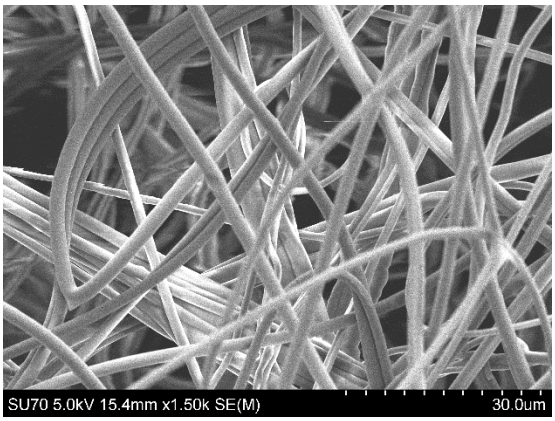

Upper layers

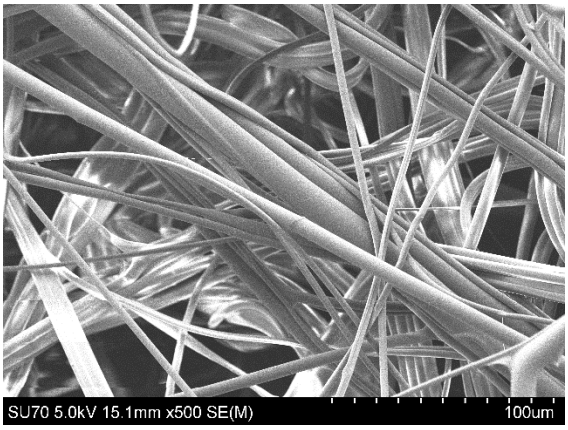

Lower layer

(d) Respirator filter media type-4

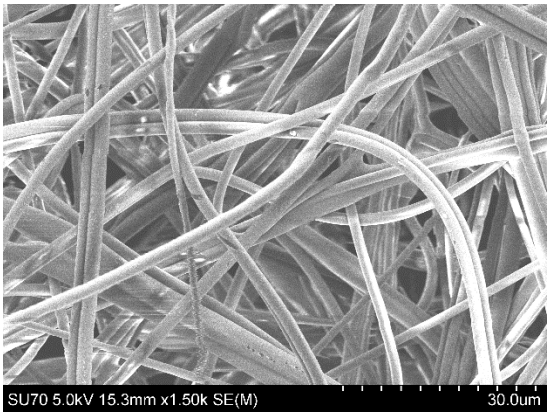

Upper layers

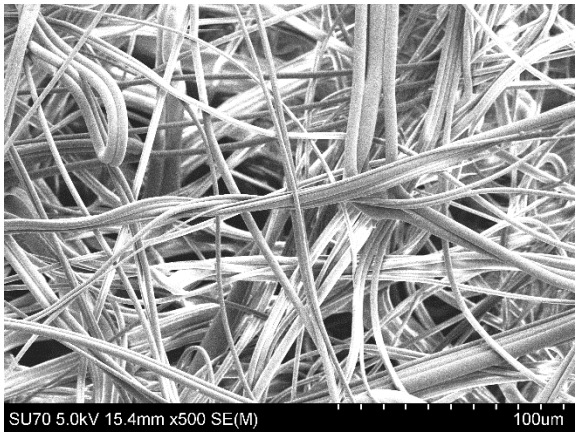

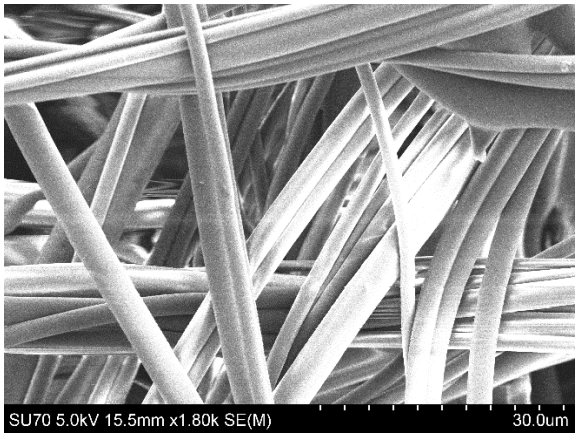

Lower layer

(e) Respirator filter media type-5

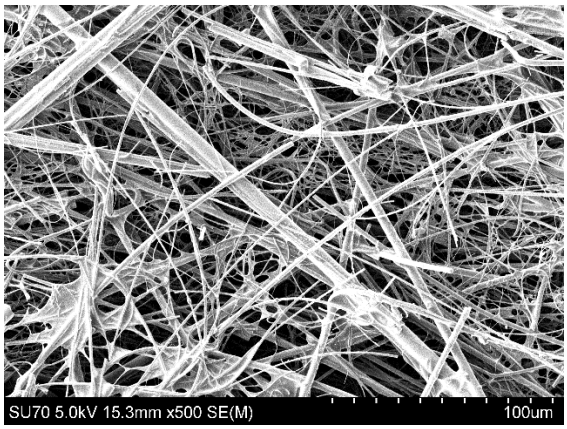

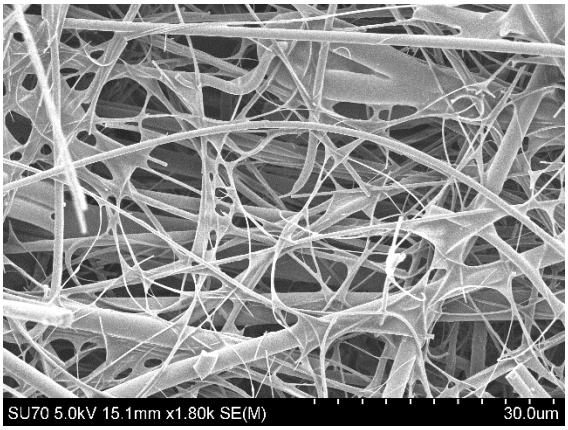

(f) Glass fibrous filter media (Cummins_GF)

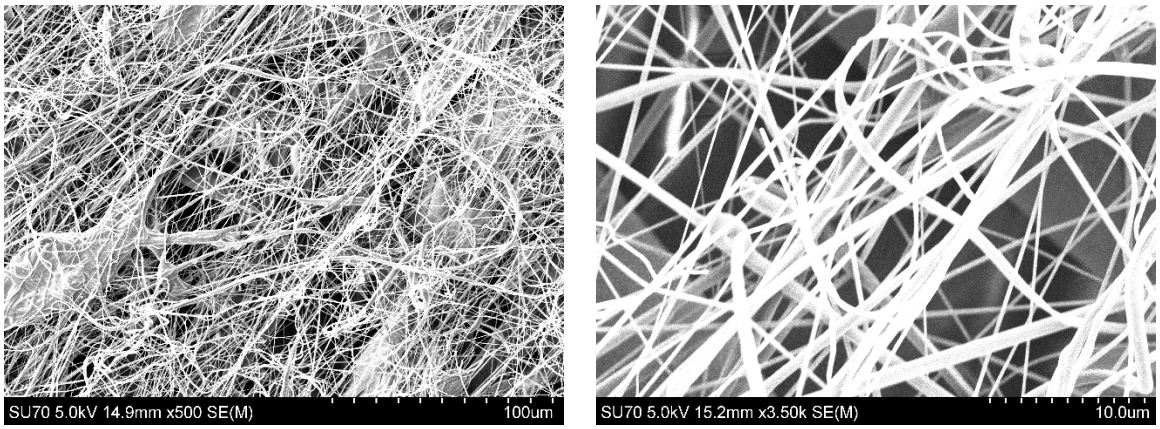

(g) Glass fibrous filter media (Cummins_Nanofiber)

APPENDIX B

Peak Penetration of respirator filter media:

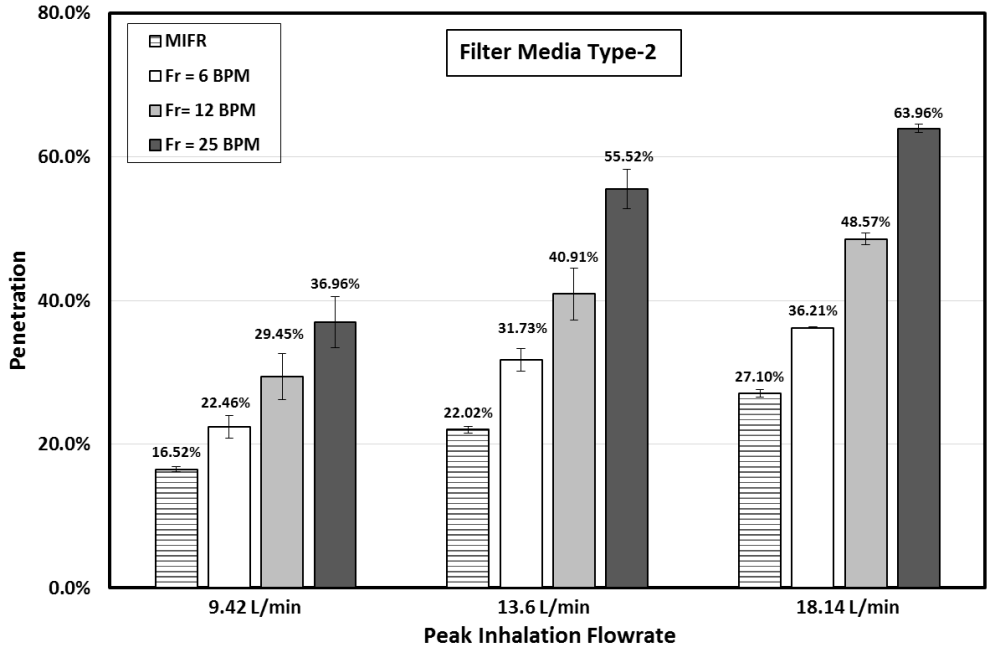

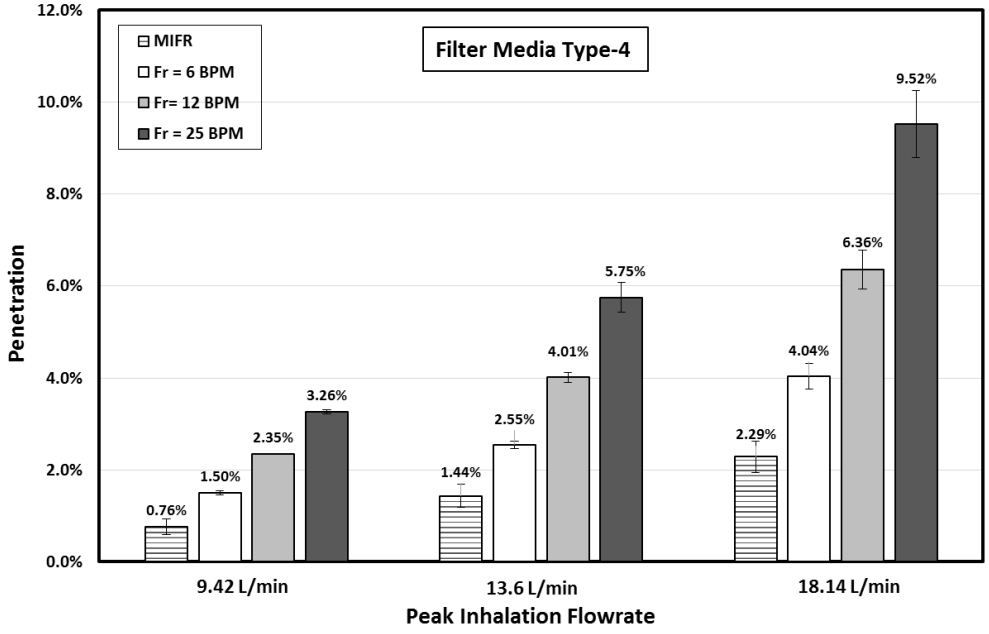

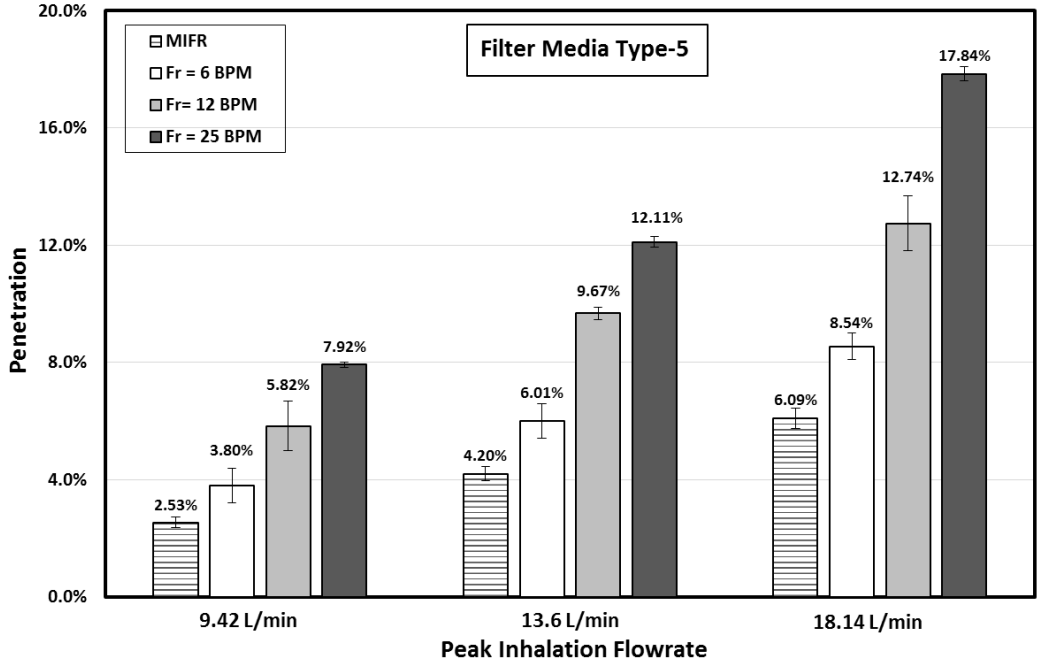
Filter Media Type-5
MIFR
Fr = 6 BPM
Fr= 12 BPM
Fr = 25 BPM
Penetration
20.0%
16.0%
12.0%
8.0%
4.0%
0.0%
2.53%
3.80%
5.82%
7.92%
4.20%
6.01%
9.67%
12.11%
6.09%
8.54%
12.74%
17.84%
9.42 L/min
13.6 L/min
18.14 L/min
Peak Inhalation Flowrate

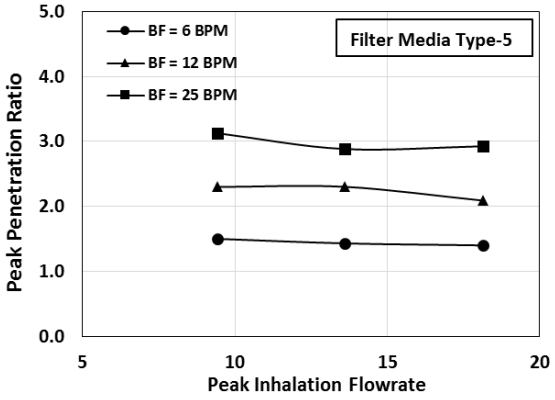
Filter Media Type-5
BF = 6 BPM
BF = 12 BPM
BF = 25 BPM
Peak Penetration Ratio
5.0
4.0
3.0
2.0
1.0
0.0
5
10
15
20
Peak Inhalation Flowrate

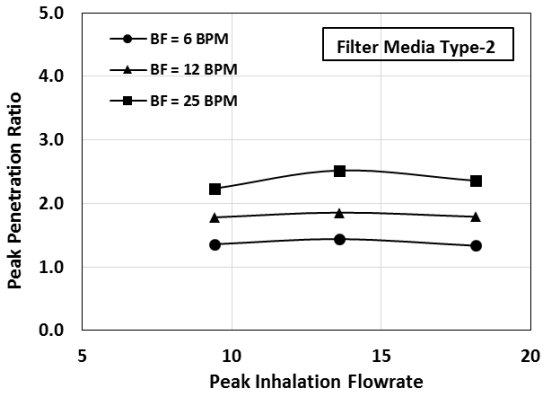
Filter Media Type-2
BF = 6 BPM
BF = 12 BPM
BF = 25 BPM
Peak Penetration Ratio
5.0
4.0
3.0
2.0
1.0
0.0
5
10
15
20
Peak Inhalation Flowrate

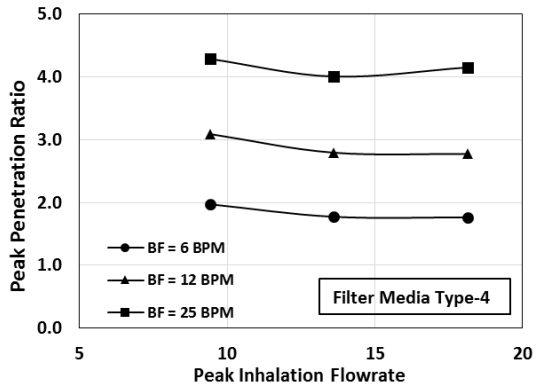
Filter Media Type-4
BF = 6 BPM
BF = 12 BPM
BF = 25 BPM
Peak Penetration Ratio
5.0
4.0
3.0
2.0
1.0
0.0
5
10
15
20
Peak Inhalation Flowrate

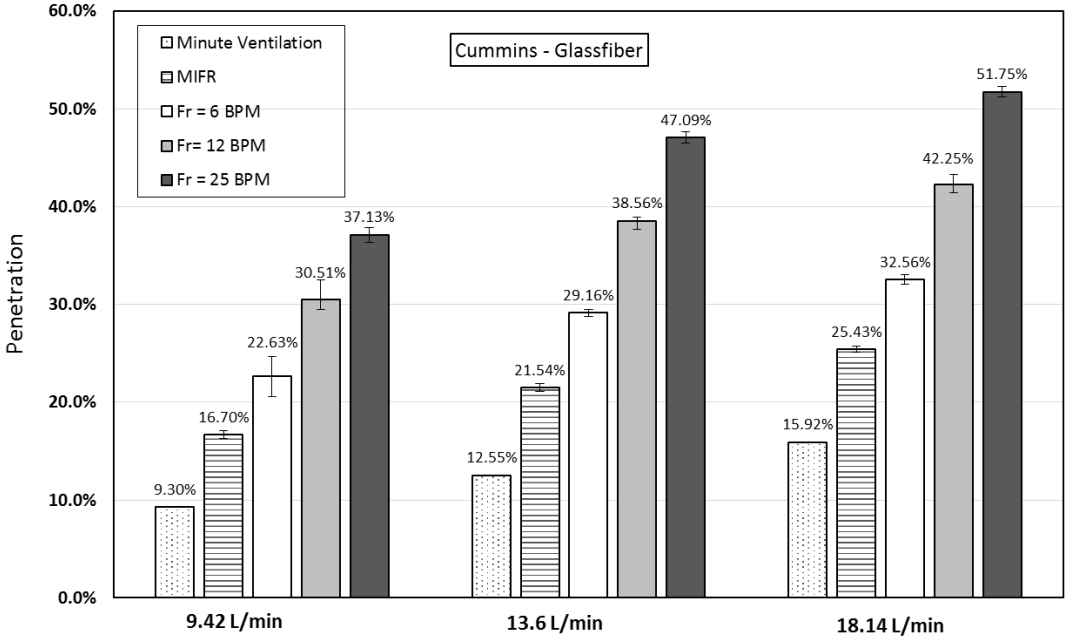
Cummins - Glassfiber
Minute Ventilation
MIFR
Fr = 6 BPM
Fr= 12 BPM
Fr = 25 BPM
Penetration
60.0%
50.0%
40.0%
30.0%
20.0%
10.0%
0.0%
9.30%
16.70%
22.63%
30.51%
37.13%
12.55%
21.54%
29.16%
38.56%
47.09%
15.92%
25.43%
32.56%
42.25%
51.75%
9.42 L/min
13.6 L/min
18.14 L/min

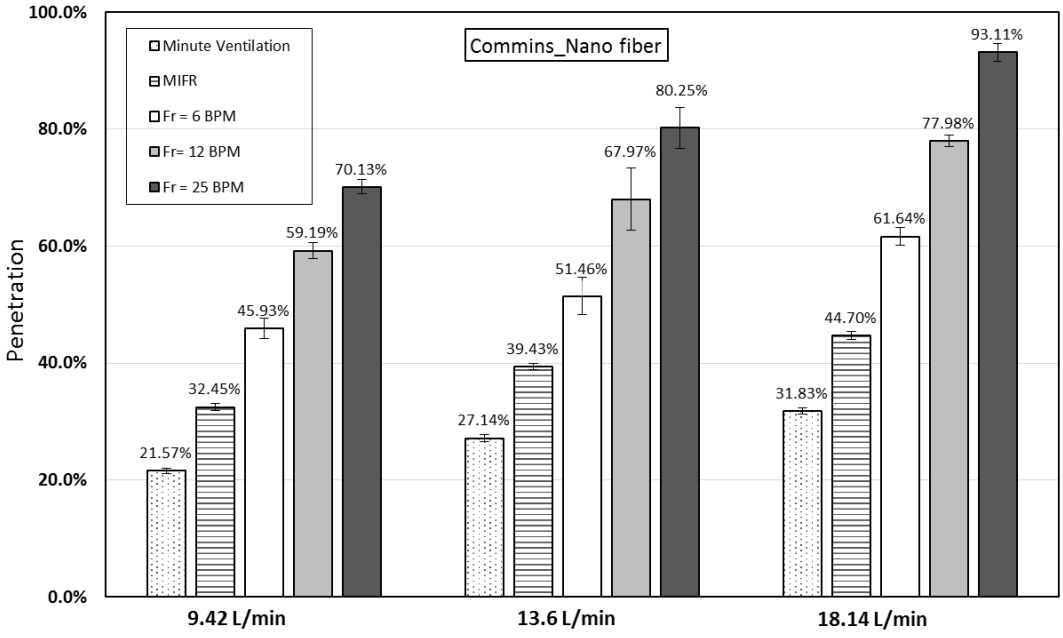
Commins_Nano fiber
Minute Ventilation
MIFR
Fr = 6 BPM
Fr= 12 BPM
Fr = 25 BPM
Penetration
100.0%
80.0%
60.0%
40.0%
20.0%
0.0%
21.57%
32.45%
45.93%
59.19%
70.13%
27.14%
39.43%
51.46%
67.97%
80.25%
31.83%
44.70%
61.64%
77.98%
93.11%
9.42 L/min
13.6 L/min
18.14 L/min

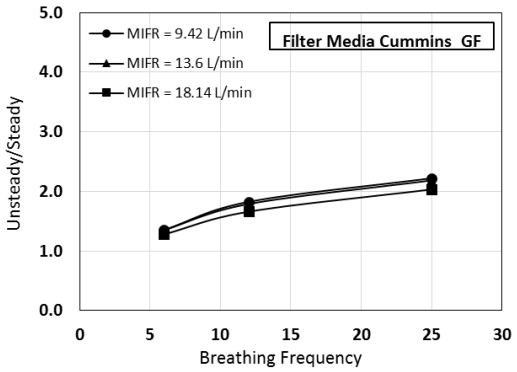
MIFR = 9.42 L/min
MIFR = 13.6 L/min
MIFR = 18.14 L/min
Filter Media Cummins_GF
Unsteady/Steady
Breathing Frequency
0.0
1.0
2.0
3.0
4.0
5.0
0
5
10
15
20
25
30

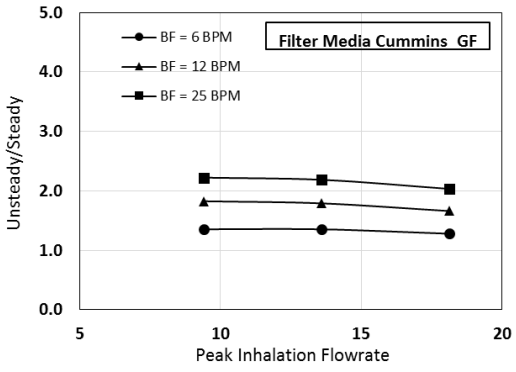
BF = 6 BPM
BF = 12 BPM
BF = 25 BPM
Filter Media Cummins_GF
Unsteady/Steady
Peak Inhalation Flowrate
0.0
1.0
2.0
3.0
4.0
5.0
5
10
15
20

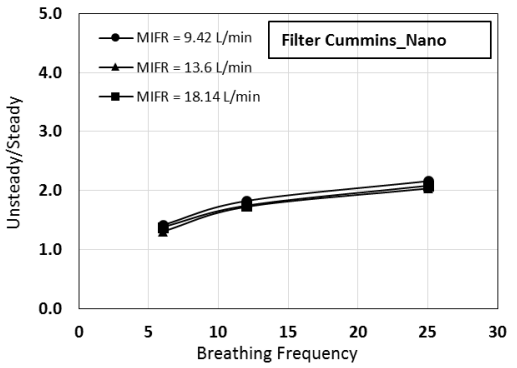
MIFR = 9.42 L/min
MIFR = 13.6 L/min
MIFR = 18.14 L/min
Filter Cummins_Nano
Unsteady/Steady
Breathing Frequency
0.0
1.0
2.0
3.0
4.0
5.0
0
5
10
15
20
25
30

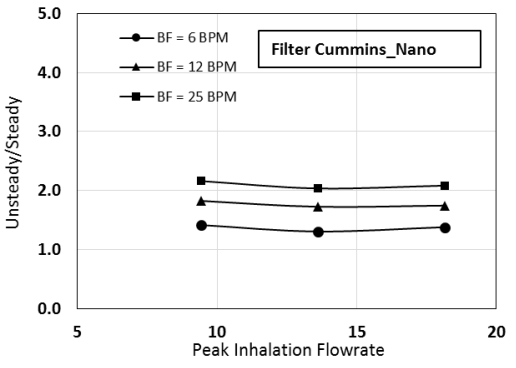
BF = 6 BPM
BF = 12 BPM
BF = 25 BPM
Filter Cummins_Nano
Unsteady/Steady
Peak Inhalation Flowrate
0.0
1.0
2.0
3.0
4.0
5.0
5
10
15
20

VITA

Qiang Wang

EDUCATION

PH.D. in MECHANICAL ENGINEERING

Virginia Commonwealth University (VCU), Richmond, VA 01/2013 - 08/2016

M.S. in MECHANICAL & NUCLEAR ENGINEERING

Virginia Commonwealth University (VCU), Richmond, VA 08/2010 - 12/2012

B.S. in MATERIAL FORMATION AND CONTROL ENGINEERING

China Three Gorges University (CTGU), Yichang, China 08/2006 - 06/2010

AWARDS & HONORS

VCU Dean's Fellowship & Research Assistant Scholarship 08/2010 - 12/2012

President: Engineering of Graduate Student Association at VCU 04/2012 - 12/2013

PUBLICATIONS

- **Wang, Qiang,** Laleh Golshahi, and Da-Ren Chen. "Advanced Testing Method to Evaluate the Performance of Respirator Filter Media." *Journal of Occupational and Environmental Hygiene* just-accepted (2016): 00-00.
- **Wang, Qiang**, Xiuli Lin, and Da-Ren Chen. "Effect of Dust Loading Rate on the Loading Characteristics of High Efficiency Filter Media." *Powder Technology* 287 (2016): 20-28.
- **Wang, Qiang**, Laleh Golshahi and Da-Ren Chen. "Evaluation of Respirator Filter." *World Filtration Congress 2016*
- **Wang, Qiang,** Laleh Golshahi and Da-Ren Chen. "Evaluation of Respirator Filter Media under Inhalation-only Condition." *Annals of Occupational Hygiene* , 2016 (in press)
- **Wang, Qiang**, Laleh Golshahi and Da-Ren Chen. "Evaluation of the Electrical Charged Aerosol Effect on the Performance of Respirator Filter." *Journal of Aerosol Science, 2016* (in preparation)
- Shaowen Chen, **Wang, Qiang** and Da-Rren Chen. "Pleat Shape Effect on Reverse Pulsed-jet Cleaning of Pleated Filter Cartridges." *Filtration and Separation, 2016* (in press)
- **Qiang Wang** and Da-Ren Chen. "The Performance of HVAC Filter Panels under Non-uniform Particle Loading Conditions" *Power Technology, 2016 (in preparation)*
- **Qiang Wang** and Da-Ren Chen. "The Effect of Filter Pleat Geometry on the Performance of HVAC Filter " *Power Technology, 2016 (in preparation)*

- Yi, Zhang, **Wang Qiang**, Fang Zi-fan, and Zhang Hu. "Static Decoupling Design Method of Electromechanical System Mechanical Structure." In *Computational Intelligence and Industrial Applications, 2009. PACIIA 2009. Asia-Pacific Conference on*, vol. 1, pp. 313-316. IEEE, 2009.
- Yi, Zhang, Zhang Hu, Fang Zi-fan, and **Wang Qiang**. "Study on the Facility Layout in Workshop Based on Improved Adaptive Genetic Algorithm." In *Computational Intelligence and Software Engineering, 2009. CiSE 2009. International Conference on*, pp. 1-4. IEEE, 2009.

ACADEMIC ACTIVITIES

- **Qiang Wang**, Laleh Golshahi and Da-Ren Chen, "Investigation of Breathing Frequency and Inhalation Flow Rate on the Performance of Respirator Filter Medium", American Association for Aerosol Research (AAAR) 35th Annual Conference, Portland, OR, October 2016.
- **Qiang Wang**, Laleh Golshani and Da-Ren Chen, "Performance Evaluation of Respirator Filter Media under the Simulated Breath Condition", World Filtration Congress 12th, Taipei, Taiwan, April, 2016
- **Qiang Wang** and Da-Ren Chen. "Unsteady Loading Test for Filter Media", Filtration & Separations in Power Generation (AFS Spring Conference), Charlotte, NC, April 2015.
- **Qiang Wang** and Da-Ren Chen. "Effect of Particle Loading Rate on Flat Filter Medium Performance", American Association for Aerosol Research (AAAR) 33rd Annual Conference, Orlando, FL, October 2015.

- **Qiang Wang** and Brian Hinderliter. “The Influence of Zin Particle Sizes and Volume Fraction on the Electrochemical”, Physical and Reaction Rate Properties of Coatings, CoatingsTech Conference, Chicago, IL, February 2013.